(12)

AD

CONTRACT REPORT BRL-CR-568

STOCHASTIC GUN DYNAMICS

S&D DYNAMICS, INC.
755 NEW YORK AVE.
HUNTINGTON, NY 11743

APRIL 10, 1987

US ARMY BALLISTIC RESEARCH LABORATORY
ABERDEEN PROVING GROUND, MARYLAND

Destroy this report when it is no longer needed.
Do not return it to the originator.

Additional copies of this report may be obtained from the National Technical Information Service, U. S. Department of Commerce, Springfield, Virginia 22161.

The findings in this report are not to be construed as an official Department of the Army position, unless so designated by other authorized documents.

The use of trade names or manufacturers' names in this report does not constitute indorsement of any commercial product.

UNCLASSIFIED
SECURITY CLASSIFICATION OF THIS PAGE

AD-A180 866

REPORT DOCUMENTATION PAGE

Form Approved
OMB No 0704-0188
Exp Date Jun 30, 1986

1a REPORT SECURITY CLASSIFICATION Unclassified	1b RESTRICTIVE MARKINGS
2a SECURITY CLASSIFICATION AUTHORITY	3 DISTRIBUTION / AVAILABILITY OF REPORT
2b DECLASSIFICATION / DOWNGRADING SCHEDULE	
4 PERFORMING ORGANIZATION REPORT NUMBER(S)	5 MONITORING ORGANIZATION REPORT NUMBER(S) DAAK11-83-C-0054
6a NAME OF PERFORMING ORGANIZATION USA Ballistic Research Laboratory 6b OFFICE SYMBOL (If applicable) SLCBR-IB-W	7a NAME OF MONITORING ORGANIZATION S&D Dynamics, Inc.
6c. ADDRESS (City, State, and ZIP Code) Aberdeen Proving Ground, MD 21005-5066	7b ADDRESS (City, State, and ZIP Code) 755 New York Ave. Huntington, NY 11743
8a. NAME OF FUNDING / SPONSORING ORGANIZATION - 8b OFFICE SYMBOL (If applicable)	9 PROCUREMENT INSTRUMENT IDENTIFICATION NUMBER -
8c. ADDRESS (City, State, and ZIP Code)	10 SOURCE OF FUNDING NUMBERS PROGRAM ELEMENT NO: 612618 / PROJECT NO: AH80 / TASK NO: / WORK UNIT ACCESSION NO:

11 TITLE (Include Security Classification)
Stochastic Gun Dynamics

12 PERSONAL AUTHOR(S)
Martin T. Soifer and Robert S. Becker

13a TYPE OF REPORT	13b TIME COVERED	14 DATE OF REPORT (Year, Month, Day)	15 PAGE COUNT
FINAL	FROM Oct 86 TO Feb 87		

16 SUPPLEMENTARY NOTATION The view, opinions, and/or findings contained in this report are those of the author(s) and should not be construed as an official Department of the Army position, policy, or decision, unless so designated by other documentation.

17 COSATI CODES			18 SUBJECT TERMS (Continue on reverse if necessary and identify by block number)
FIELD	GROUP	SUB-GROUP	
19	C5		Gun Dynamics; Monte-Carlo Routine; Gun Tube Muzzle Motion; Shot-to-Shot Variability; DYNACODE-G; Probabilistic Muzzle Behavior; Stochastic Gun Dynamics; Fire Control
19	06		

19 ABSTRACT (Continue on reverse if necessary and identify by block number)

Employing a Monte-Carlo routine and random number generator, a stochastic version of DYNACODE-G has been developed and implemented for the purpose of assessing probalistic gun tube muzzle motion behavior due to shot-to-shot variations in pertinent forcing functions which arise during firing. In addition, DYNACODE-G has been modified to accomodate input accelerations at the trunnion level to simulate vehicle motion over prescribed terrain, an externally supplied numerical integration scheme.

20 DISTRIBUTION / AVAILABILITY OF ABSTRACT	21 ABSTRACT SECURITY CLASSIFICATION
☒ UNCLASSIFIED/UNLIMITED ☐ SAME AS RPT ☐ DTIC USERS	UNCLASSIFIED
22a NAME OF RESPONSIBLE INDIVIDUAL James O. Pilcher II	22b TELEPHONE (Include Area Code) (301) 278-6127 22c OFFICE SYMBOL SLCBR-IB-W

DD FORM 1473, 84 MAR 83 APR edition may be used until exhausted
All other editions are obsolete

SECURITY CLASSIFICATION OF THIS PAGE
UNCLASSIFIED

TABLE OF CONTENTS

LIST OF FIGURES

LIST OF FIGURES (Cont'd.)

LIST OF TABLES

1. INTRODUCTION

This final report documents work performed by S&D Dynamics, Inc. under Contract No. DAAK11-83-C-0054 to the U.S. Army Ballistic Research Laboratory, Aberdeen Proving Ground, MD.

The primary objective of this effort is the extension of the deterministic gun dynamics simulation code, DYNACODE-G, to accommodate shot-to-shot variations in pertinent forcing functions which arise during firing, in order to assess gun system performance on a probabilistic basis. Additional objectives include introduction of gun mount excitation to simulate vehicle motion and introduction of an externally supplied firing signal to prescribe burst-mode fire.

For the purposes of this study the 75mm ADMAG served as baseline gun system, 75mm LAV firings conducted at Aberdeen Proving Ground, November 1984, served as forcing function data base, and M1 vehicle-hull accelerations for the Munson straight, full and washboard courses served as vehicle motion data base.

In order to achieve the cited objectives, DYNACODE-G was first modified to accommodate independent right and left recoil accumulator loads. Forcing function data consisting of propellant generated gas pressure, right and left recoil accumulator pressures and recoil motion obtained from seventeen LAV firings were statistically analyzed by Mrs. Melinda B. Krummerich, Mechanics and Structures Branch, Interior Ballistics Division, U.S. Army Ballistic Research Laboratory, to serve as data base. DYNACODE-G was then modified to include a Monte-Carlo routine (with BRL supplied random number generator) to operate on the data base to produce a statistically meaningful sample of "mathematical" firings. M1 vehicle-hull accelerations were statistically analyzed by Miss Susan A. Coates, Mechanics and Structures Branch, IBD, BRL, and DYNACODE-G was modified to accommodate mount excitation (i.e., simulated vehicle motion). In order to efficiently handle gun system response to mount excitation, firing excitation and the response time between successive firings, DYNACODE-G was modified by replacing the fixed time-step Runge-Kutta integration scheme with an automated (self-determining) variable time-step routine. Finally, DYNACODE-G was modified to accommodate an externally supplied firing signal to prescribe the timing between successive rounds in burst-mode fire, based on gun tube muzzle motion parameters falling within a prescribed "window" of acceptable values.

2. MONTE-CARLO ROUTINE

DYNACODE-G was modified to include a Monte-Carlo routine for the purpose of generating a statistically meaningful sample of "mathematical" firings based on a limited sample of actual firings. An overview of the technique is depicted in Fig. 1.

Referring to Fig. 1, test results for pertinent forcing function data obtained from "M" firings are statistically analyzed. A random number generator is introduced to produce pertinent forcing function data for "N" (>> "M") "mathematical" firings. Each set of forcing function data obtained for each "mathematical" firing is input into DYNACODE-G for the purpose of generating muzzle motion data. The resulting muzzle motion data are then statistically analyzed to produce a probabilistic assessment of muzzle motion for the class of ammunition considered.

2.1 Statistical Analysis of Pertinent Forcing Function Data

Forcing function data consisting of propellant generated gas pressure, right and left recoil accumulator pressures and recoil velocity for each of seventeen 75mm LAV firings conducted at Aberdeen Proving Ground, November 1984, were statistically analyzed by Mrs. Melinda B. Krummerich, Mechanics and Structures Branch, Interior Ballistics Division, U.S. Army Ballistic Research Laboratory.

Individual shot data for propellant generated gas pressure was first normalized with respect to time-to-peak-pressures, t^*, as depicted schematically in Fig. 2. Assuming a normal distribution for t^*, the statistical distribution for propellant generated gas pressure as a function of time, namely $p_c(t/t^*)$, was obtained for the sample of seventeen firings, as schematically depicted in Fig. 2.

Examination of individual shot data revealed two distinct patterns for right recoil accumulator pressure data, a single pattern for left recoil accumulator pressure data and a single pattern for recoil velocity data, as schematically depicted in Fig. 3. Right recoil accumulator pressure data for eight of the firings, Pattern "A", were identical with corresponding left accumulator data; whereas, right recoil accumulator data for the remaining nine firings, Pattern "B", were consistently higher than corresponding left recoil pressure data. Statistical distributions for right recoil accumulator pressure Patterns "A" and "B", left recoil accumulator pressure and recoil velocity were obtained as schematically depicted in Fig. 3.

Having defined the statistical distributions associated with the pertinent forcing functions for the limited sample of firings, the Monte-Carlo routine was introduced to define the variables associated with each of "N" mathematical firings, as depicted in Fig. 4. Referring to Fig. 4, a two-state random number generator selects either Pattern "A" or "B" for the right recoil accumulator, while a normally distributed random number generator defines a compatible set of forcing function data for each of the "N" mathematical firings for input (on a deterministic basis) into DYNACODE-G.

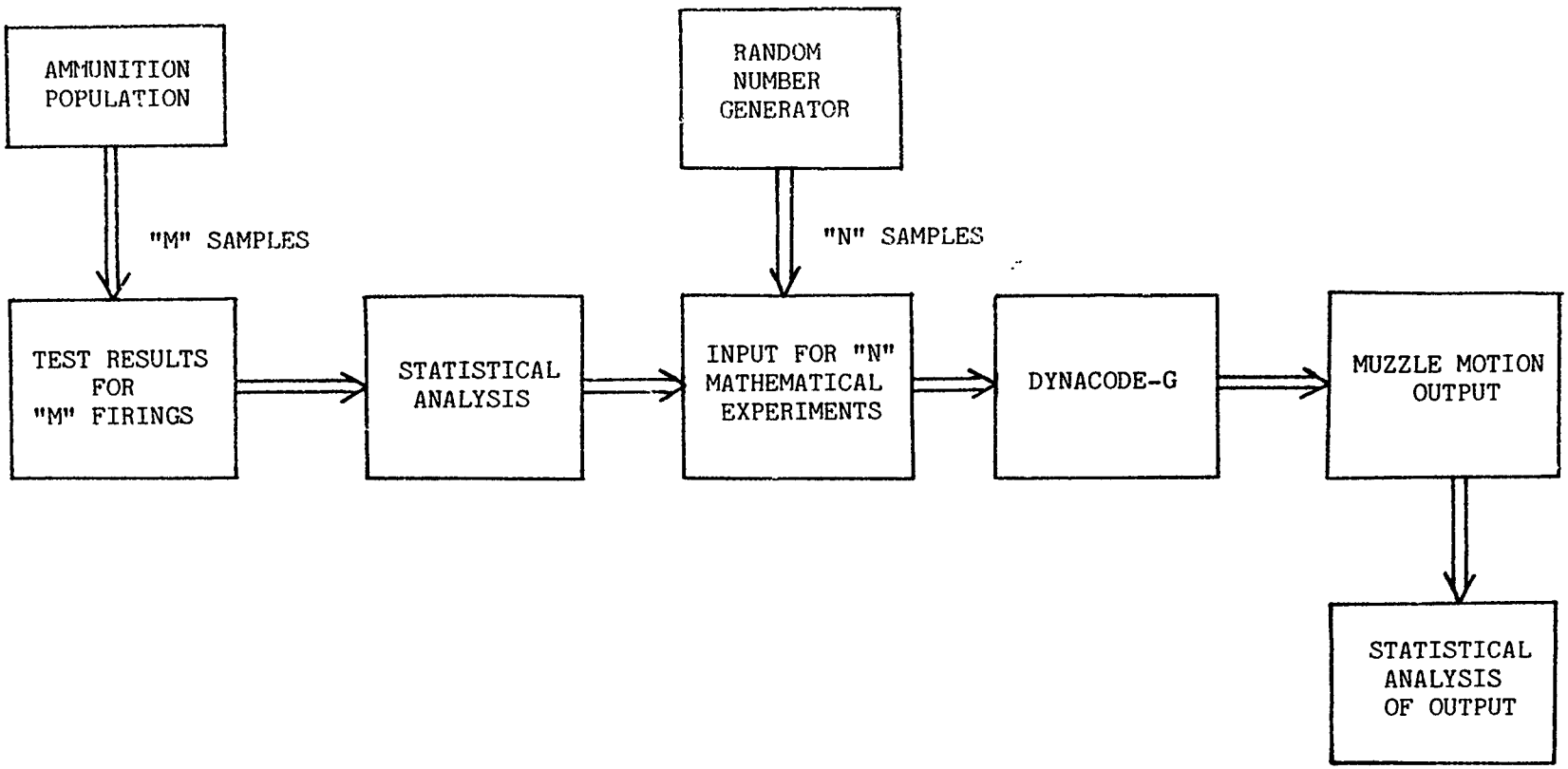

Fig. 1 - Overview of Technique

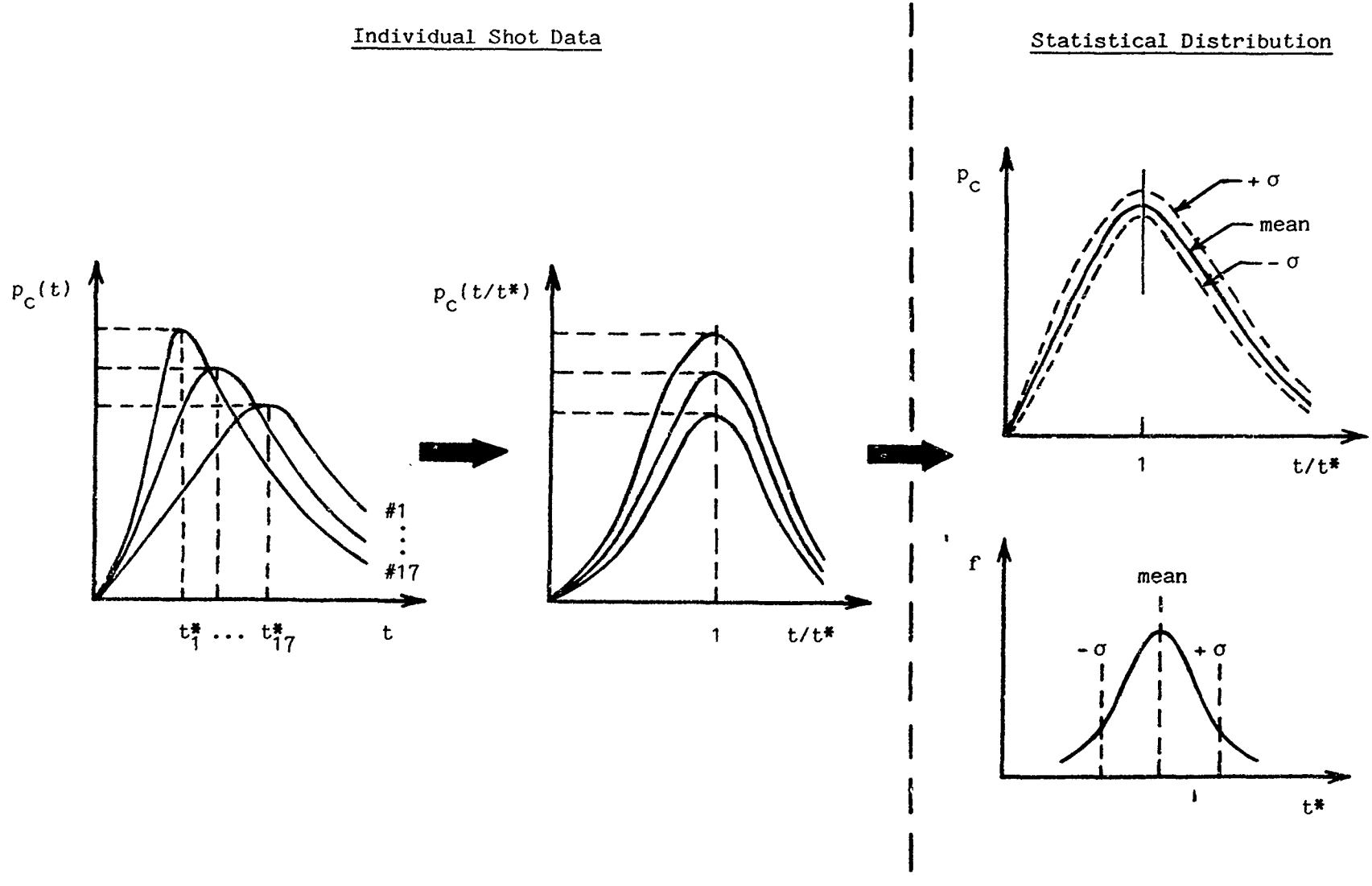

Fig. 2 - Statistical Distribution of Propellant Generated Gas Pressure

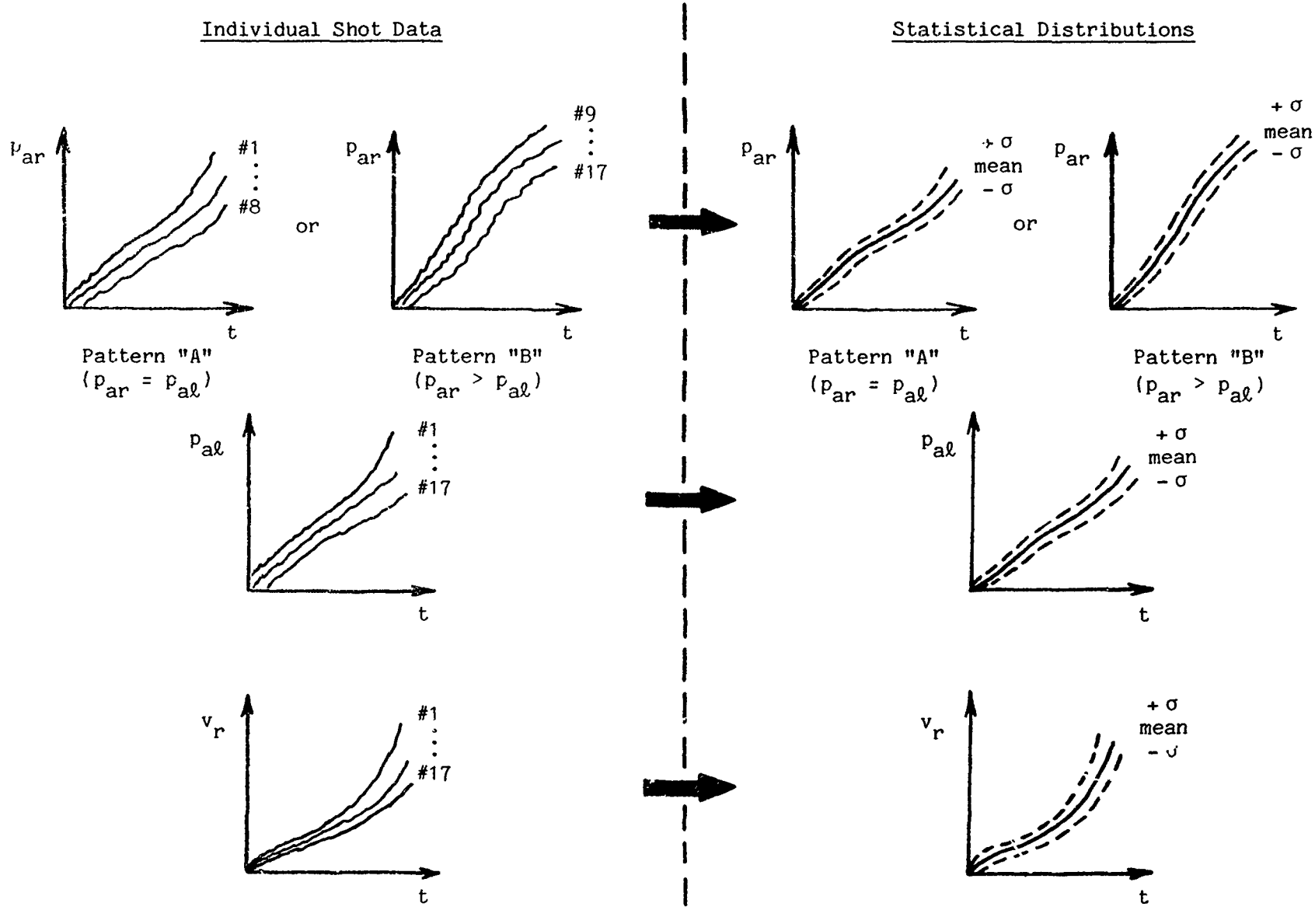

Fig. 3 - Statistical Distributions of Recoil Accumulator Pressure and Recoil Motion

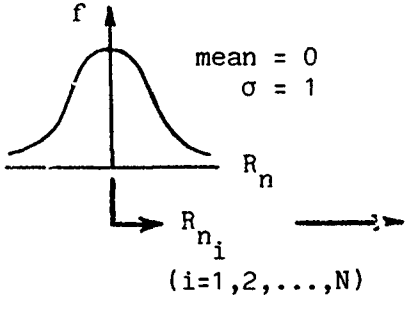

Normally Distributed
Random Number Generator

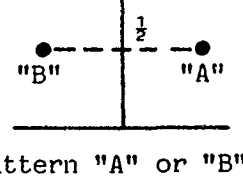

Pattern "A" or "B"

Two-State Random
Number Generator

$$
\left\{
\begin{array}{l}
p_c(t/t^*) = p_c(t/t^*)\big|_{mean} + R_{n_i}\,\sigma(t/t^*) \quad ; \quad i=1,2,\ldots,N \\
\\
t^* = t^*_{mean} - R_{n_i}\,\sigma^* \\
\\
p_{ar}(t) = \left\{
\begin{array}{l}
p_{ar}^{"A"}(t)\big|_{mean} + R_{n_i}\,\sigma_{ar}^{"A"}(t) \\
\qquad\qquad \text{or} \\
p_{ar}^{"B"}(t)\big|_{mean} + R_{n_i}\,\sigma_{ar}^{"B"}(t)
\end{array}
\right. \\
\\
p_{a\ell}(t) = p_{a\ell}(t)\big|_{mean} + R_{n_i}\,\sigma_{a\ell}(t) \\
\\
v_r(t) = v_r(t)\big|_{mean} + R_{n_i}\,\sigma_{v_r}(t)
\end{array}
\right\} \rightarrow \boxed{\text{DYNACODE-G}}
$$

Fig. 4 - Application of Monte-Carlo Routine

2.2 Application of Monte-Carlo Routine

In general, a sample population size of thirty data sets is sufficient to achieve a meaningful statistical analysis. However, since a two-state random number generator is needed to define the right recoil accumulator pressure pattern, twice this number, or sixty data sets, are appropriate. The Monte-Carlo routine and modified version of DYNACODE-G were employed as depicted in Fig. 4 to produce sixty, single-shot, "mathematical" firings, based on the seventeen 75mm LAV firings, using the BRL Cyber 7600 system. The results of these runs have been statistically analyzed. It is noted that the fixed time-step, fourth-order, Runge-Kutta integration scheme has been retained in this version of DYNACODE-G.

Population means and standard deviations were computed for shot-exit time, muzzle velocity, (total) transverse muzzle displacement at shot-exit, (total) transverse linear velocity at shot-exit, and (total) pitch rate at shot-exit, as presented in Table I. As may be seen from Table I, the greatest sensitivity in terms of shot-to-shot variations occur in transverse linear velocity and pitch rate. Since these parameters dominate the "jump" equations it may be concluded that shot-to-shot variations can account for a 10% to 20% increase in dispersion at the target.

In addition, the total population of sixty "mathematical" firings was segregated into two separate populations characterized by the distinction between right recoil accumulator pressure Patterns "A" and "B". Twenty-six data sets contained Pattern "A"; thirty-four data sets contained Pattern "B". Student t-tests on the resulting means and standard deviations obtained for all parameters examined within each population showed no statistically significant difference between the two populations. Hence, it may be concluded that the noted anomalous recoil accumulator pressure patterns have insignificant effect on the total dispersion budget.

Finally, a Chi-Square analysis was performed to determine the correlation between transverse linear velocity and pitch rate at shot-exit. Examination of the individual "mathematical" firings relative to the overall population means yielded the 2 x 2 matrix in Table II. The calculated value of χ^2 for this table, namely 35.4, is highly significant and indicates a high degree of coupling between linear and angular muzzle velocities at shot-exit. Hence, it may be expected that these parameters will have an additive effect in terms of the total error budget for target dispersion.

TABLE I - STATISTICAL ANALYSIS OF PERTINENT SHOT-EXIT PARAMETERS FOR POPULATION OF SIXTY "MATHEMATICAL" FIRINGS*

VARIABLE	MEAN	STANDARD DEVIATION	STANDARD DEVIATION AS % OF MEAN
Transverse Displacement (in)	1.94×10^{-3}	$.1134 \times 10^{-3}$	5.8
Transverse Velocity (fps)	.6485	.1101	17.0
Pitch Rate (rad/sec)	4.527	.4387	9.7
Muzzle Velocity (fps)	5696.	34.62	.61
Exit Time (ms)	6.305	.06	.95

* Generated using Monte-Carlo technique and modified version of DYNACODE-G.

TABLE II - CORRELATION BETWEEN TRANSVERSE LINEAR VELOCITY AND PITCH RATE AT SHOT-EXIT*

	PITCH RATE > MEAN	PITCH RATE < MEAN	ROW SUM
TRANSVERSE VELOCITY > MEAN	Observed - 28	Observed - 4	32
	Expected - 16	Expected - 16	
TRANSVERSE VELOCITY < MEAN	Observed - 2	Observed - 26	28
	Expected - 14	Expected - 14	
COLUMN SUM	30	30	

* $\chi^2 = \sum_{\text{Boxes}} \frac{(\text{Obs} - \text{Exp} - 0.5)^2}{\text{Exp}} = 35.4$

3. VEHICLE MOTION

Algorithms were developed to recover pitch, roll and vertical accelerations at the gun trunnions in terms of bed mounted accelerometer data obtained for M1 vehicle test runs on the Munson straight, full and washboard courses. Miss Susan A. Coates, Mechanics and Structures Branch, Interior Ballistics Division, U.S. Army Ballistic Research Laboratory, implemented the algorithms and, in addition, performed a power spectral density analysis of the acceleration traces.

Sample traces of pitch, roll and vertical accelerations as recovered by the algorithms for the Munson full course (BRL Ident 1) are presented in Figs. 5a, 6a and 7a, respectively. Results of the corresponding power spectral density analyses are presented in Figs. 5b, 6b and 7b.

A functional representation (based on frequency content) was developed to simulate a typical cycle of acceleration data. Simulated traces of pitch, roll and vertical accelerations (based on the functional representation developed and power spectral density analyses performed) are presented in Figs. 5c, 6c and 7c, respectively.

In addition, expressions for inertia loads due to mount excitation were developed and incorporated within DYNACODE-G. Within the framework of small displacement theory, and in accordance with the notation of DYNACODE-G, these loads, applied to each mass point of the gun system, take the form

$$\begin{Bmatrix} r_{y_i} \ddot{\psi}_g \\ -\ddot{y}_g - r_{x_i} \ddot{\psi}_g + r_{z_i} \ddot{\varphi}_g \\ -r_{y_i} \ddot{\varphi}_g \\ -\ddot{\varphi}_g \\ 0 \\ -\ddot{\psi}_g \end{Bmatrix}$$

where $\ddot{\psi}_g$, $\ddot{\varphi}_g$ and $\ddot{y}_g$ respectively denote pitch, roll and vertical input accelerations at the trunnions, and r_{x_i}, r_{y_i} and r_{z_i} denote components of the position vector of the i^{th} mass point relative to the trunnions.

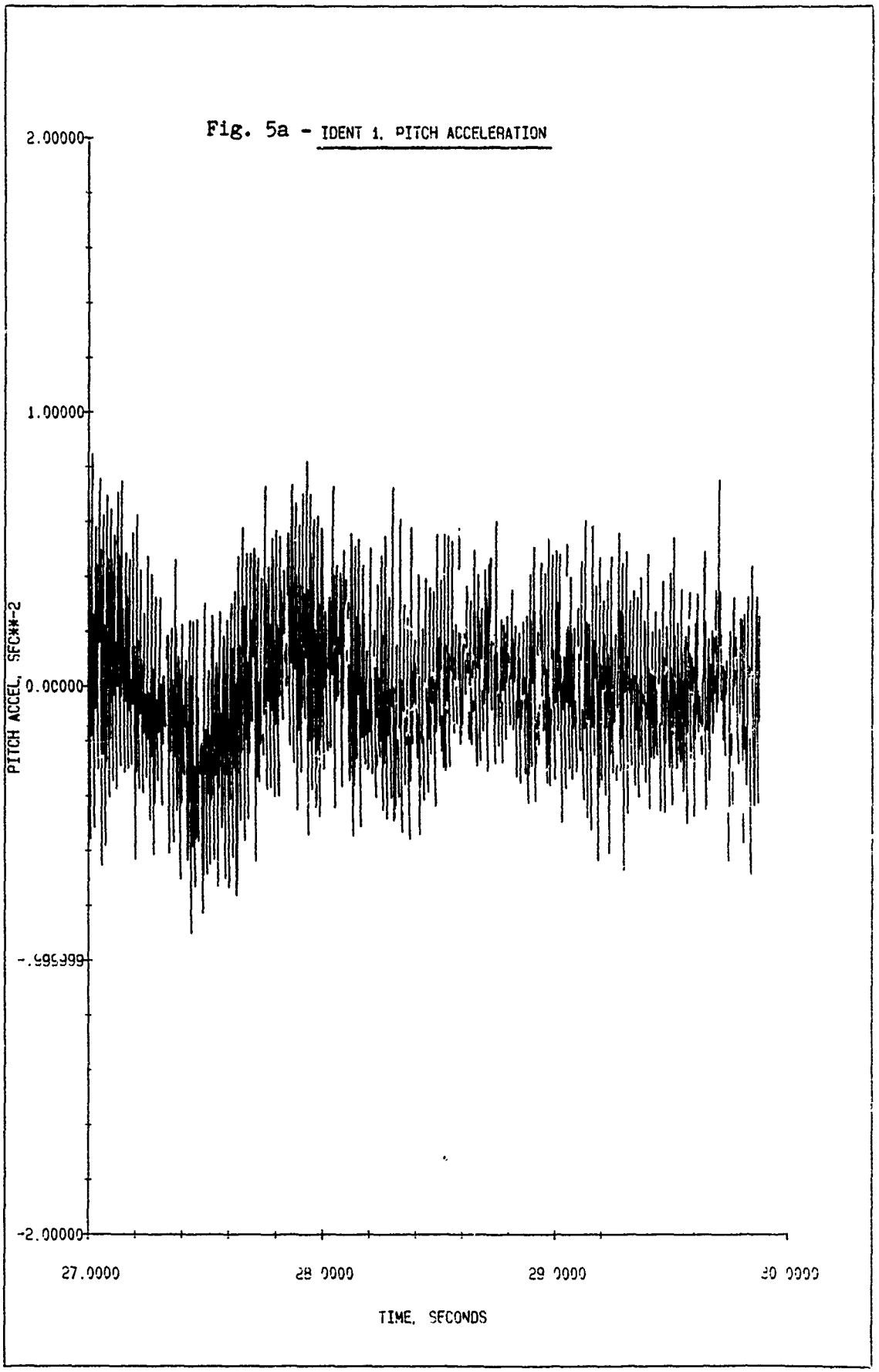
Fig. 5a - IDENT 1. PITCH ACCELERATION
2.00000
1.00000
0.00000
-.999999
-2.00000
PITCH ACCEL, SEC**-2
27.0000
28.0000
29.0000
30.0000
TIME, SECONDS

Fig. 5b - ID1, PSD PITCH ACCEL, 27001-30000

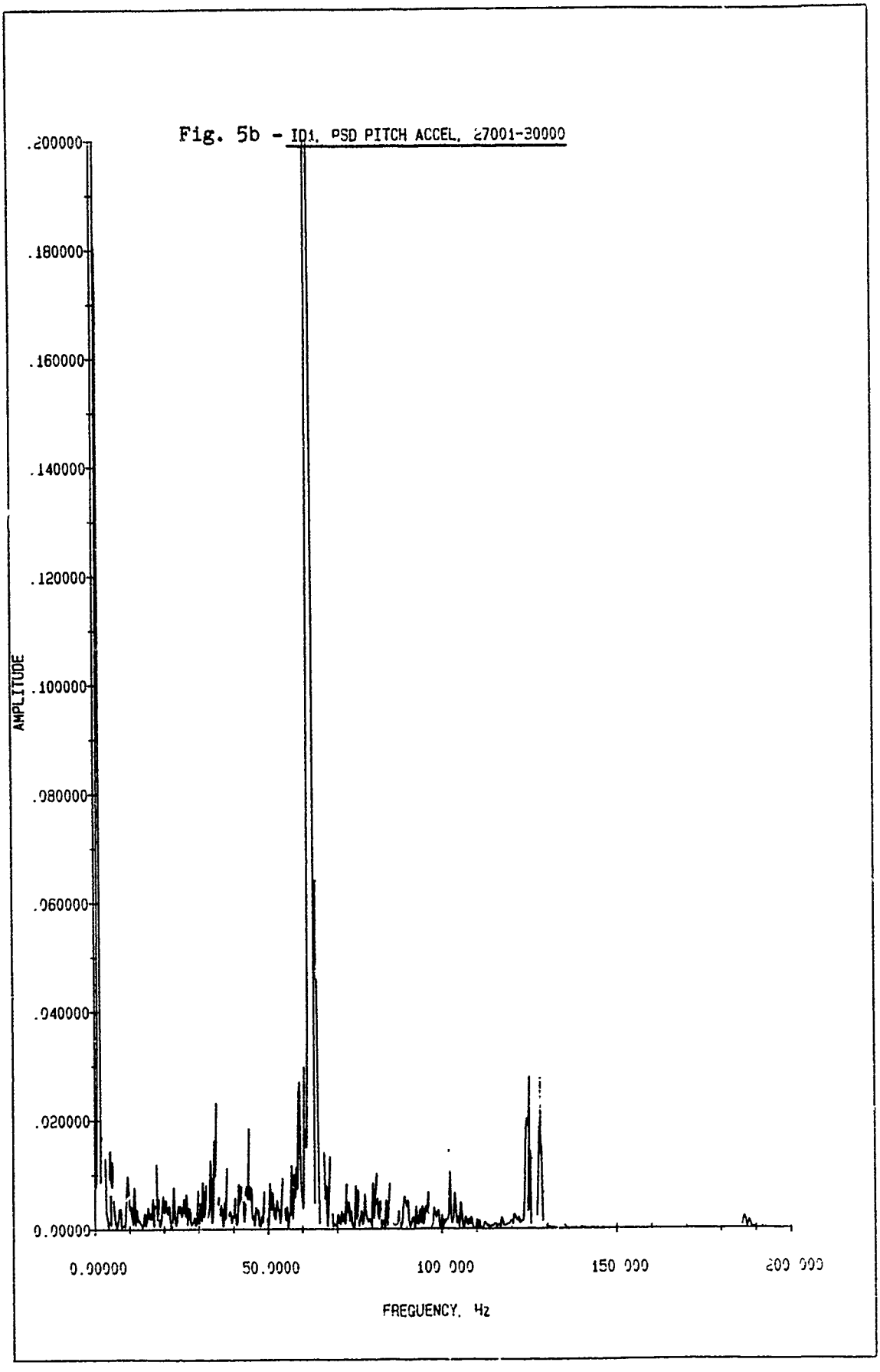

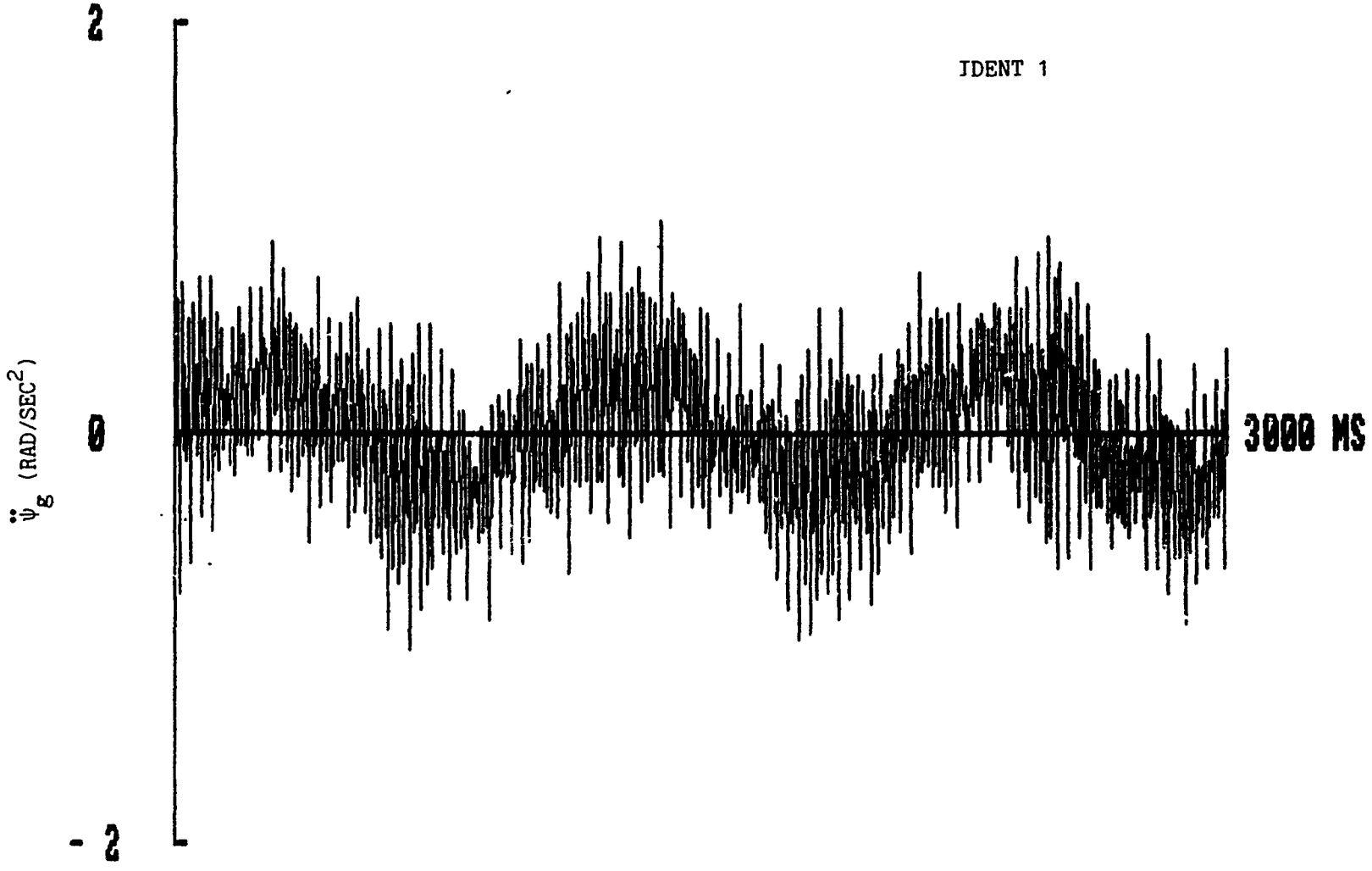

Fig. 5c - Simulated Pitch Acceleration

Fig. 6a - IDENT 1, ANGULAR ROLL ACCEL

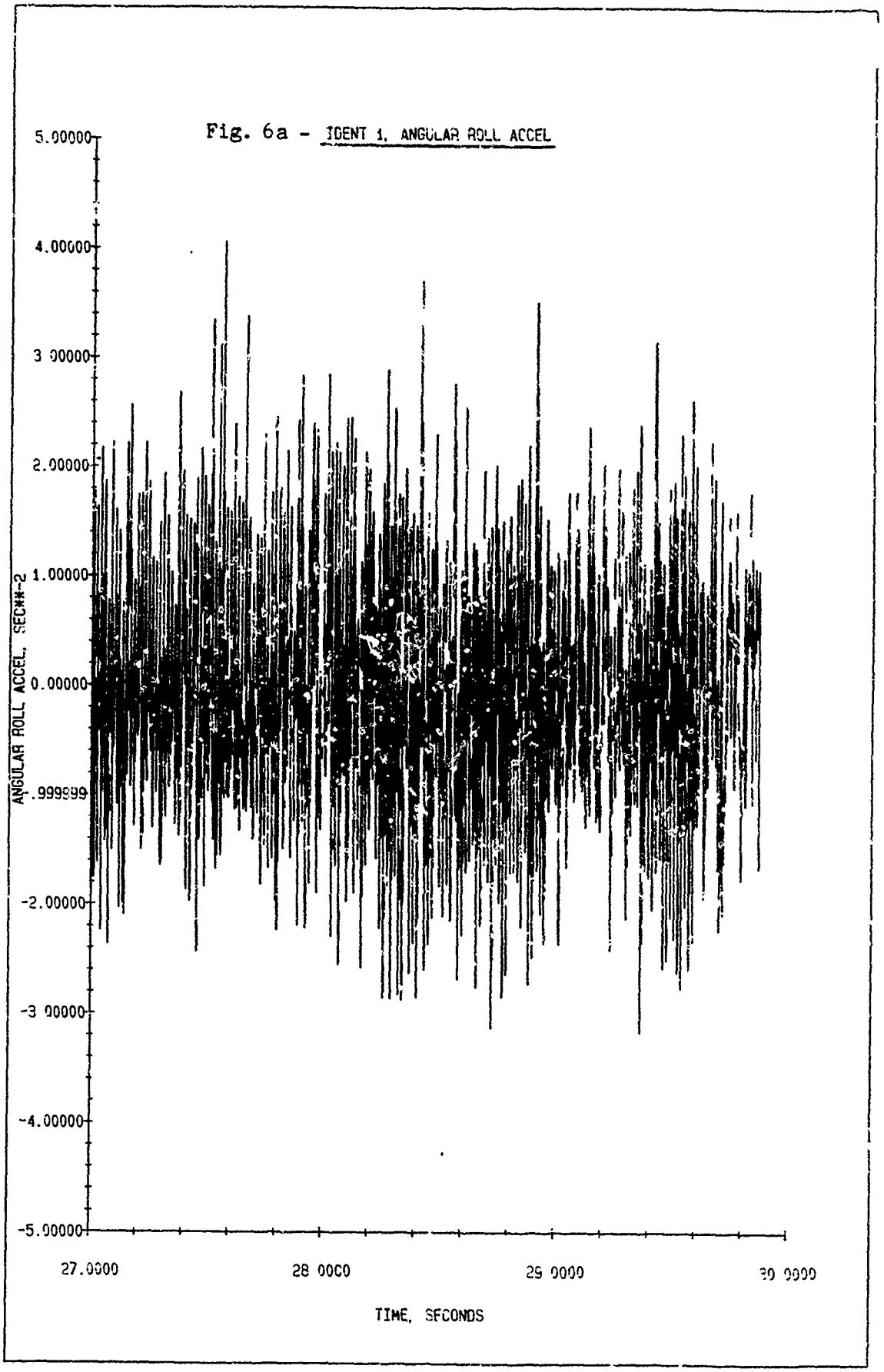

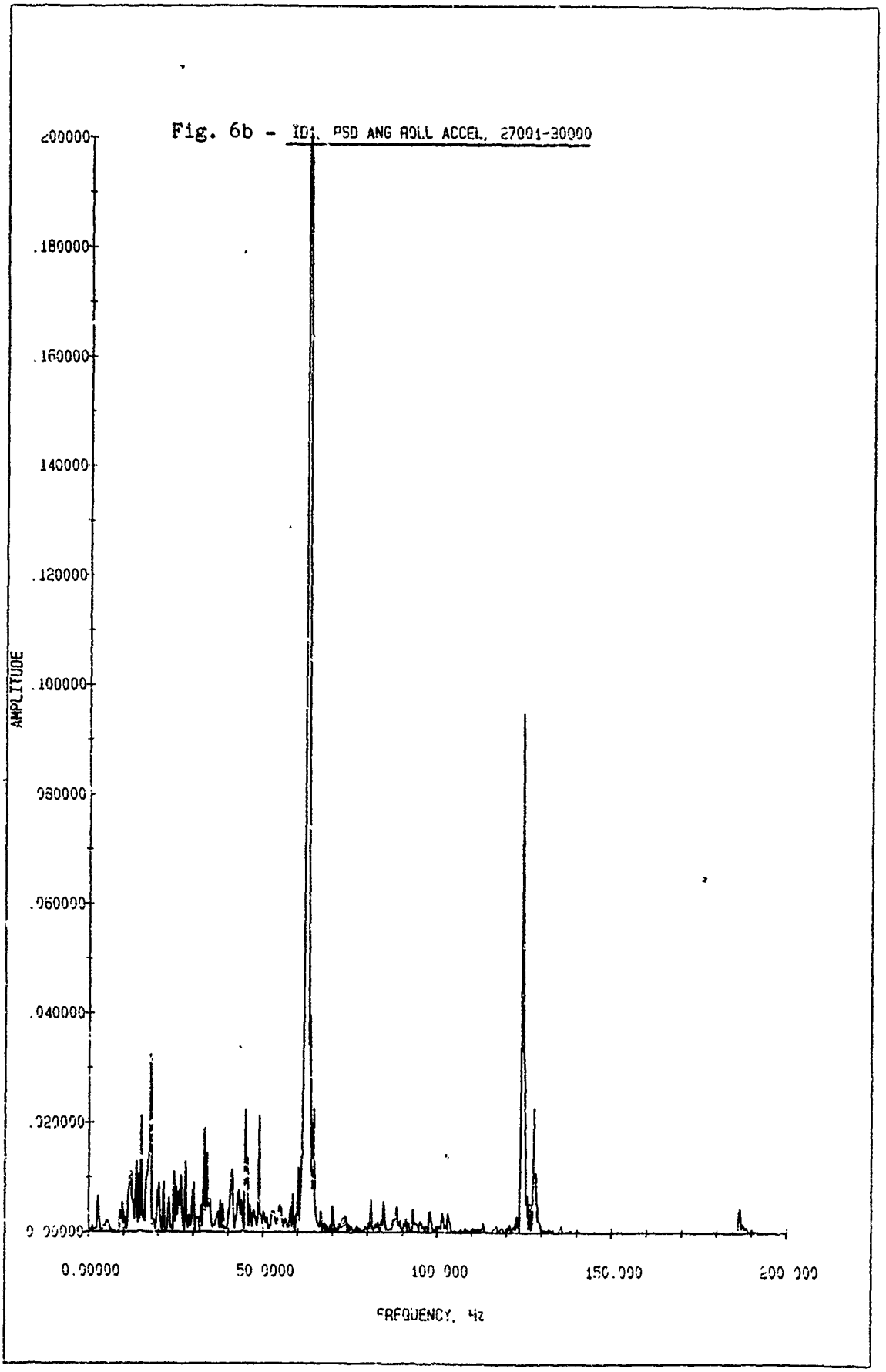
Fig. 6b - ID1. PSD ANG ROLL ACCEL. 27001-30000
.200000
.180000
.160000
.140000
.120000
.100000
.080000
.060000
.040000
.020000
0.00000
AMPLITUDE
0.00000
50.0000
100.000
150.000
200.000
FREQUENCY, Hz

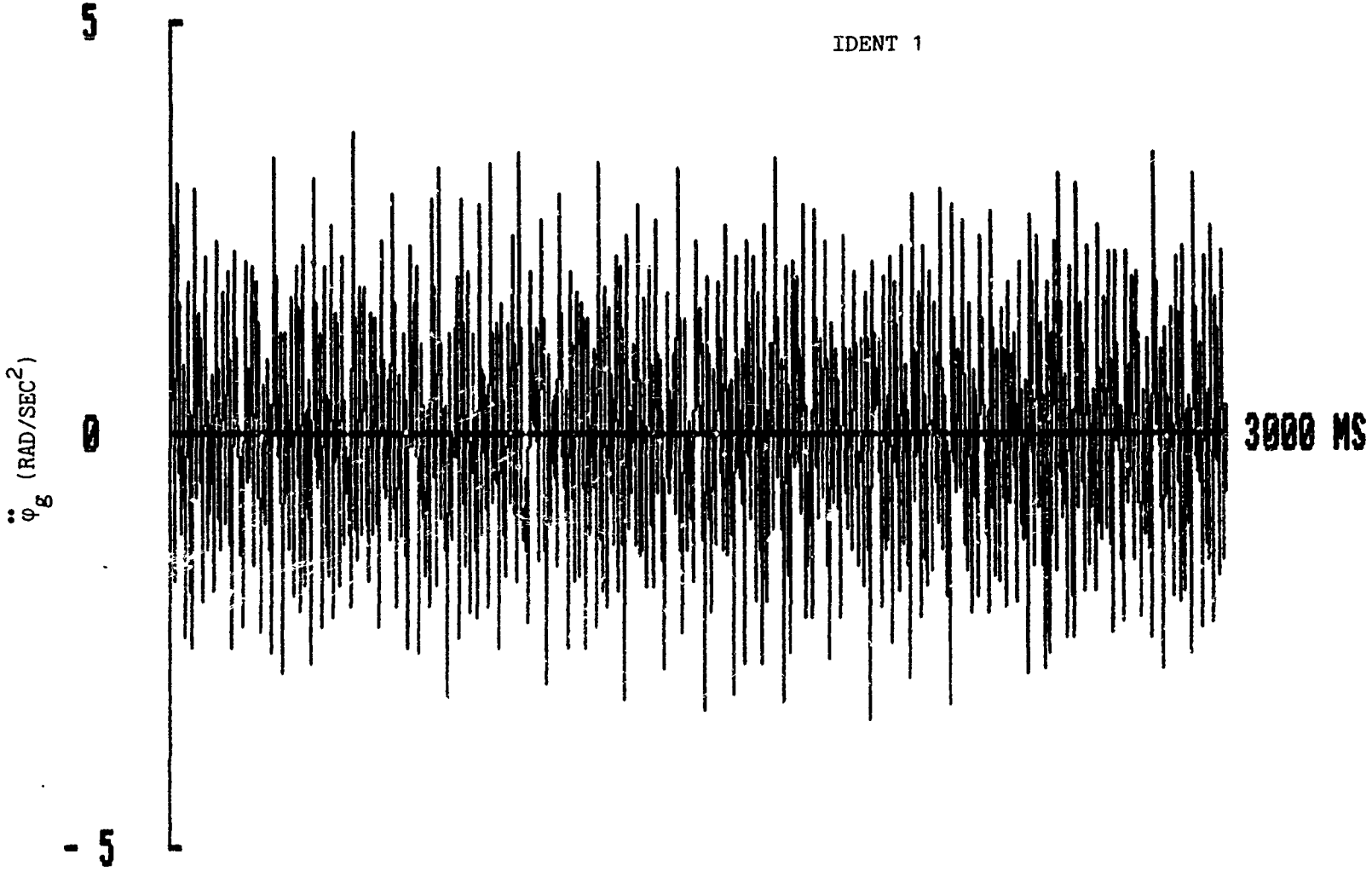

Fig. 6c - Simulated Roll Acceleration

Fig. 7a - IDENT 1, VERTICAL ACCEL

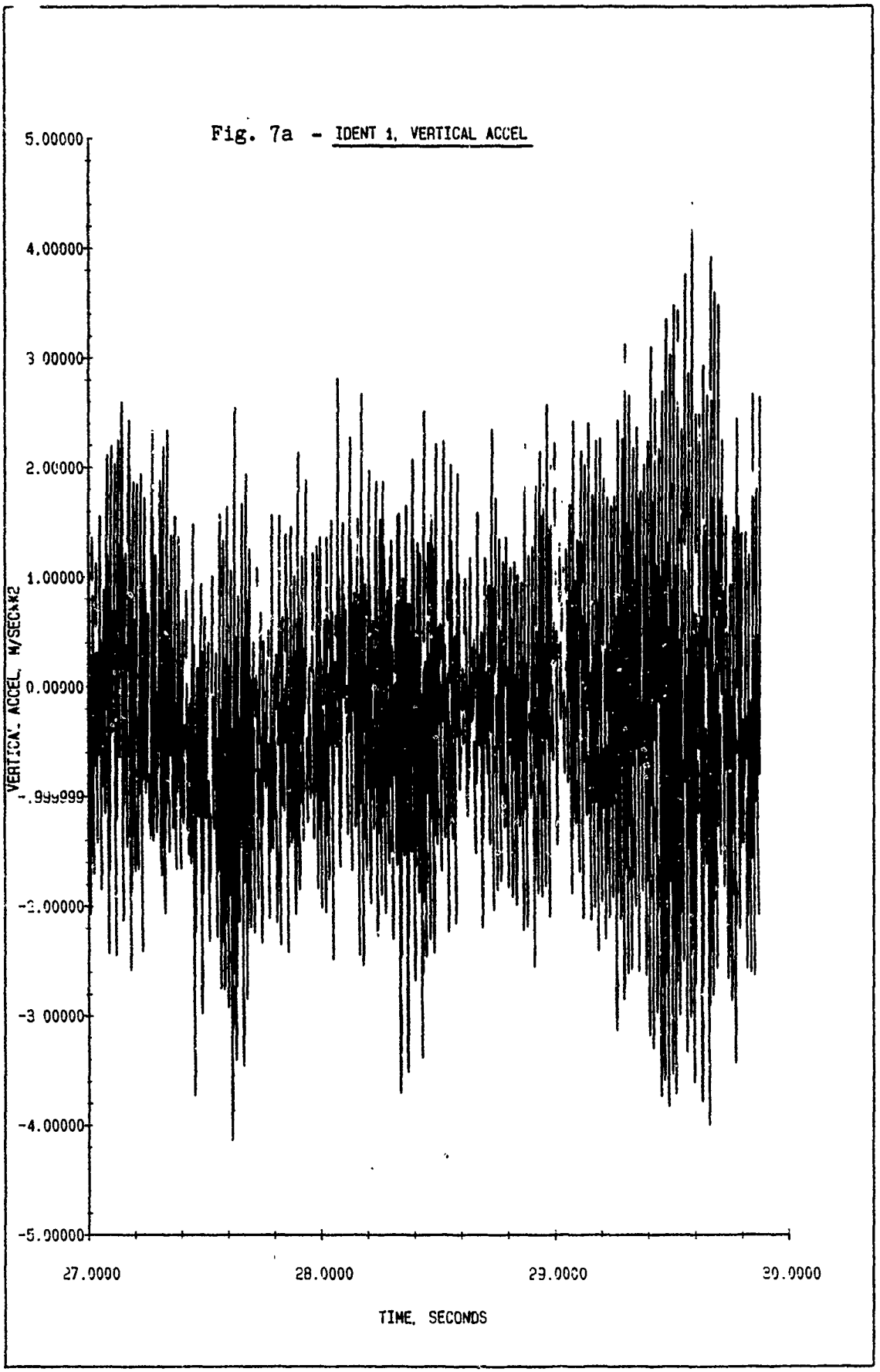

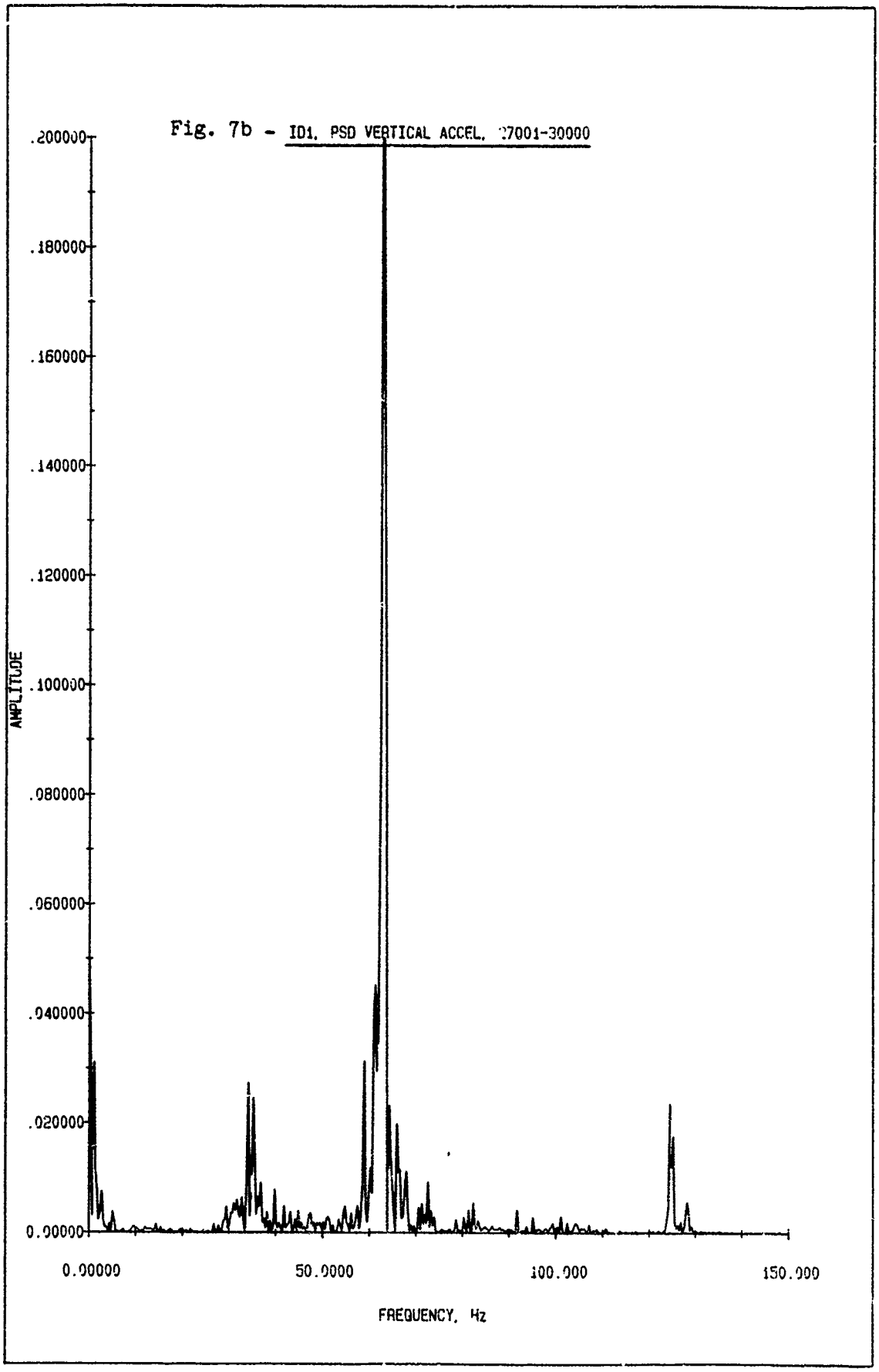
Fig. 7b - ID1, PSD VERTICAL ACCEL, 27001-30000
.200000
.180000
.160000
.140000
.120000
.100000
.080000
.060000
.040000
.020000
0.00000
AMPLITUDE
0.00000
50.0000
100.000
150.000
FREQUENCY, Hz

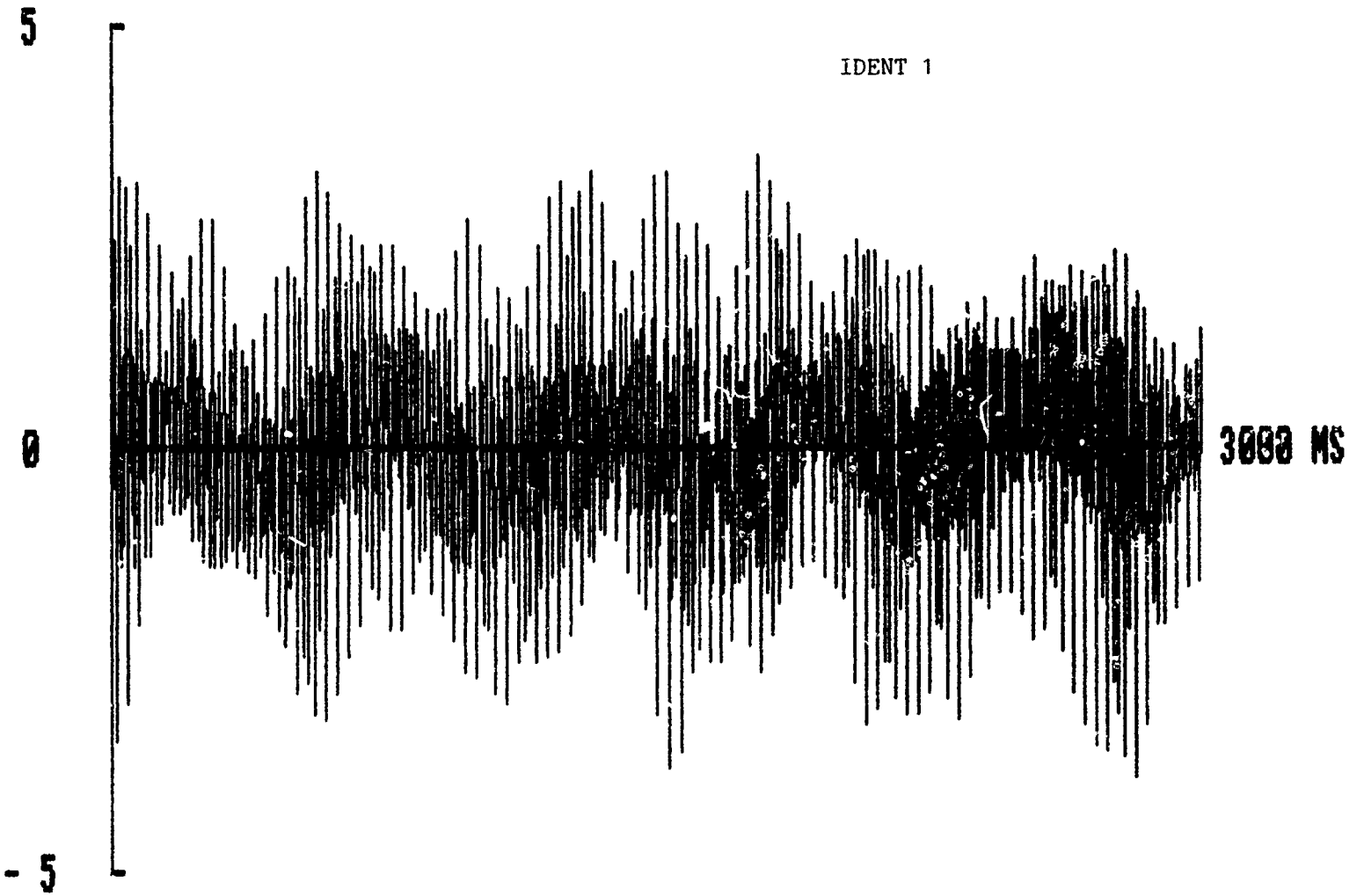

Fig. 7c - Simulated Vertical Acceleration

DYNACODE-G, with fixed time-step integration and without firing excitation, was exercised first for the purpose of demonstrating its ability to handle gun system response to a typical cycle of mount excitation (simulated vehicle motion) for each vehicle course considered. Sample output obtained for the Munson full course for vertical muzzle displacement, pitch, muzzle velocity and pitch rate are presented in Figs. 8 thru 11, respectively. Output for lateral muzzle displacement, yaw, muzzle velocity and yaw rate are presented in Figs. 12 thru 15, respectively.

Using the above version of DYNACODE-G, numerous runs were performed next to serve as baseline for establishing solution convergence of pertinent parameters as a function of integration step-size; a necessary investigation in the development of a variable time-step integration scheme, as will be discussed in the sequel.

Although not a pertinent part of the present study, it is noted that a Monte-Carlo routine, with equally weighted random number generator, could readily be introduced in this version of DYNACODE-G should the user desire to study the stochastic nature of gun system motion (due to vehicle motion) just prior to firing.

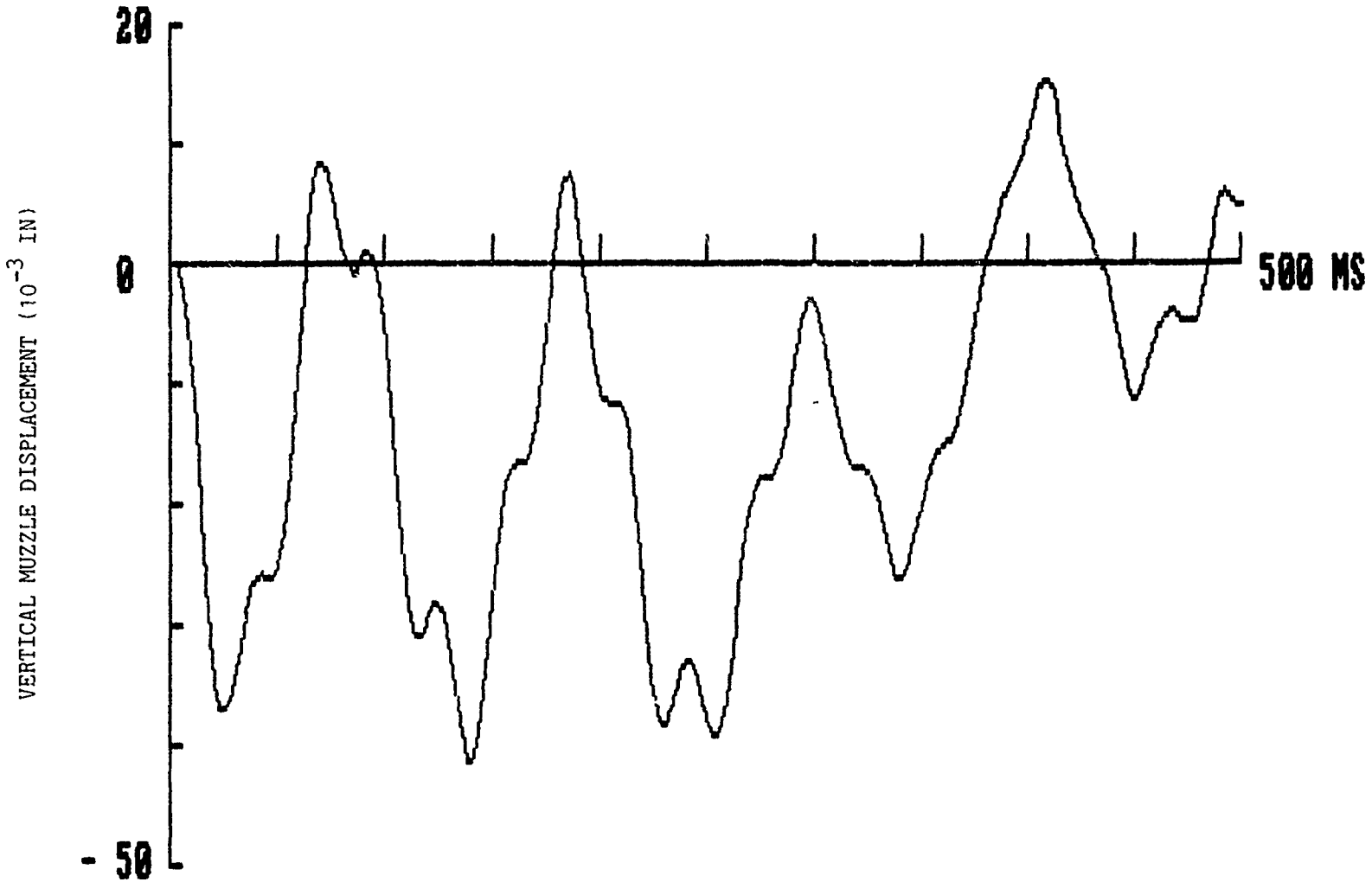

Fig. 8 - Vertical Muzzle Displacement on Munson Course

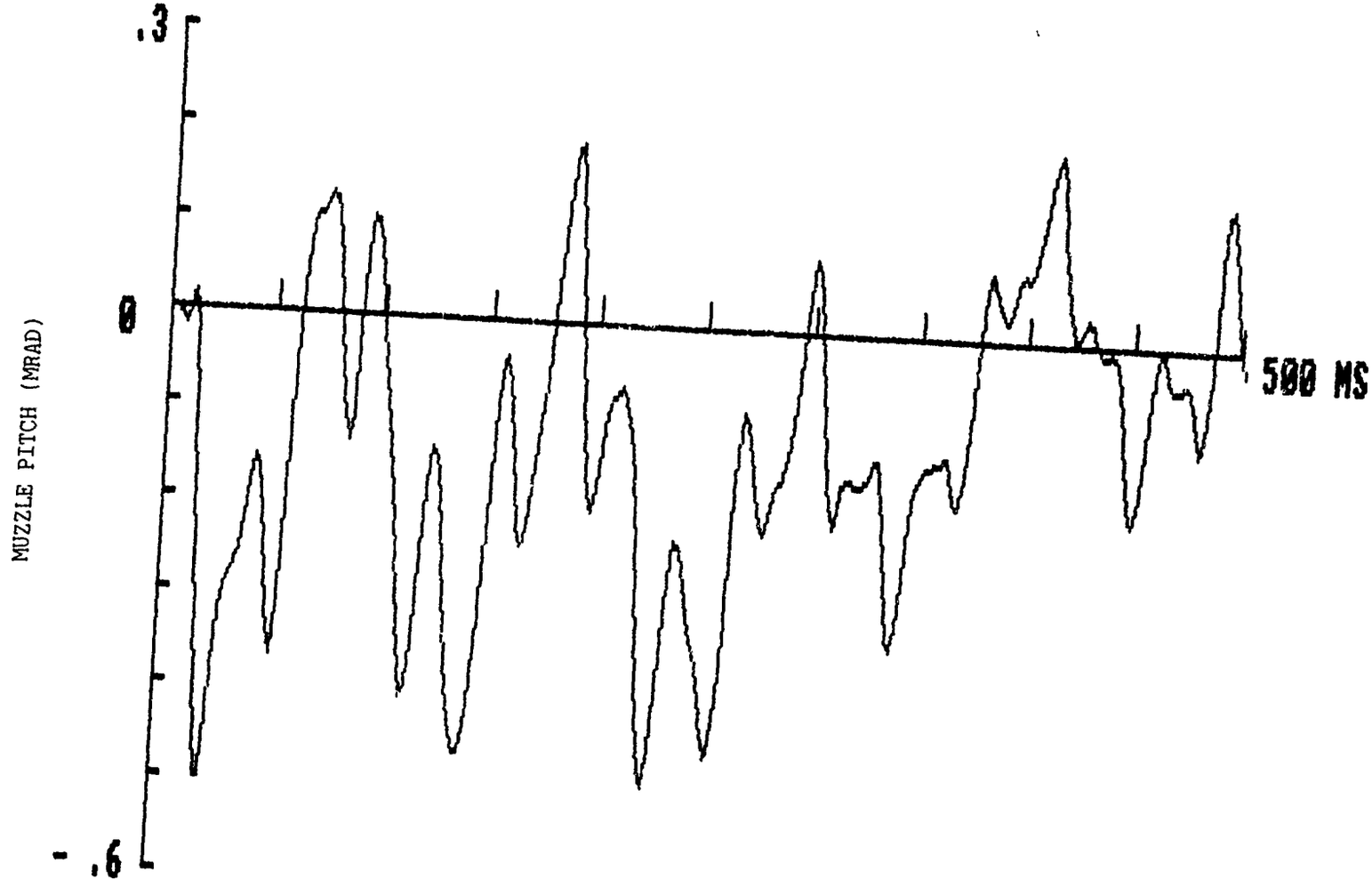

Fig. 9 - Muzzle Pitch on Munson Course

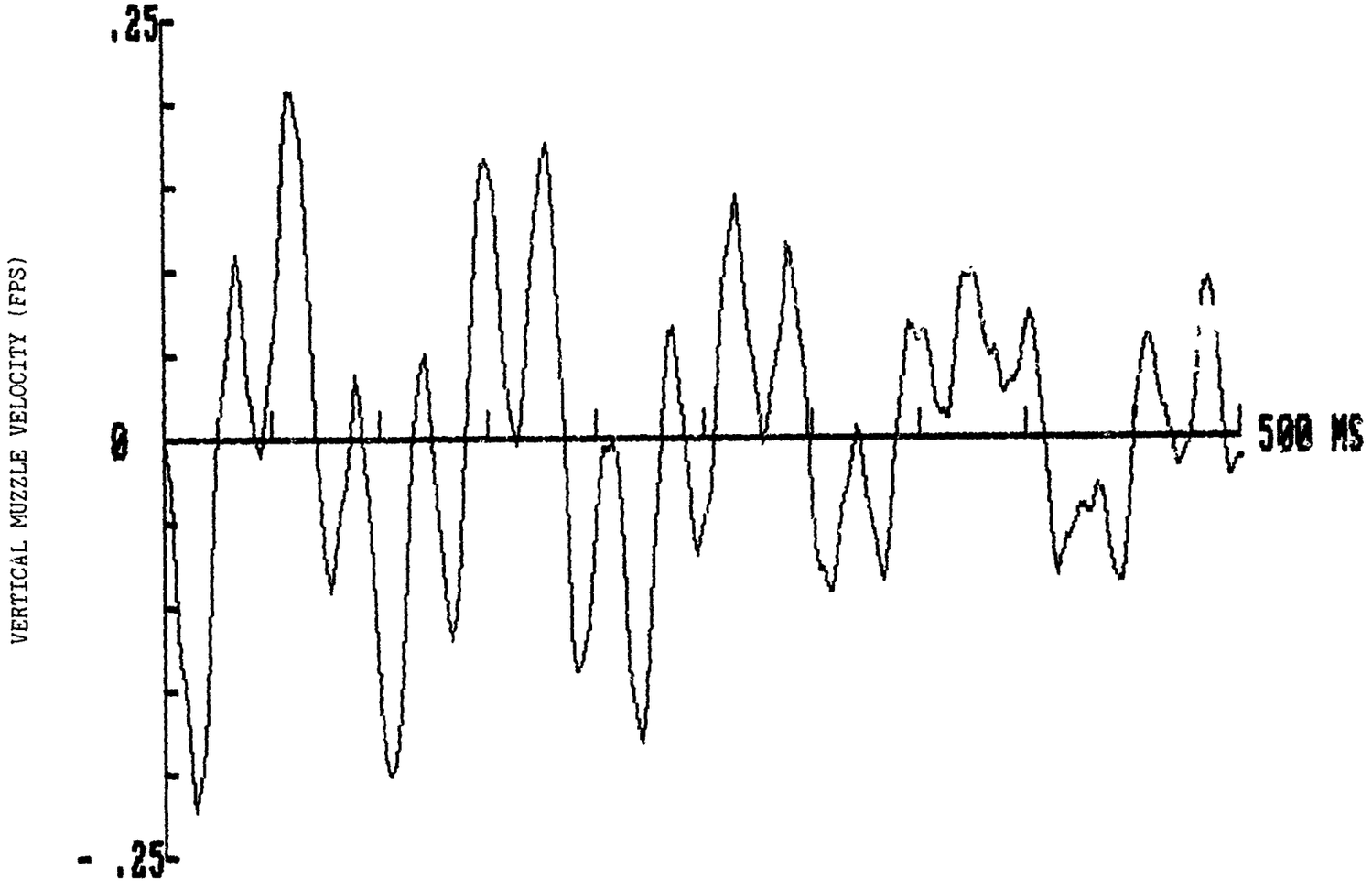

Fig. 10 - Vertical Muzzle Velocity on Munson Course

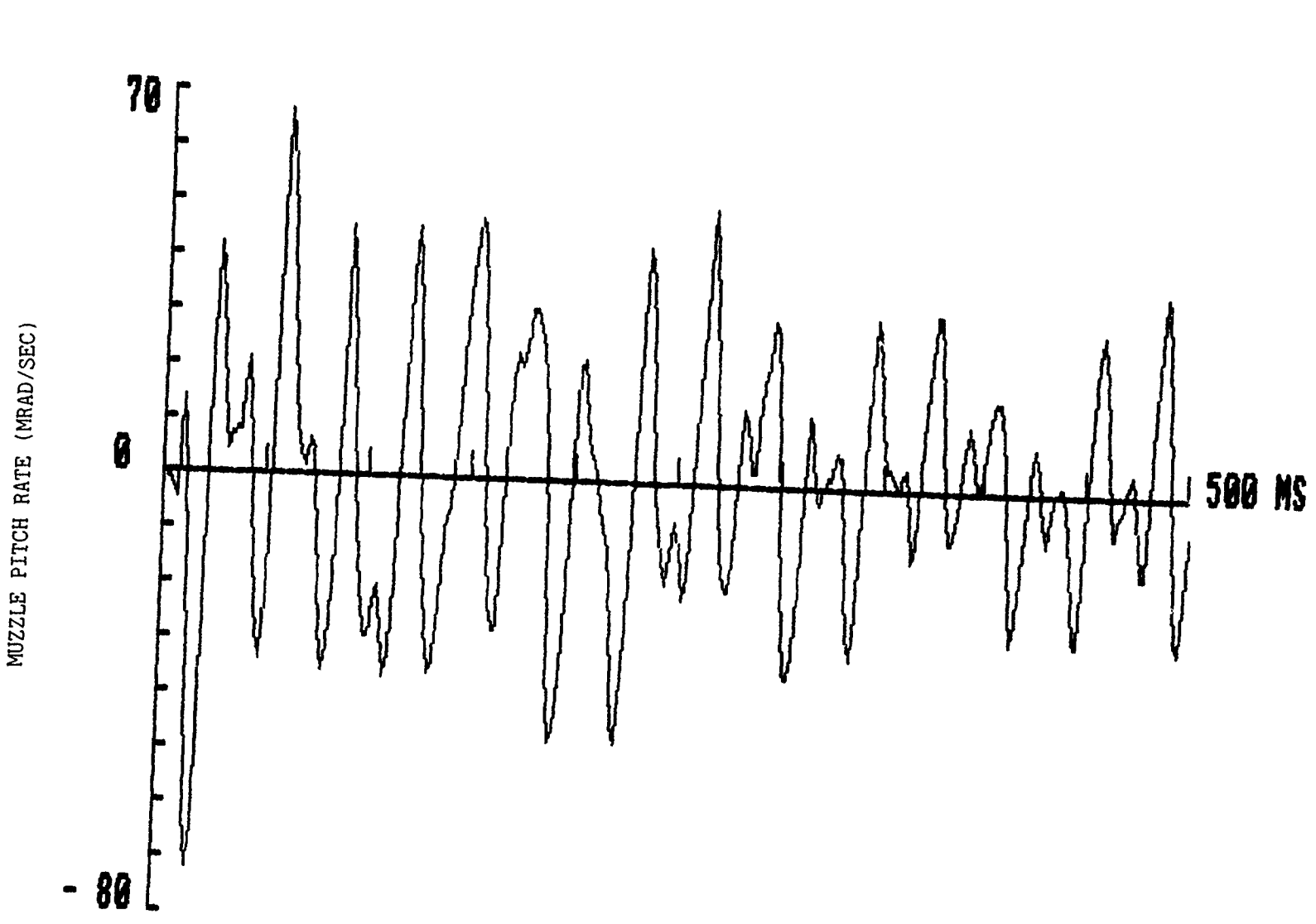

Fig. 11 - Muzzle Pitch Rate on Munson Course

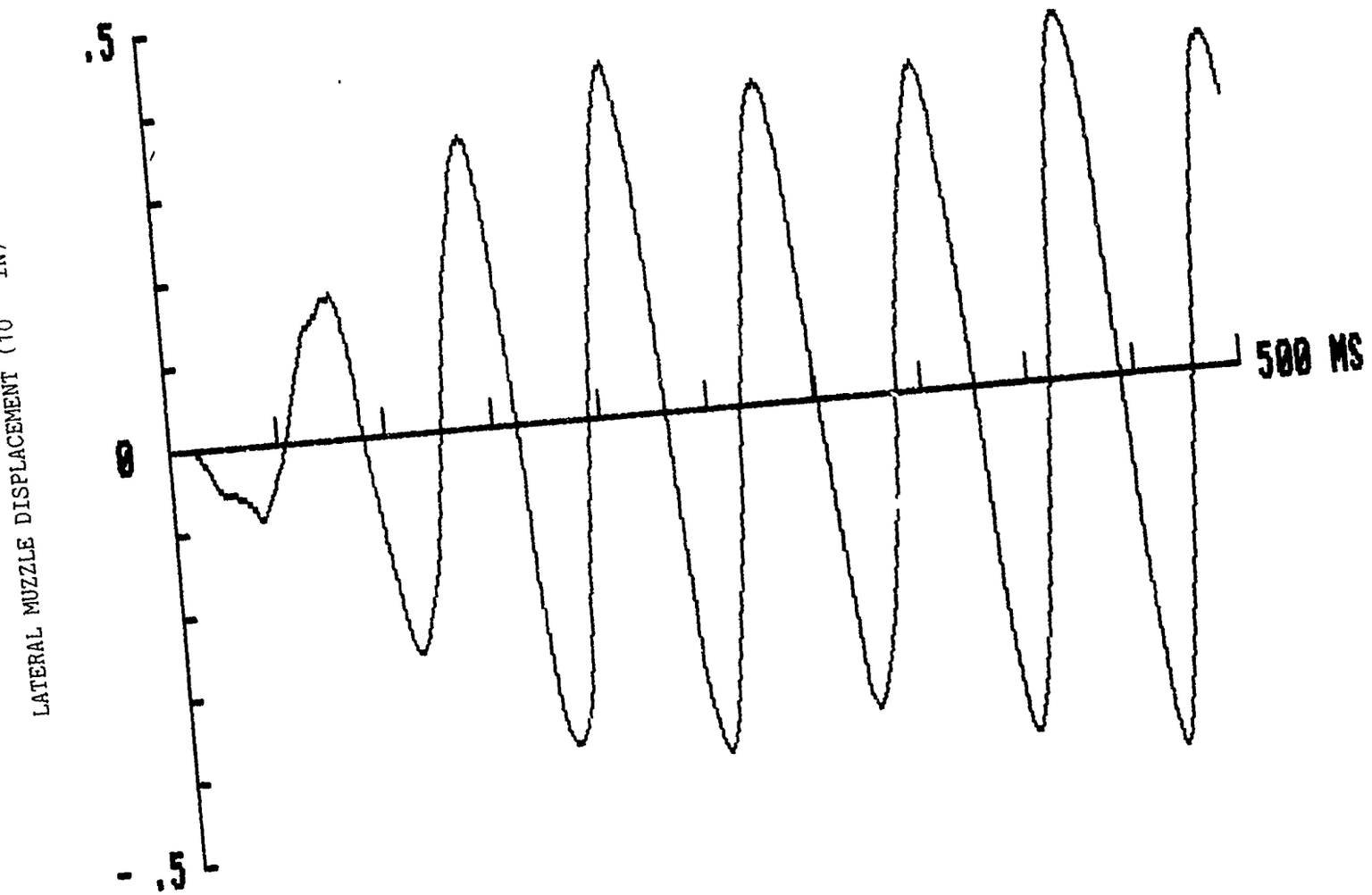

Fig. 12 - Lateral Muzzle Displacement on Munson Course

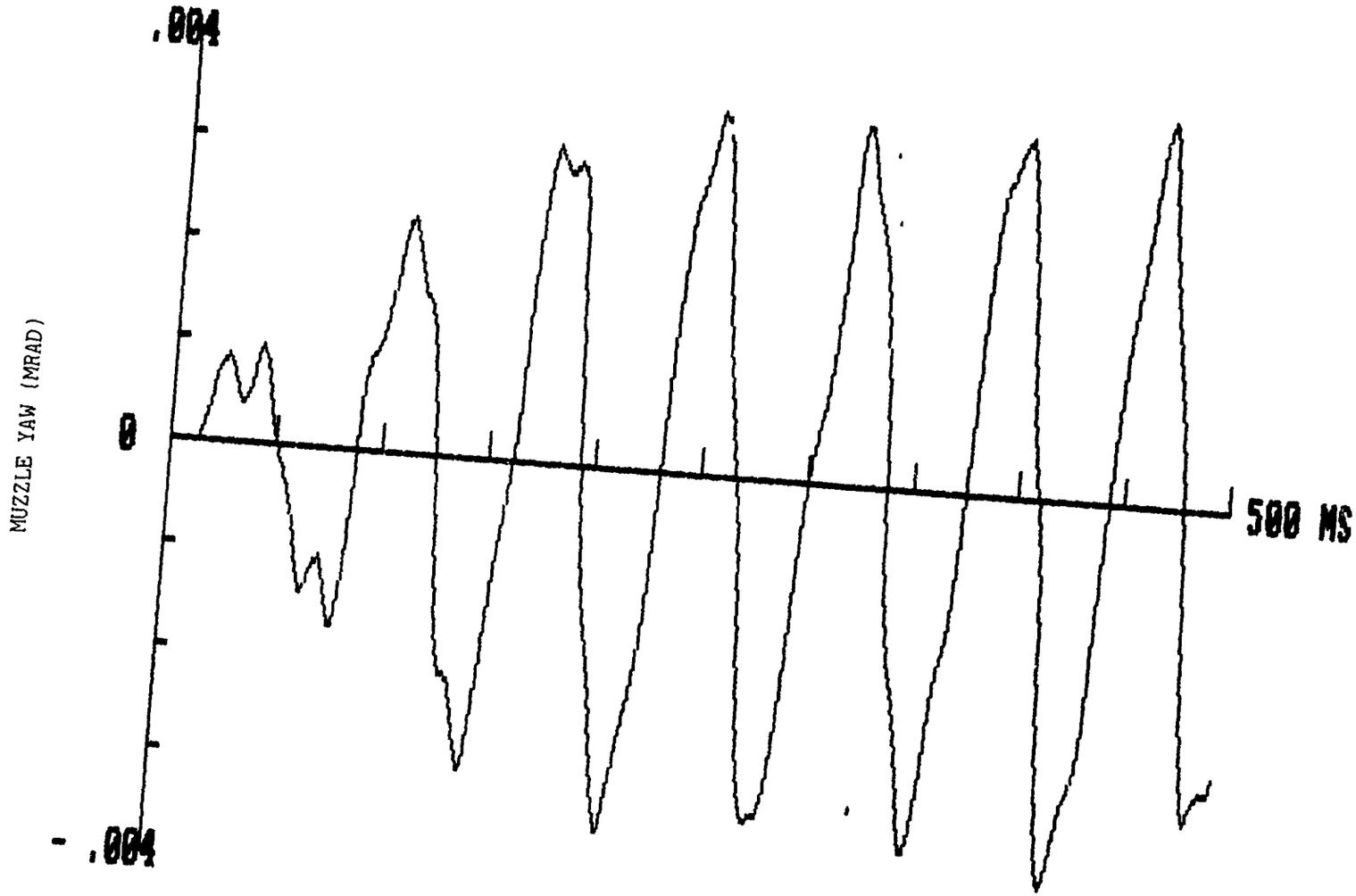

Fig. 13 - Muzzle Yaw on Munson Course

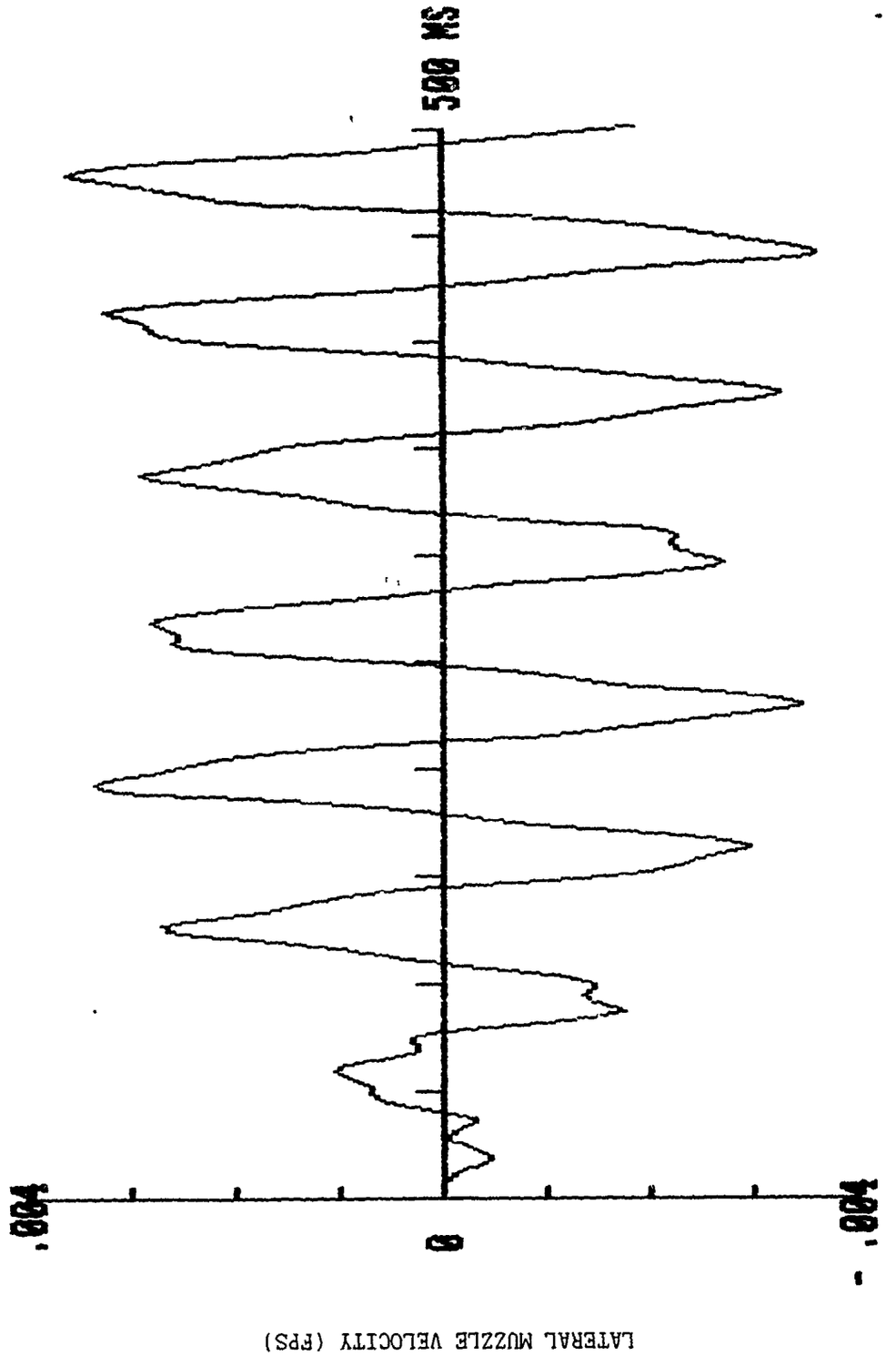

Fig. 14 - Lateral Muzzle Velocity on Munson Course

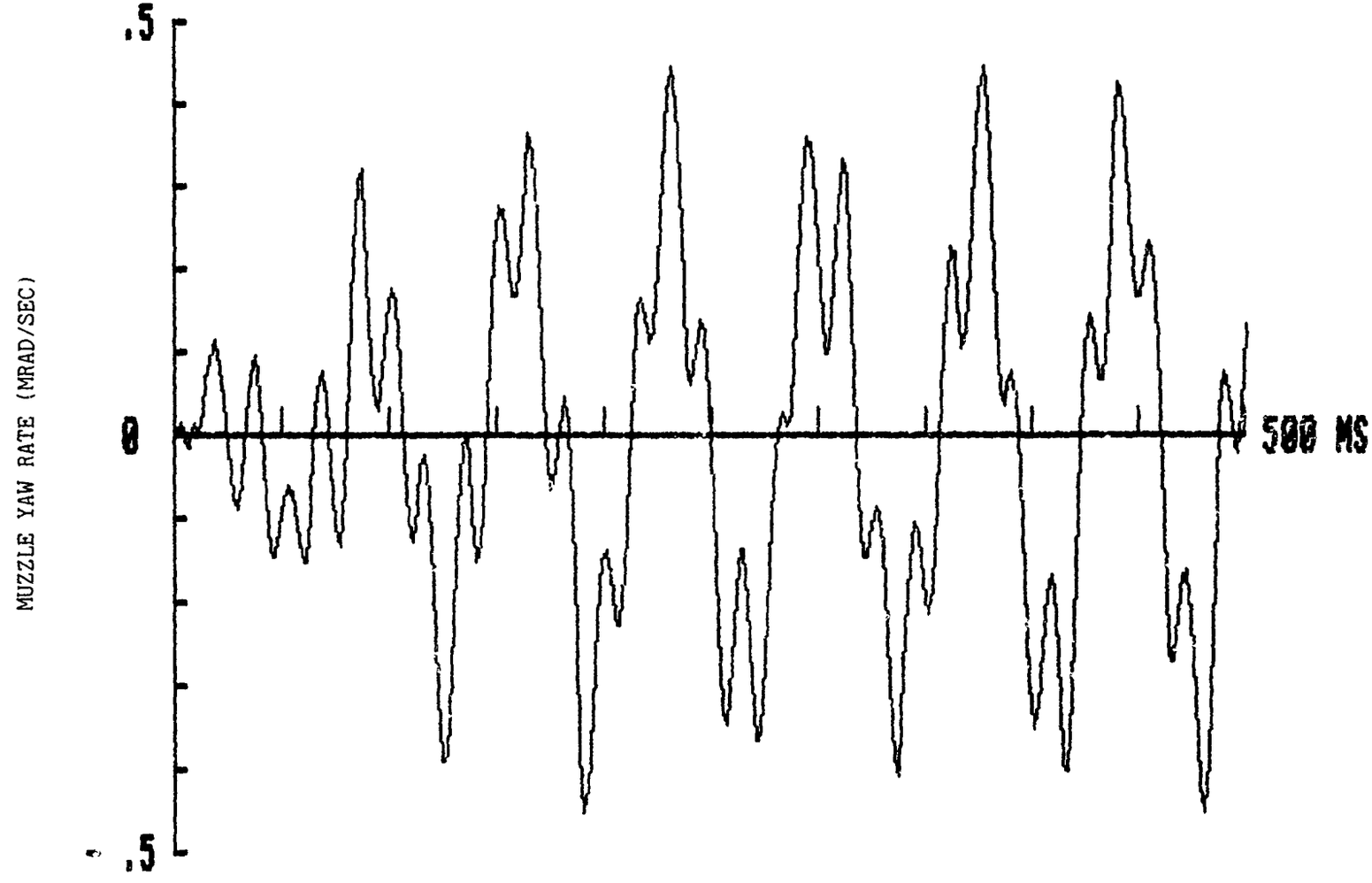

Fig. 15 - Muzzle Yaw Rate on Munson Course

4. VARIABLE TIME-STEP INTEGRATION

The fixed time-step, fourth order, Runge-Kutta integration scheme employed in DYNACODE-G is computationally efficient when treating gun system response to a single or simultaneously applied set of excitations. In general, the size of the time-step is keyed to the frequency content of the excitation -- the higher the frequency content, the smaller the required time-step for a convergent solution. However, when treating gun system response to a series of sequential excitations with intermittent time delays, the fixed time-step scheme is computationally inefficient, particularly in the time-delay regions where a far more coarse time-step would prove adequate. To handle such situations, whose scenario might consist, for example, of tracking gun tube muzzle motion during firing-on-the-move, followed by a prescribed delay before the next firing, computational efficiency dictates development of a variable time-step integration scheme.

Using the solution provided by DYNACODE-G with fixed time-step integration for gun system response to vehicle motion as baseline, it was found that velocity parameters are most sensitive to step-size variations, and, in particular, it was found that convergence of muzzle pitch-rate guarantees convergence of all other parameters at all other mass points; thereby providing an absolute error bound on the solution. Having identified a suitable parameter to establish convergence, namely muzzle pitch-rate, it remains to quantify an error estimate in choosing the step-size at a given time.

The error produced in the numerical solution of a first order, ordinary, differential equation using a fourth order Runge-Kutta integration scheme depends on the integration step size. Letting y_2 denote the solution obtained at time t^* using an integration step size of $2\,\Delta t$, and letting y_1 denote the corresponding solution at t^* obtained from two successive integrations of Δt each, the respective solution errors are

$$\varepsilon_2 = \frac{16}{15} |y_2 - y_1| \quad \text{and} \quad \varepsilon_1 = \frac{1}{16} \varepsilon_2 .$$

ε_2 and ε_1 serve as upper and lower error bounds which may be used in an automated process to determine when to increase or decrease the step size, Δt.

Since the computation of ε_2 requires calculation of both y_1 and y_2, an improved numerical solution is obtained as a by-product of this computation through the use of the Richardson estimator at t^*, namely,

$$y^* = \frac{1}{15} (16\, y_1 - y_2) .$$

It is noted that the error in the Richardson estimator is a full order of magnitude smaller than the corresponding error in y_1.

Based on the above considerations, the fixed time-step integration scheme within DYNACODE-G has been replaced with an automated variable time-step routine which employs the following logic at each integration step:

1. Starting at time t, two successive integrations of step size Δt each are performed on the generalized coordinates and velocities to determine their values at time $t + 2\Delta t$.

2. Starting again at time t, but with a step size of $2\Delta t$, the generalized coordinates and velocities are again determined at $t + 2\Delta t$.

3. The Richardson estimators for generalized coordinates and velocities are formed at $t + 2\Delta t$ using the values computed in 1 and 2. These estimators serve as solution at $t + 2\Delta t$, as well as initial conditions for the next integration.

4. Δt is determined for the next integration by forming upper and lower error bounds on muzzle pitch-rate and comparing these values against an acceptable input error, ε, as follows:

   If $\varepsilon_1 > \varepsilon$, Δt is replaced by $\Delta t/2$

   If $\varepsilon_2 < \varepsilon$, Δt is replaced by $2\Delta t$

   If $\varepsilon_1 < \varepsilon < \varepsilon_2$, Δt remains unchanged.

Although the variable time-step scheme described above requires one and a half times as many calculations at each step as does the fixed time-step scheme, comparison runs show that convergence to machine accuracy is achieved with an average integration step which is sixteen times larger than the fixed time-step. Relaxation of the acceptable error, ε, would of course allow further improvement in run time.

5. EXTERNAL FIRING SIGNAL

In order to optimize the effectiveness of burst-mode fire, the timing between rounds of a burst is keyed to pertinent muzzle motion parameters falling within an acceptable "window" of values. Specifically, DYNACODE-G with mount excitation to accommodate firing-on-the-move (as described in Section 3) and variable time-step integration (as described in Section 4) was modified to track muzzle displacement and linear and angular velocities subsequent to shot-exit of each round of a burst. At each instant these quantities are compared with acceptable predetermined "window" values. An external firing signal is then coupled, at the user's option, with either of two control modes -- a vertical-plane "window" of values (without regard to horizontal-plane motion) and combined vertical and horizontal-plane "windows" which must be satisfied simultaneously. A schematic of program events with external firing signal control is depicted in Fig. 16.

Referring to Fig. 16, the program begins by initiating vehicle motion at t=0 and tracking muzzle response in Region 1. At a preset (but variable) time, t_s, in the vehicle motion cycle, a comparison of muzzle motion parameters versus acceptable "window" values is initiated. This comparison continues, defining Region 2, until muzzle motion satisfies "window" values. The program then accepts a firing signal at t_f and tracks subsequent muzzle motion during the recoil/counter-recoil cycle in Region 3. The program continues to track muzzle motion in Region 4, which accommodates the prescribed time required to physically load the next round. The combined time elapsed in Regions 3 and 4 defines the minimum time required to fire the next round, without regard to satisfying firing "windows". Regions 2, 3 and 4 are then sequentially repeated, depending on the number of rounds in the burst. The program stops when the final round of the burst exits the muzzle.

It is noted that varying t_s allows the user to study the effect of firing at different times in the vehicle motion cycle. As previously noted in Section 3, a Monte-Carlo routine, with equally weighted random number generator, could be introduced to specify t_s on a probabilistic basis.

DYNACODE-G, with simulated vehicle motion for the Munson full course and as herein modified, was exercised for the purpose of comparing three three-round bursts fired from the 75mm ADMAG, with and without firing control signals. For the purposes of this illustrative comparison, each three-round burst was arbitrarily initiated with t_s, and consequently t_f, set equal to zero. Vertical-plane "window" values were arbitrarily set at $|y| \leq .005$ in, $|v_y| \leq .05$ fps and $|\omega_z| \leq .05$ rad/sec. Horizontal-plane "window" values were arbitrarily set at $|z| \leq .01$ in, $|v_z| \leq .01$ fps and $|\omega_y| \leq .01$ rad/sec. In addition, load time was arbitrarily set such that the minimum combined time to cycle and load is 1 sec. The user may of course vary t_s, "window" values and load time according to specific needs.

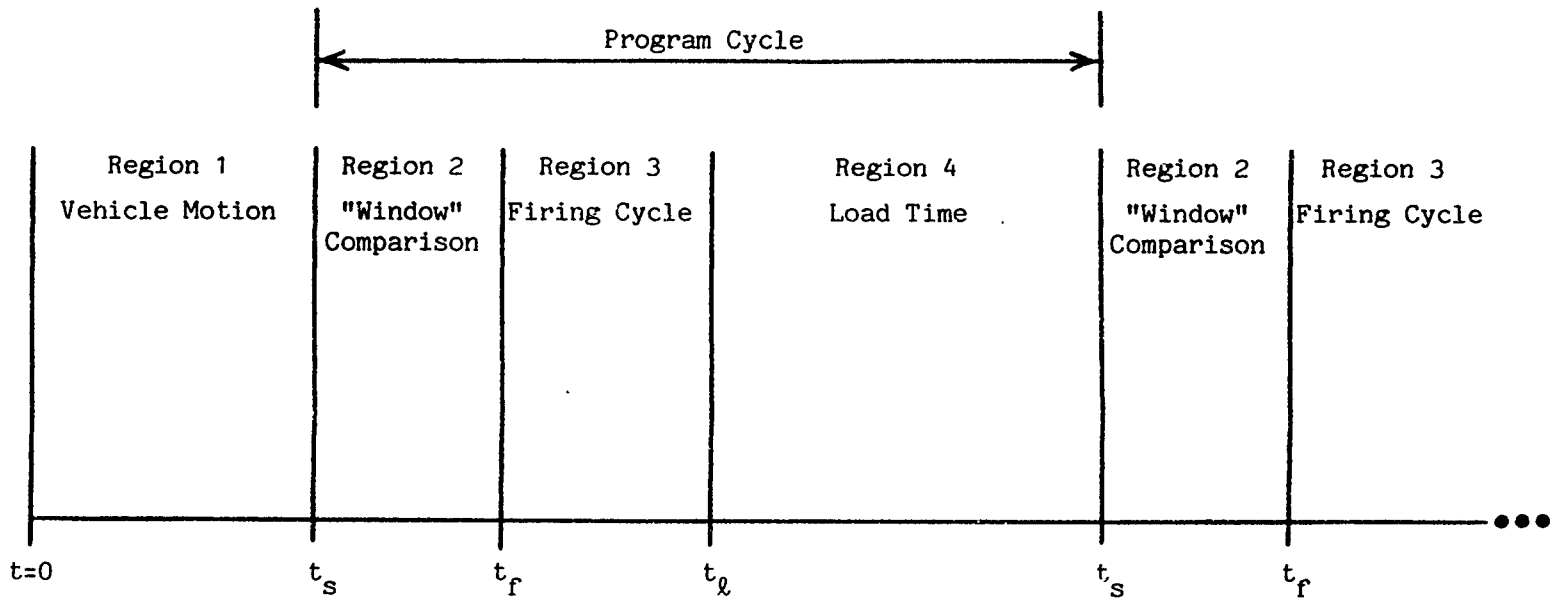

Fig. 16 - Schematic of Program Events for Controlled Burst-Mode Fire

Time-histories of vertical muzzle displacement, velocity and pitch rate are presented graphically in Figs. 17 thru 19 for a three-round burst without firing control signal, in Figs. 20 thru 22 with a vertical-plane "window" and in Figs. 23 thru 25 with combined vertical and horizontal-plane "windows". Corresponding time-histories of lateral muzzle displacement, velocity and yaw rate are presented graphically in Figs. 26 thru 28 for the three-round burst without firing control signal, in Figs. 29 thru 31 with a vertical-plane "window" and in Figs. 32 thru 34 with combined vertical and horizontal-plane "windows". In addition, a summary of pertinent muzzle motion parameters at shot-exit of each round of each burst is presented for comparison purposes in Table III.

As may be seen from the figures and comparisons presented, it is not readily obvious that requiring individual muzzle motion parameters prior to firing be bounded within acceptable "window" values guarantees optimal muzzle motion at shot-exit, particularly when firing on a moving vehicle. The concept of a firing "window" indeed seems plausible; however, it is not yet known which parameters or combinations require bounding. In addition, it is rather obvious that when firing-on-the-move, consideration must also be given to the nature of vehicle motion, the relative timing of the firing signal and phase relations between muzzle motion and vehicle motion prior to firing.

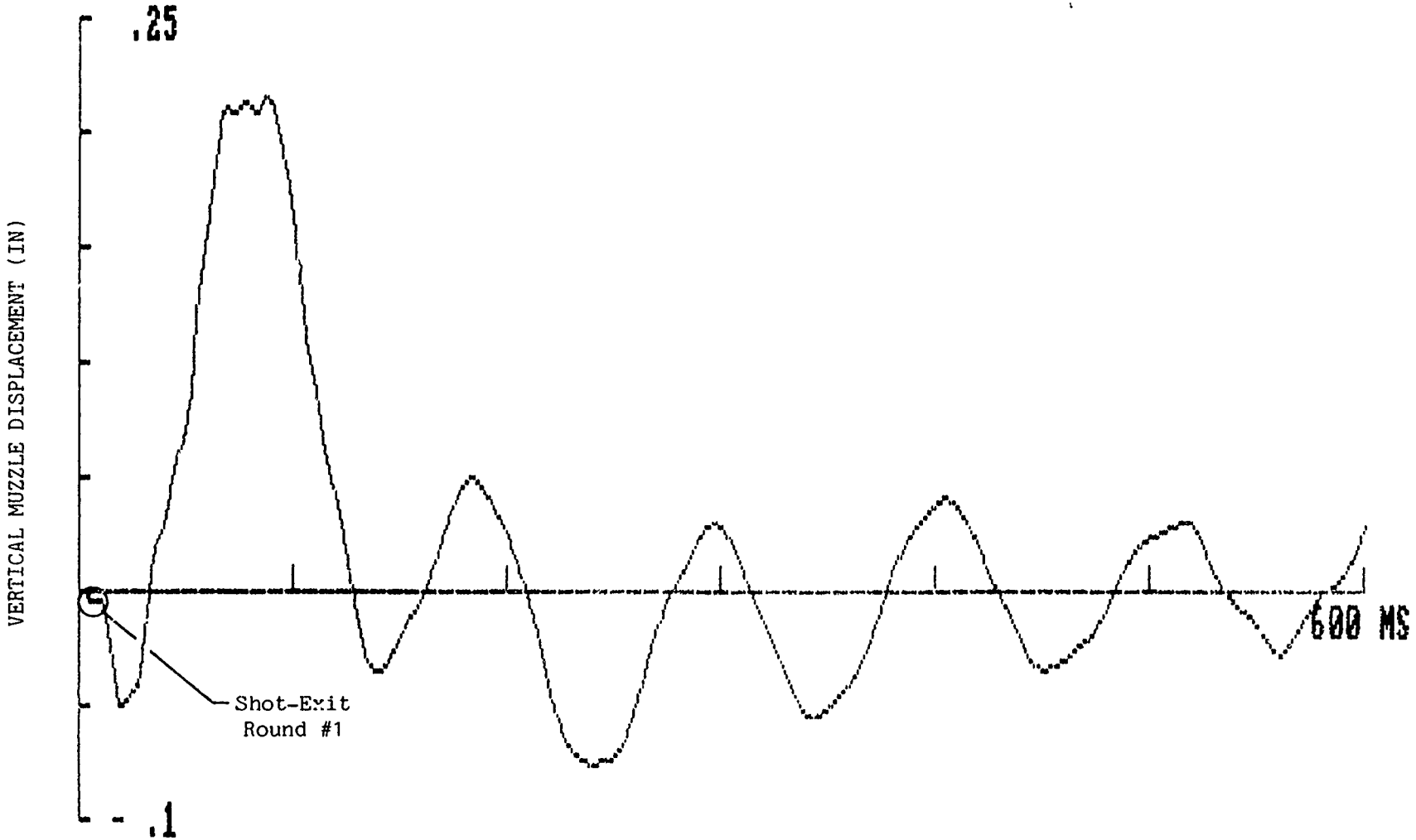

Fig. 17 - Vertical Muzzle Displacement for Three-Round Burst Without Firing Control Signal

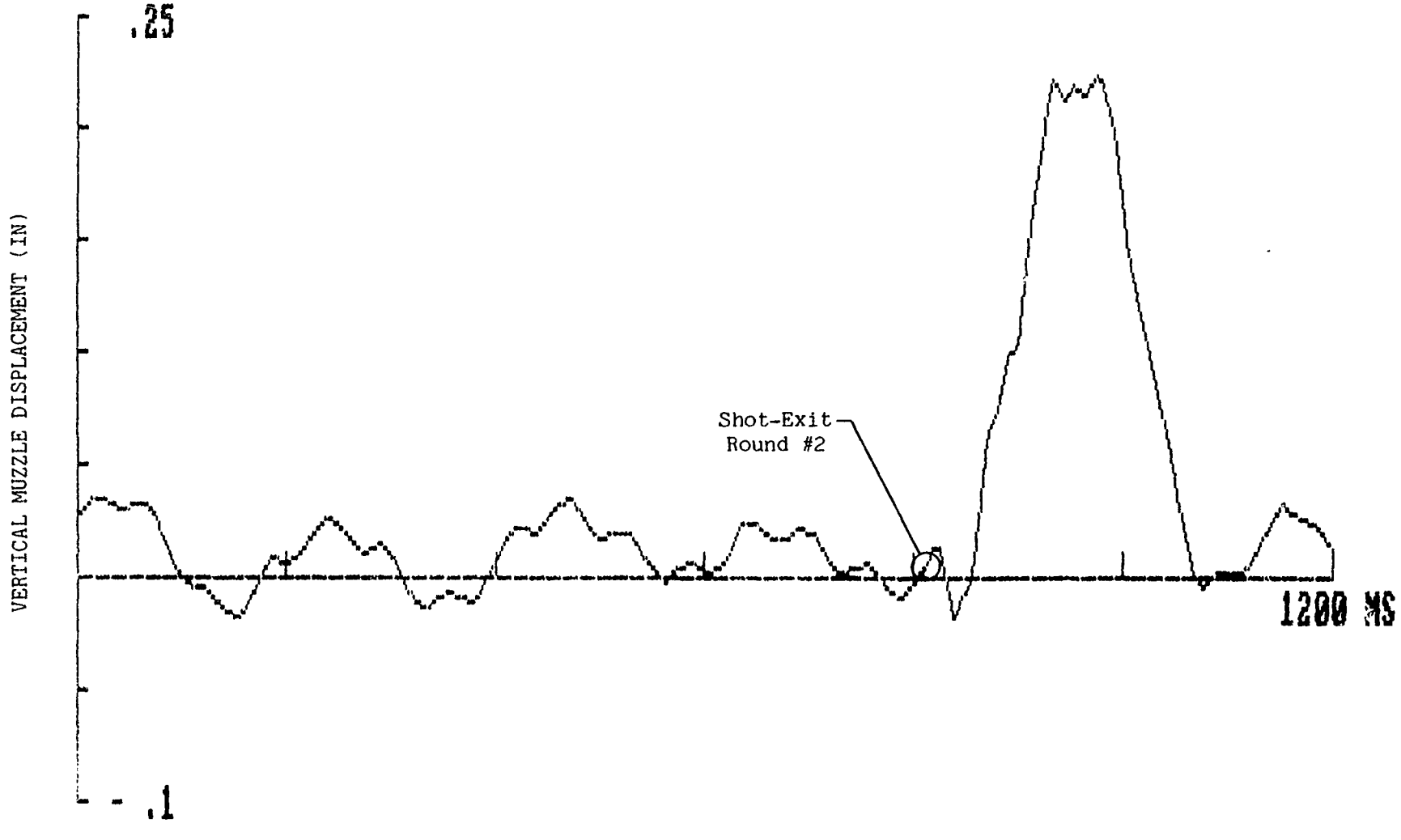
.25
VERTICAL MUZZLE DISPLACEMENT (IN)
Shot-Exit
Round #2
1200 MS
- .1

Fig. 17 (Cont'd.)

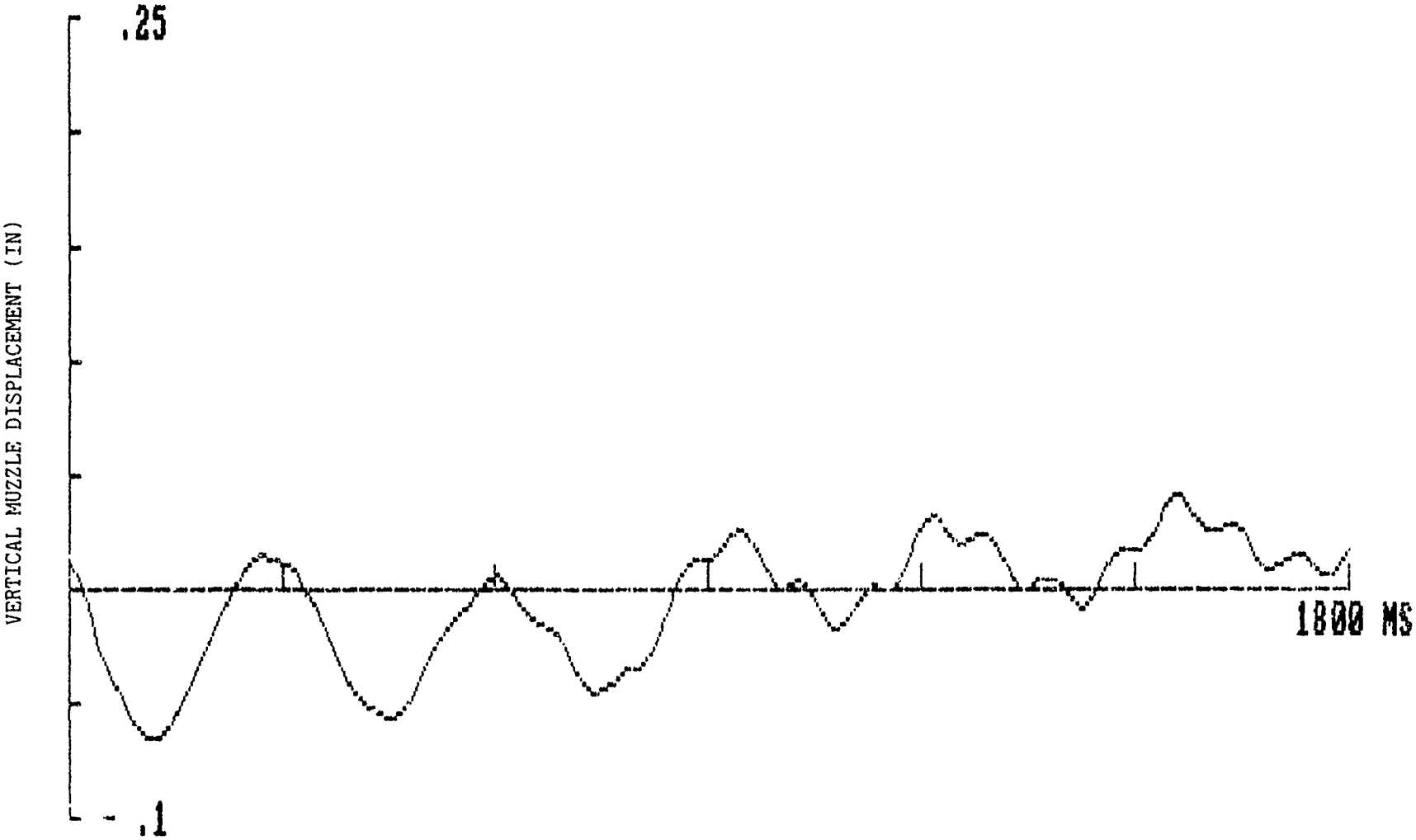

Fig. 17 (Cont'd.)

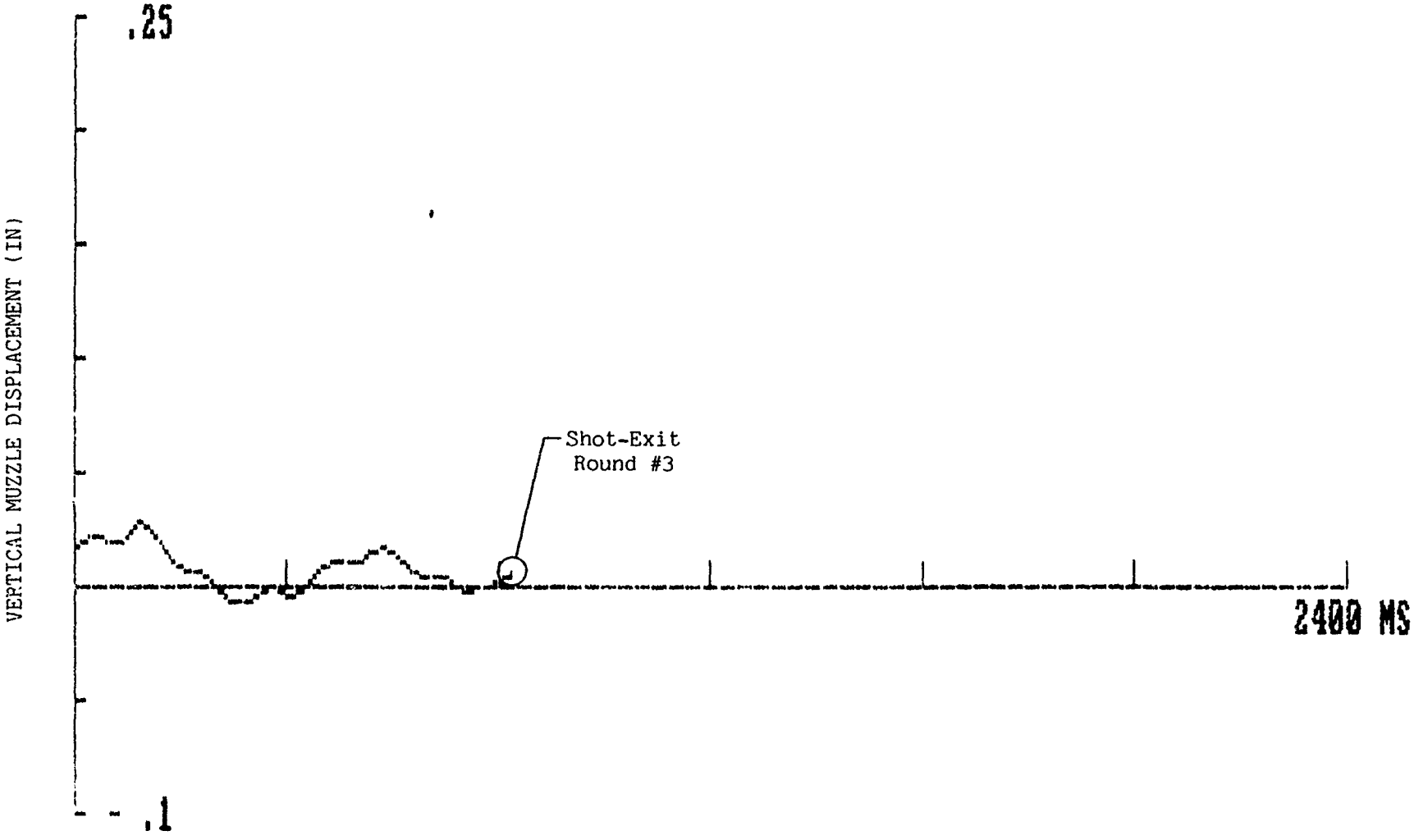
.25
VERTICAL MUZZLE DISPLACEMENT (IN)
Shot-Exit
Round #3
2400 MS
- .1

Fig. 17 - (Cont'd.)

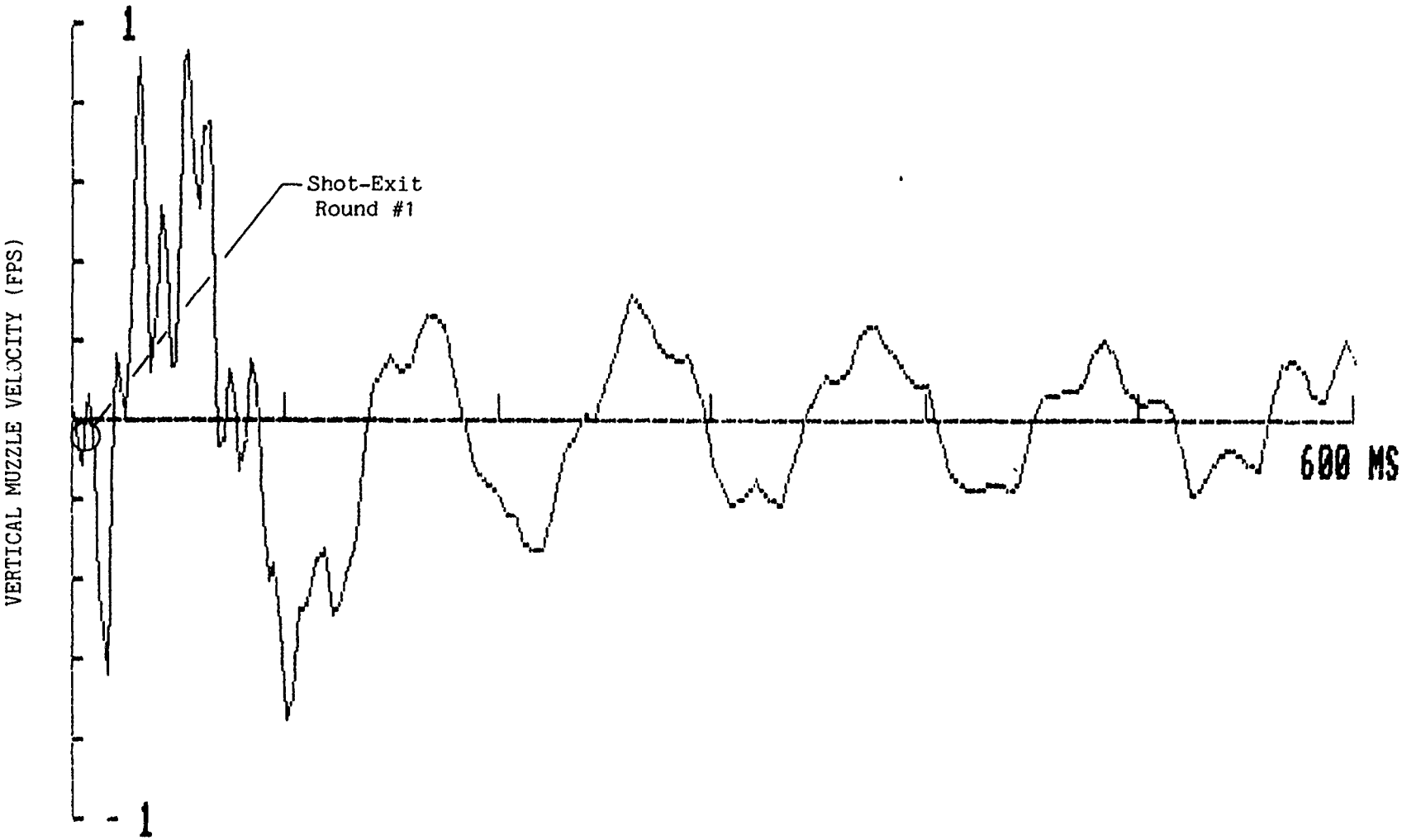

Fig. 18 - Vertical Muzzle Velocity for Three-Round Burst Without Firing Control Signal

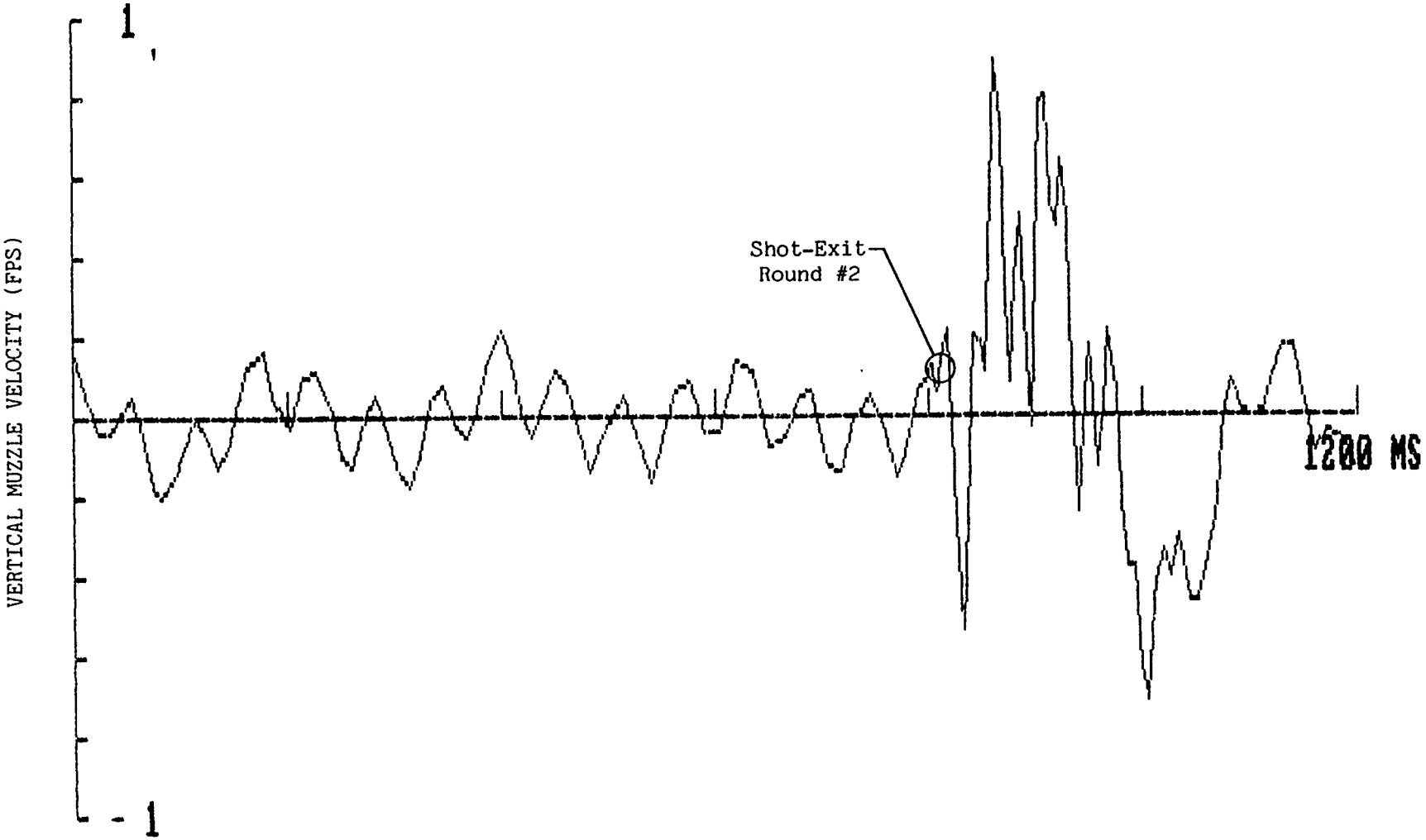

Fig. 18 (Cont'd.)

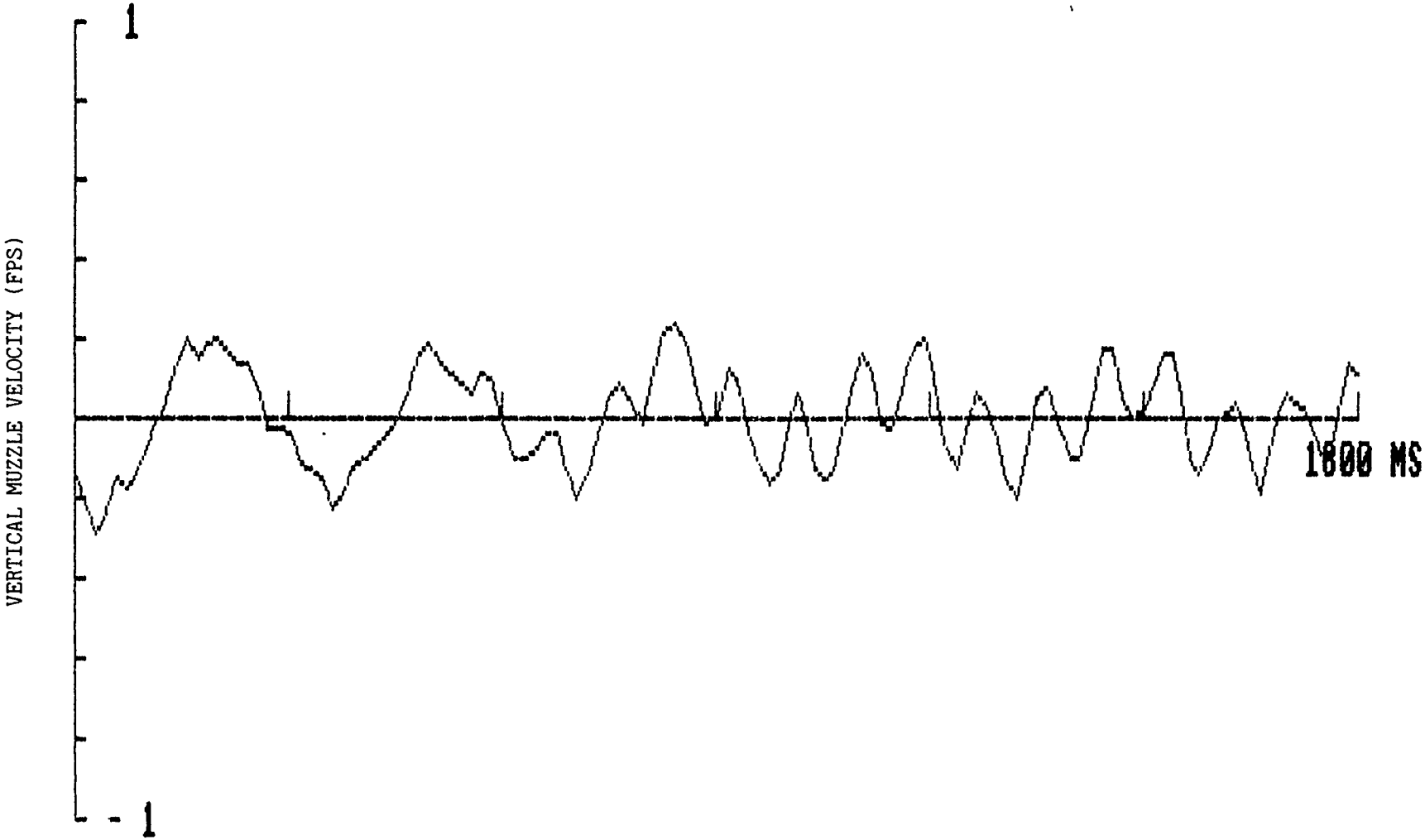

Fig. 18 (Cont'd.)

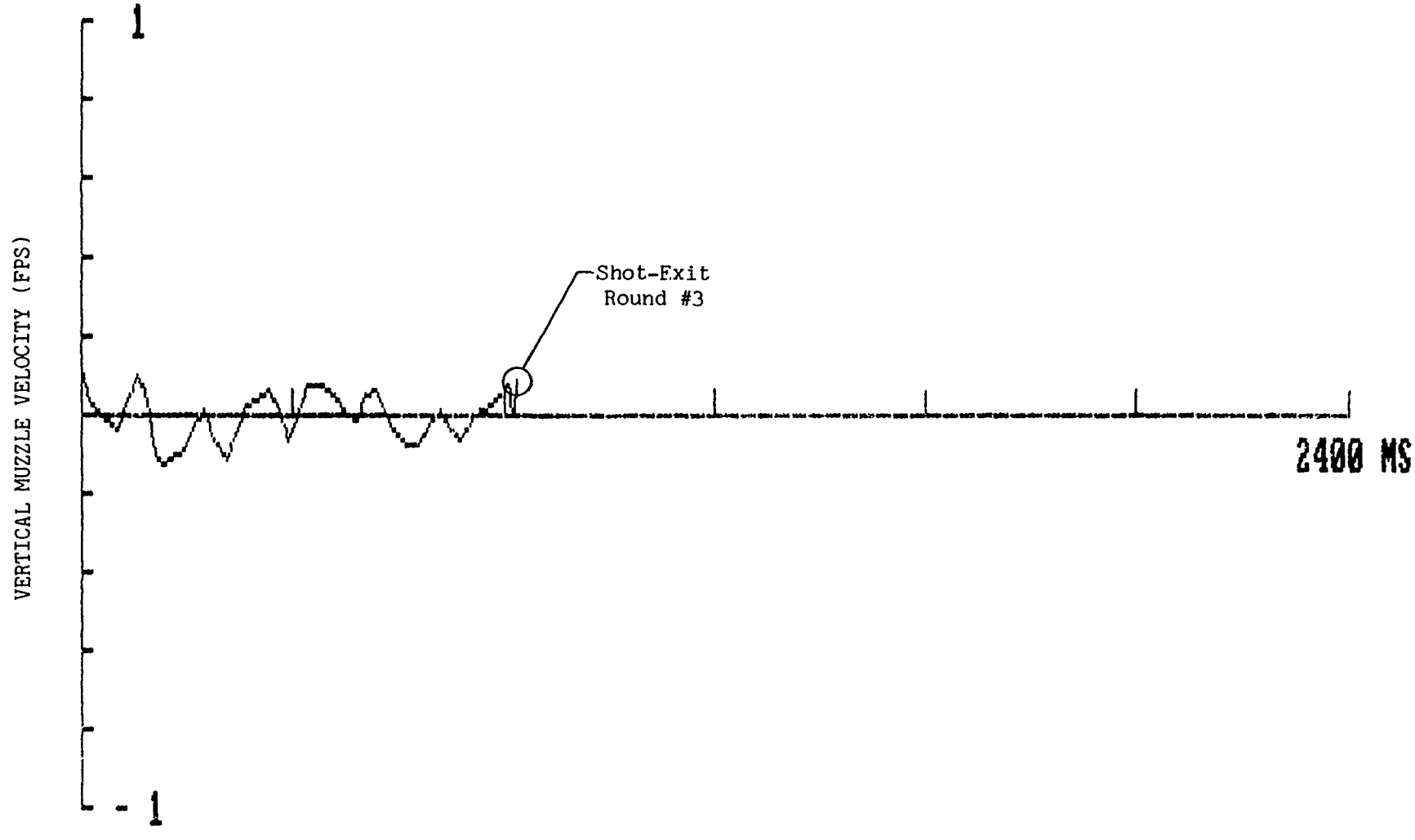

Fig. 18 (Cont'd.)

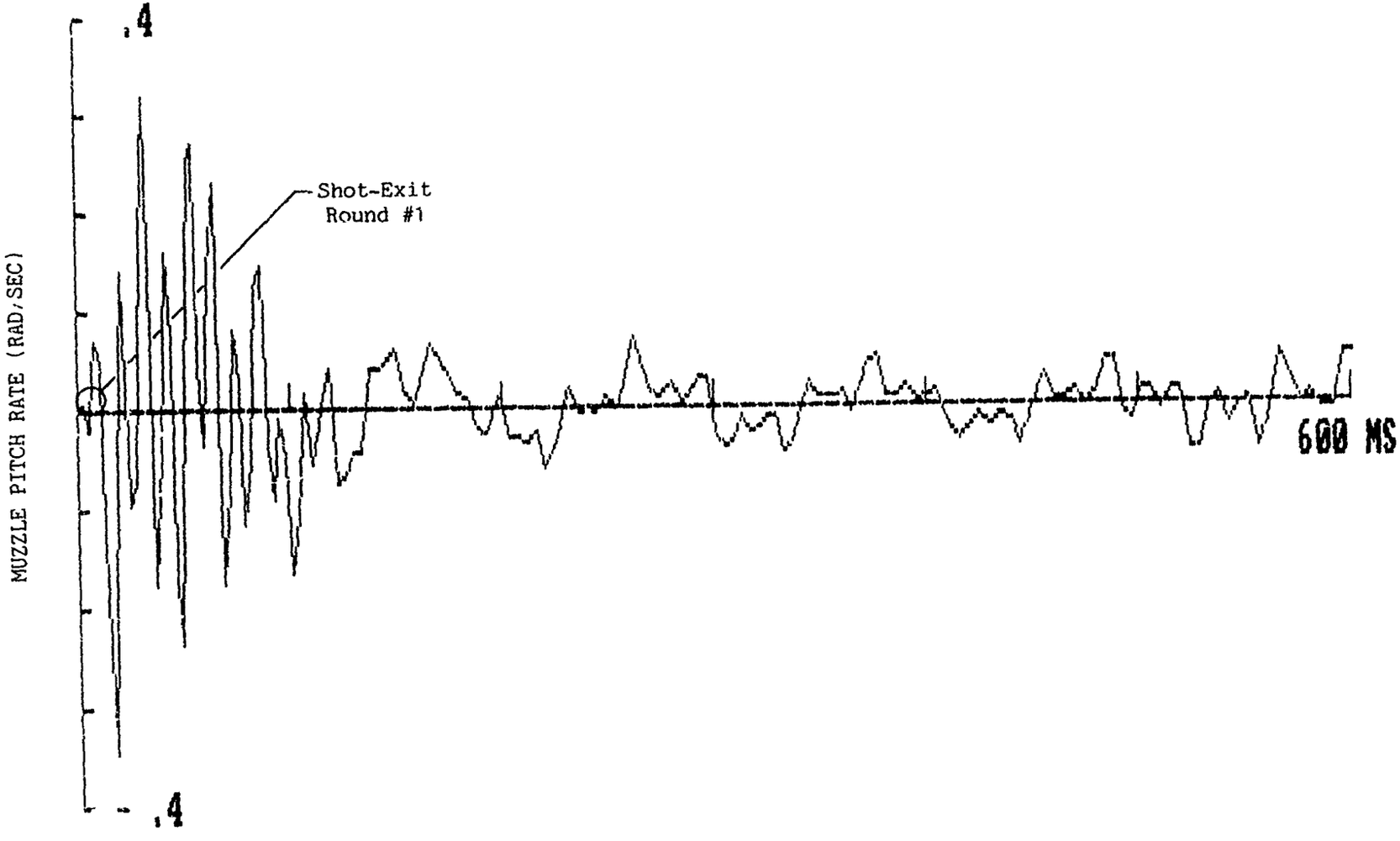

Fig. 19 - Muzzle Pitch Rate for Three-Round Burst Without Firing Control Signal

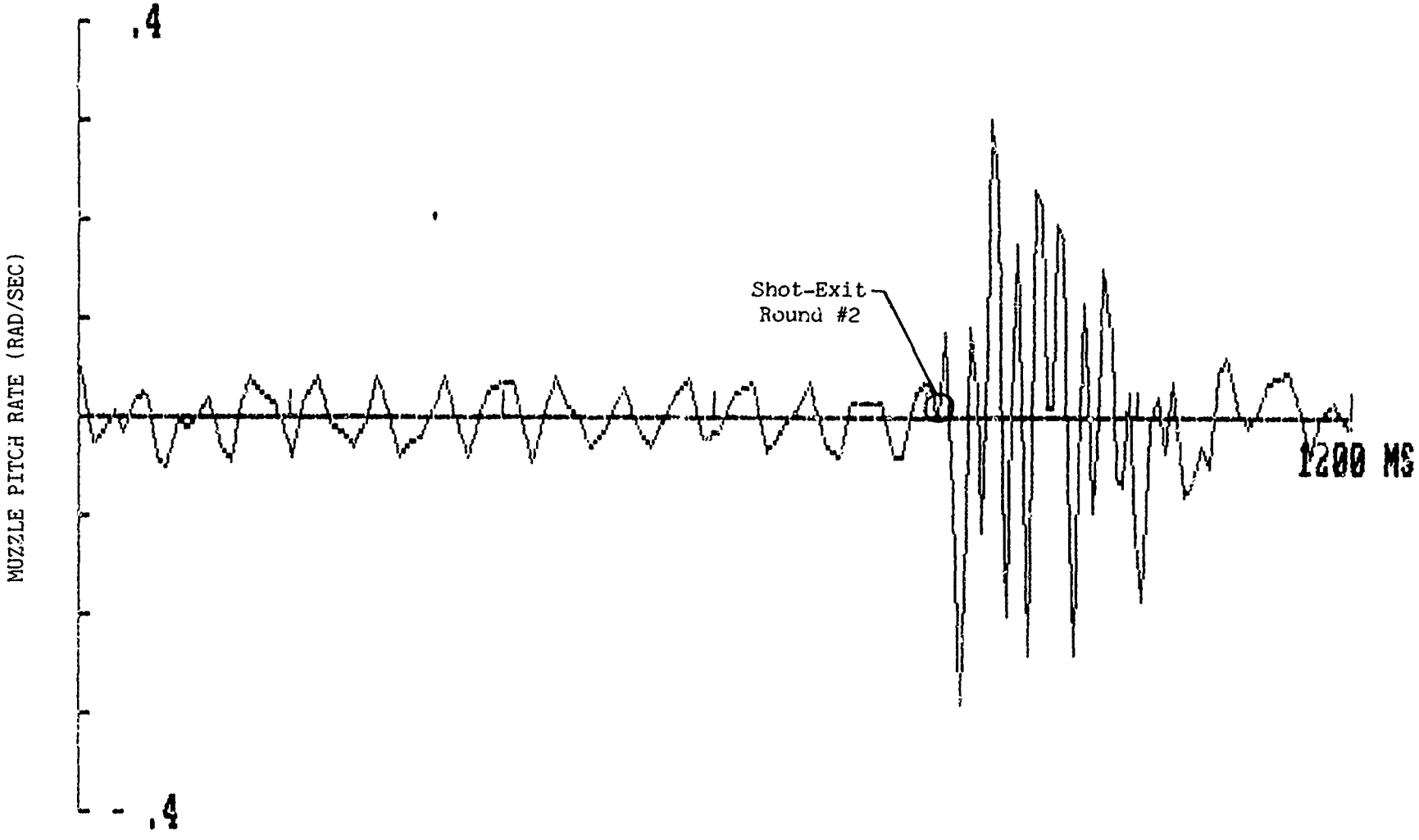

Fig. 19 (Cont'd.)

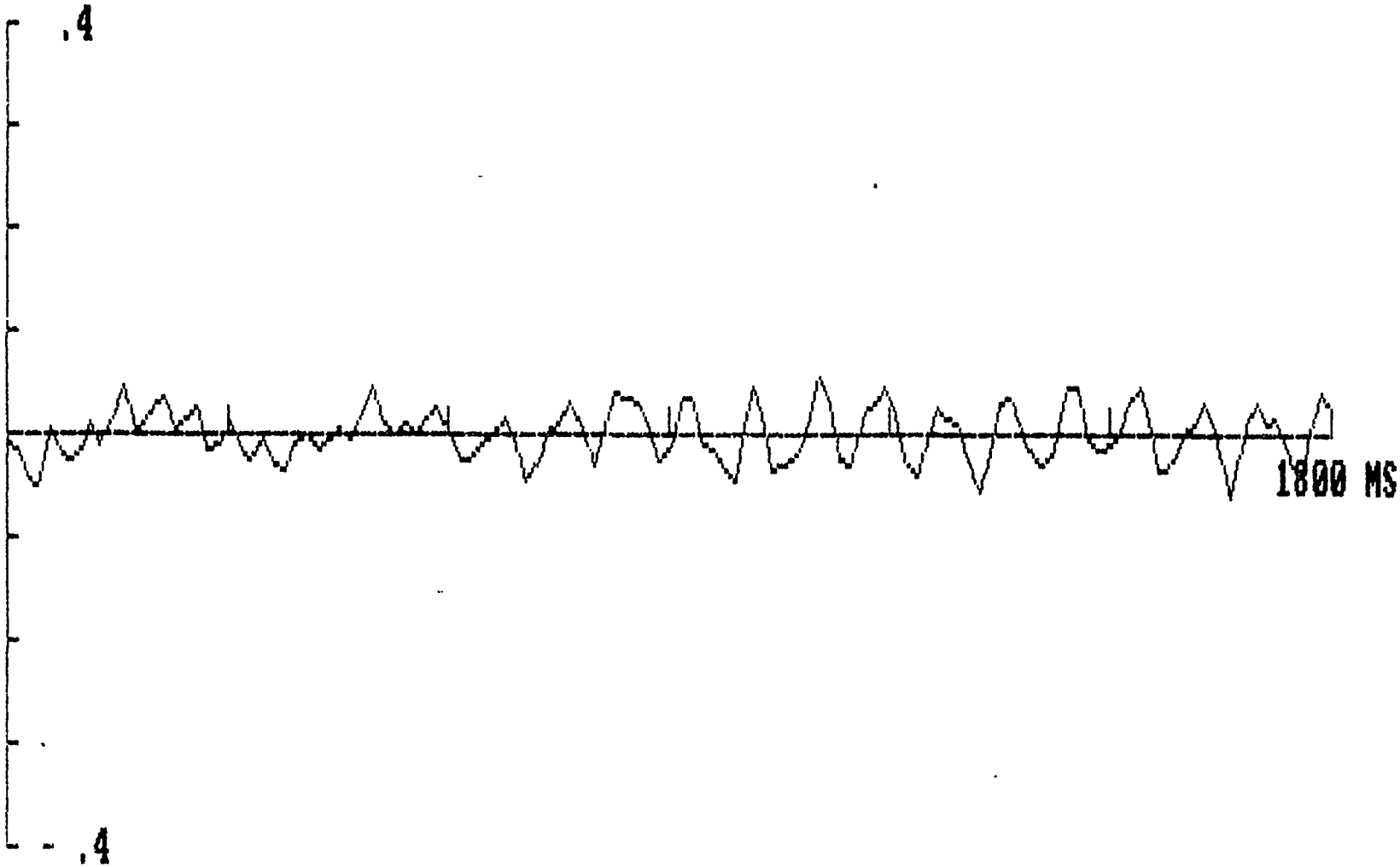

Fig. 19 (Cont'd.)

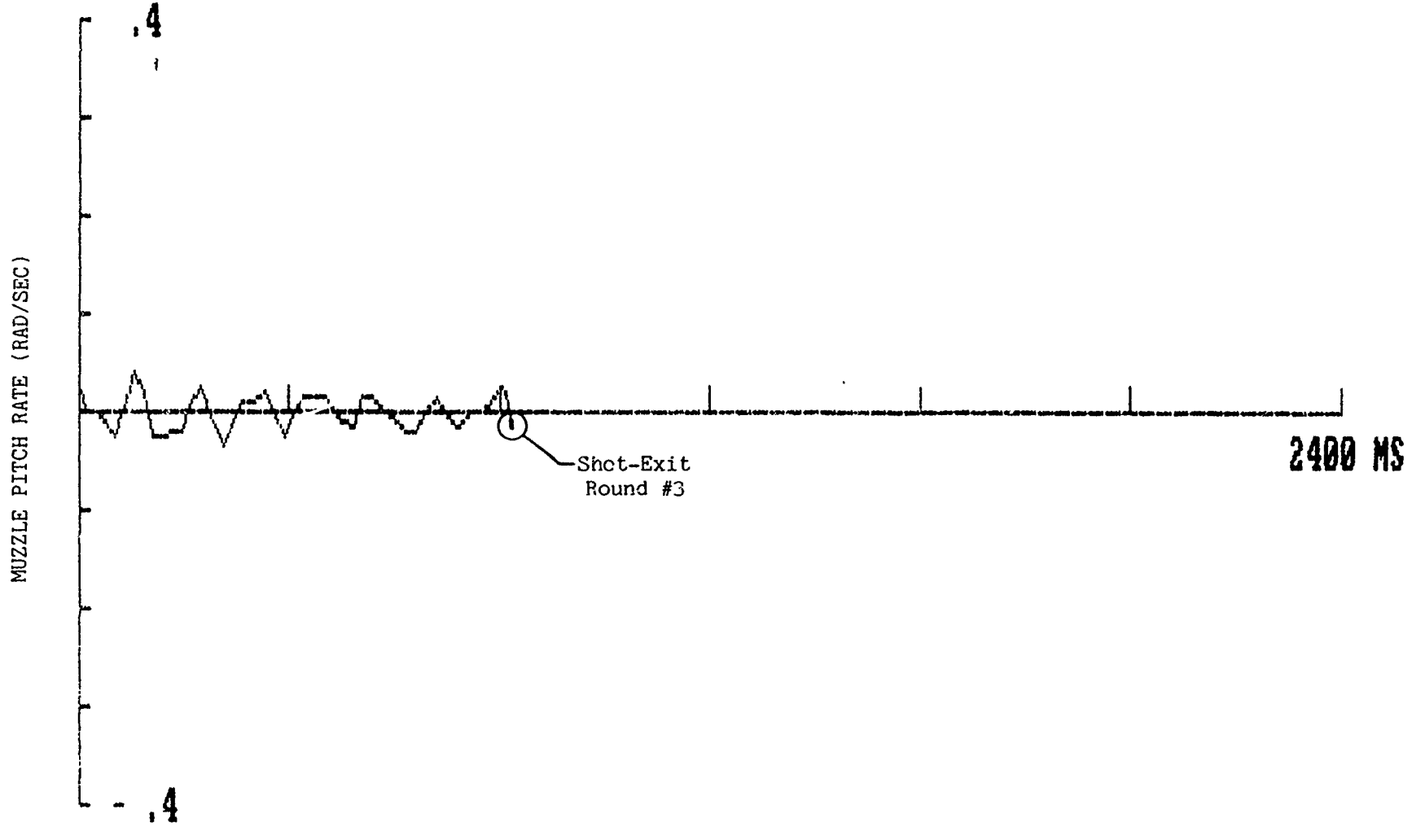

Fig. 19 (Cont'd.)

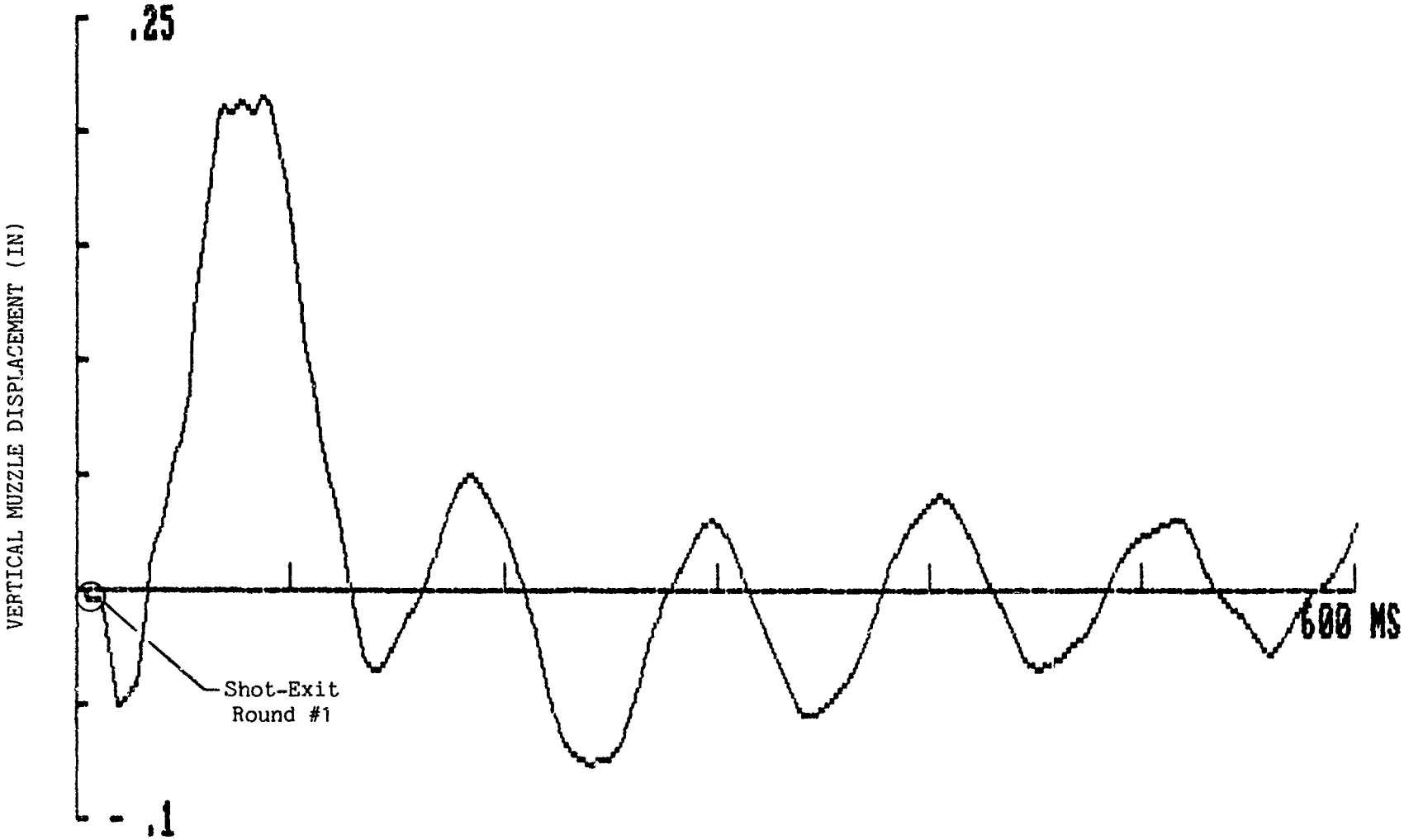

Fig. 20 - Vertical Muzzle Displacement for Three-Round Burst With Vertical-Plane "Window"

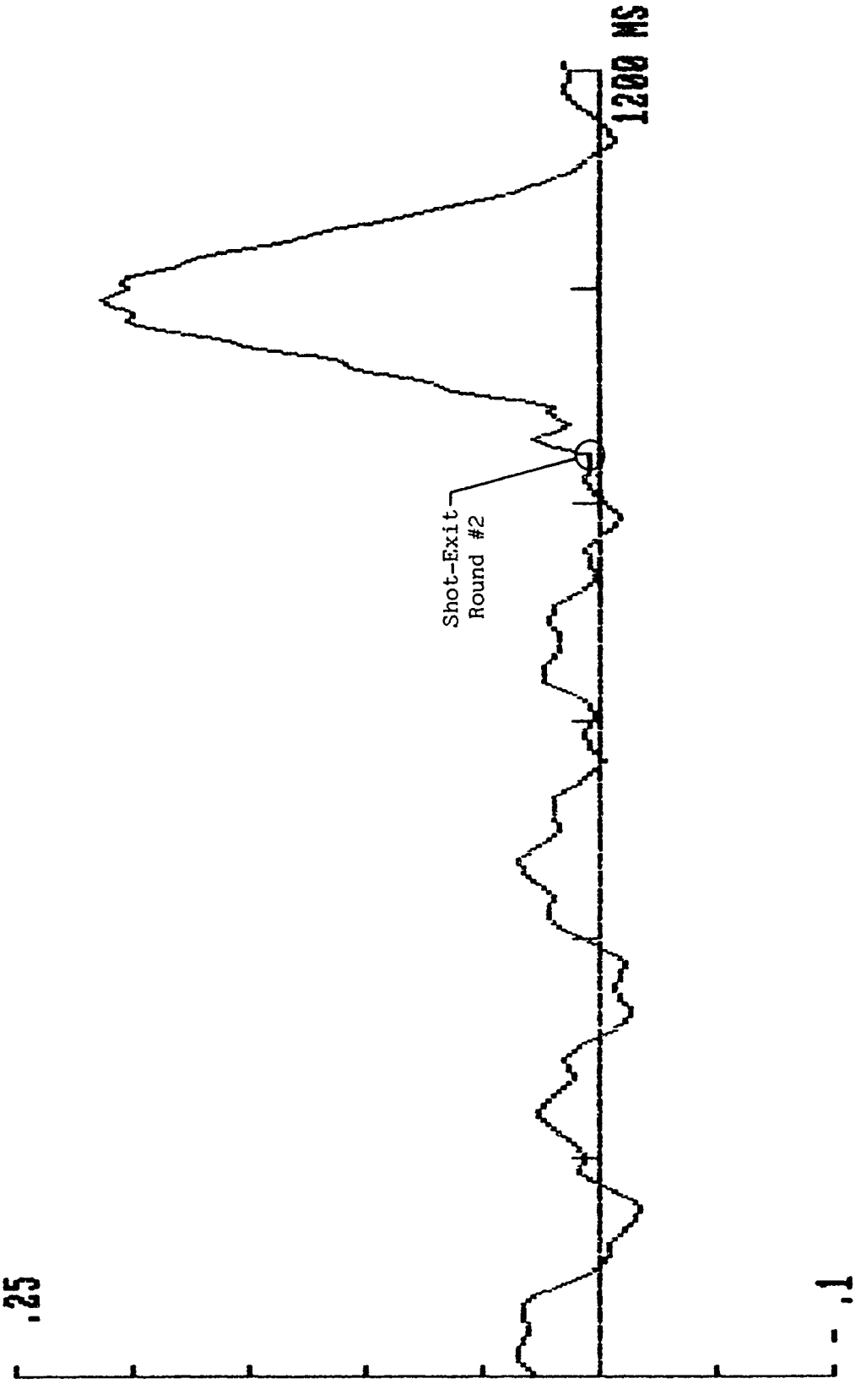
1200 MS
Shot-Exit
Round #2
.25
-.1
VERTICAL MUZZLE DISPLACEMENT (IN)

Fig. 20 (Cont'd.)

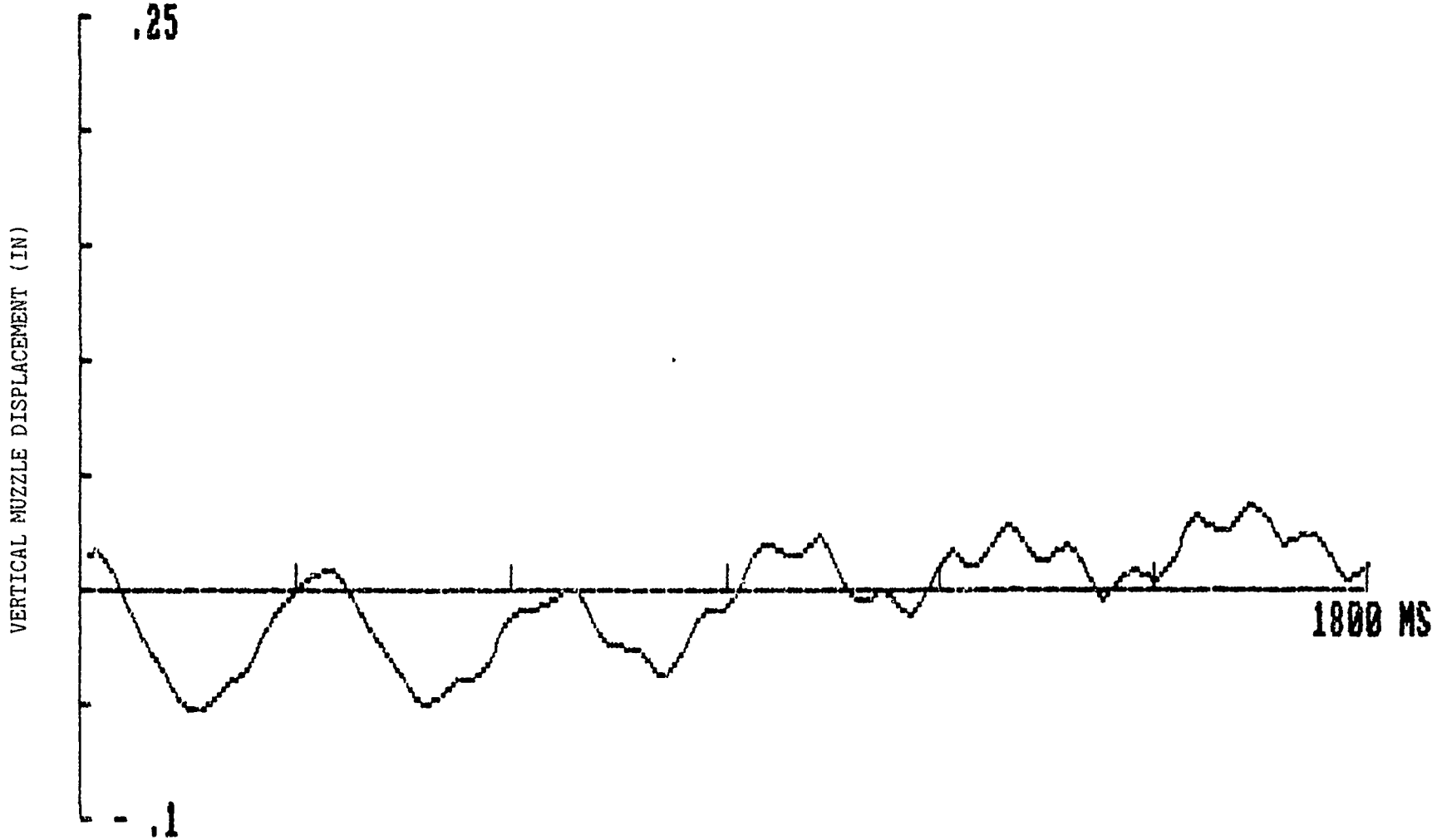

Fig. 20 (Cont'd.)

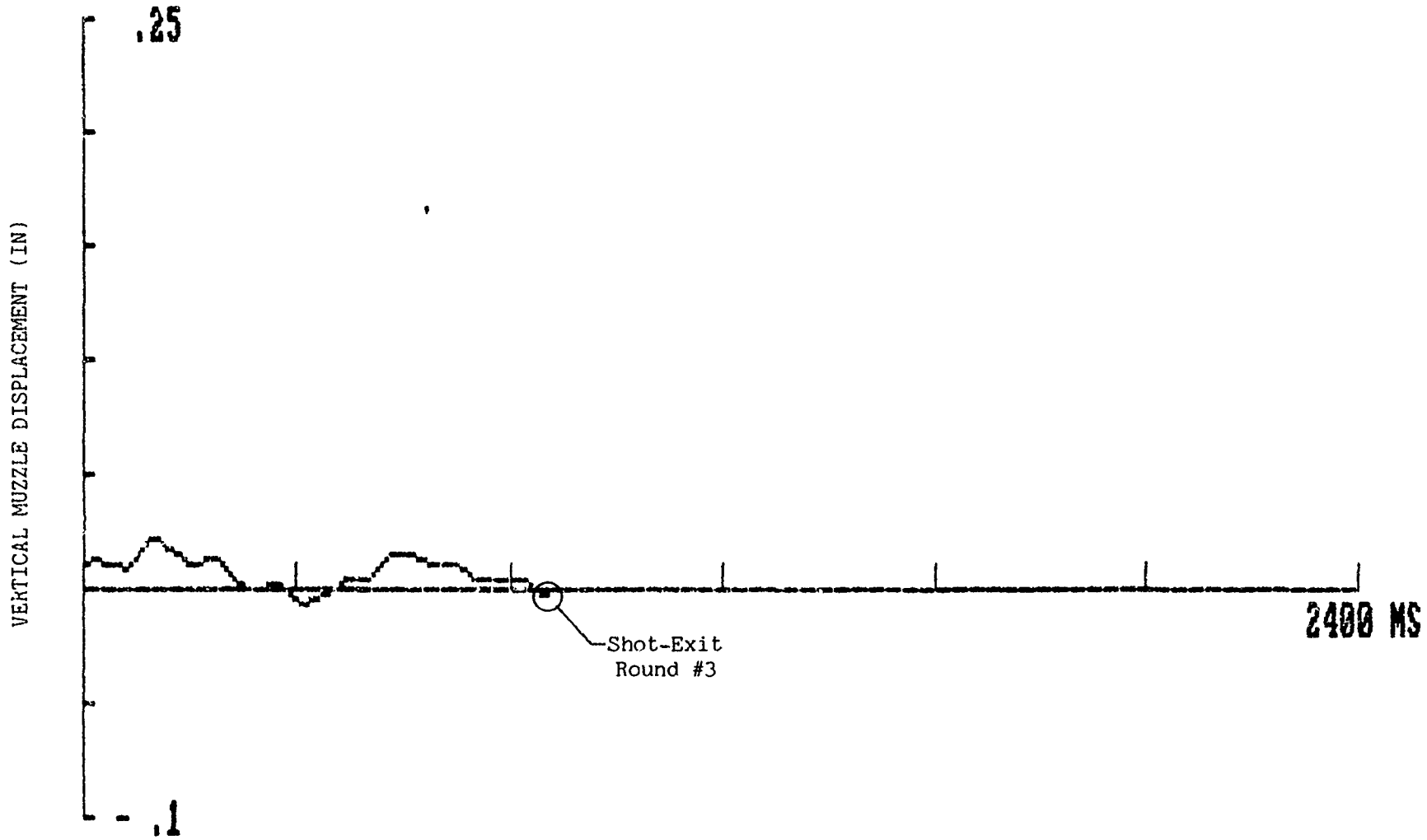
.25
VERTICAL MUZZLE DISPLACEMENT (IN)
2400 MS
Shot-Exit
Round #3
- .1

Fig. 20 (Cont'd.)

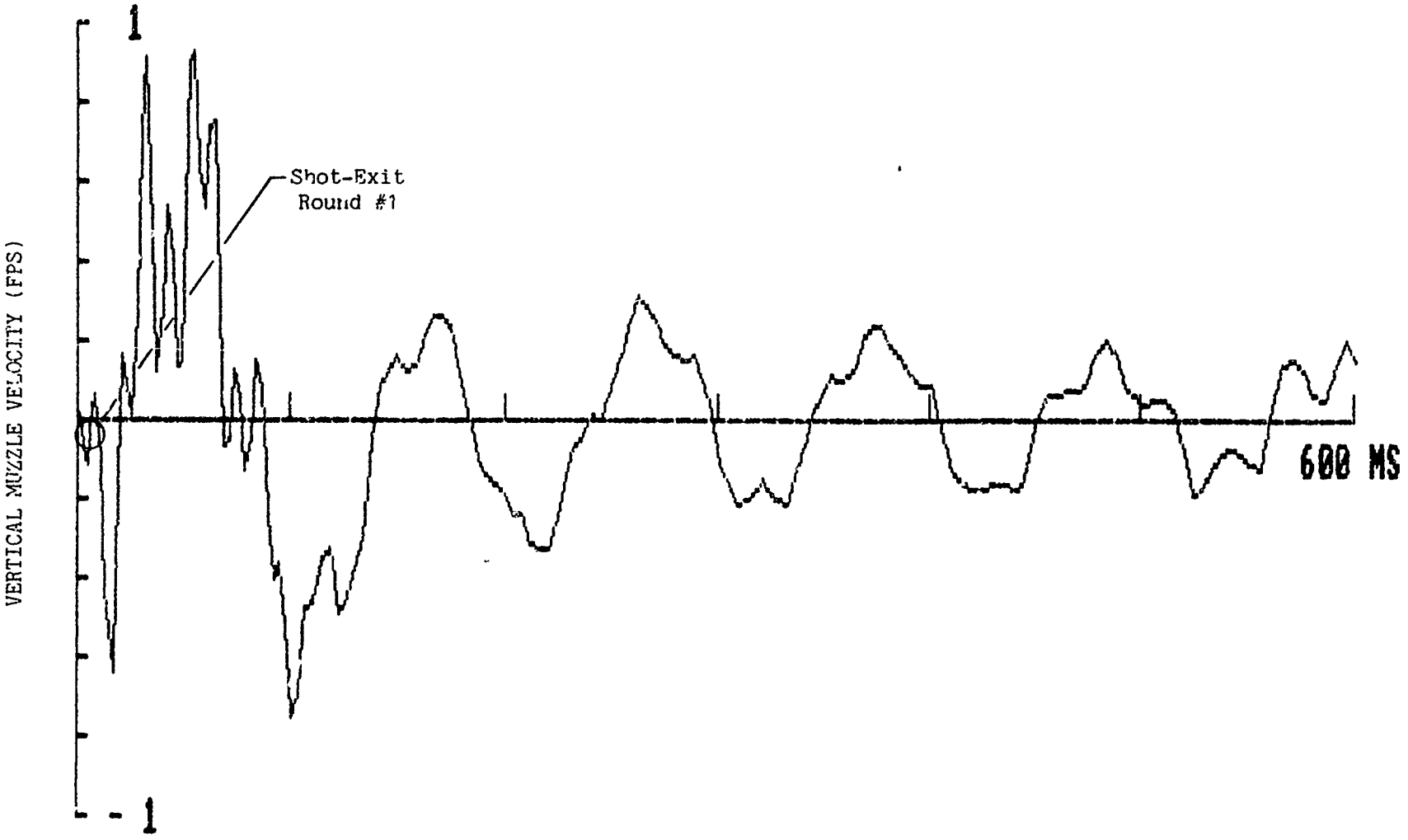

Fig. 21 - Vertical Muzzle Velocity for Three-Round Burst With Vertical-Plane "Window"

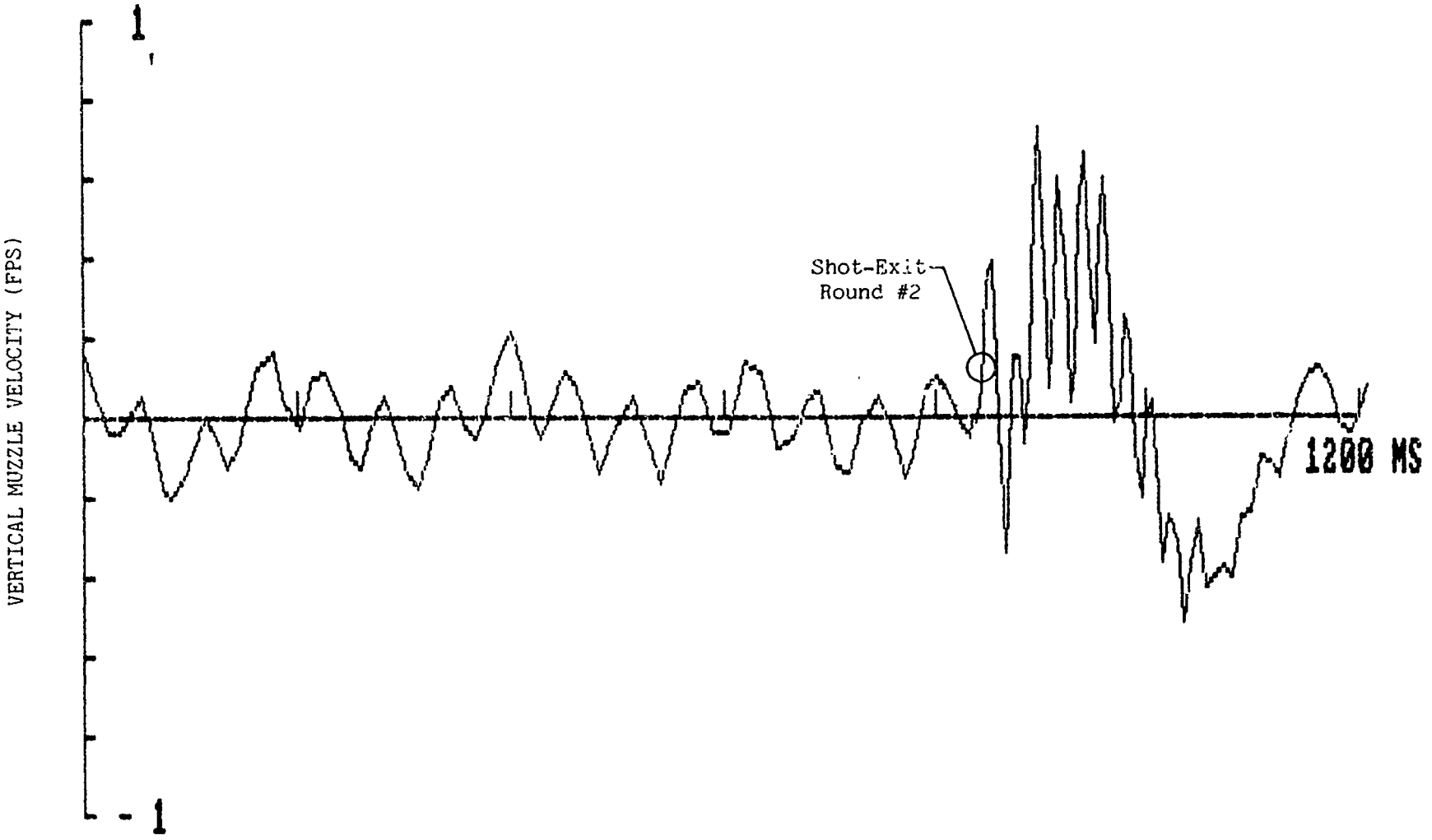

Fig. 21 (Cont'd.)

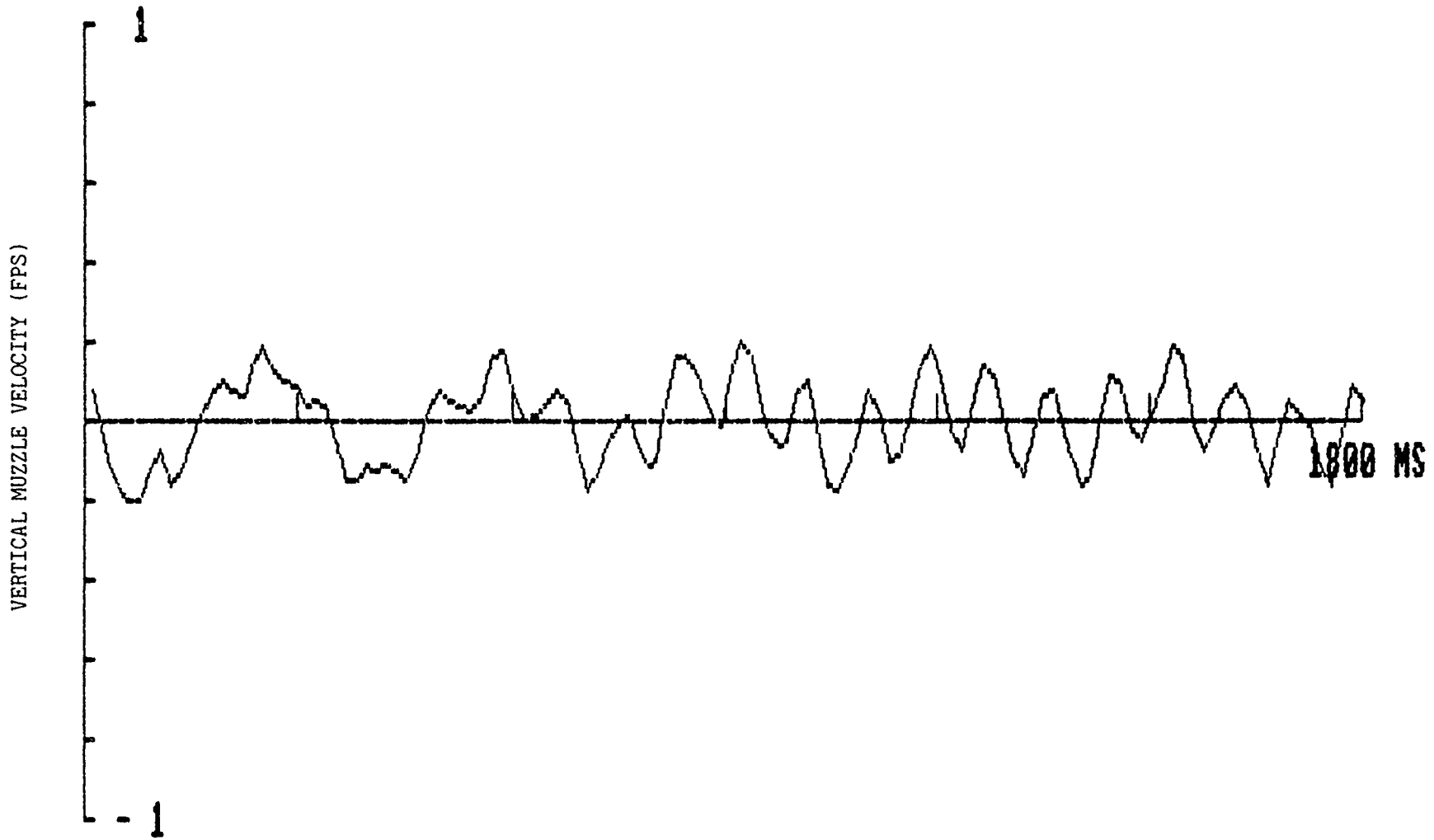

Fig. 21 (Cont'd.)

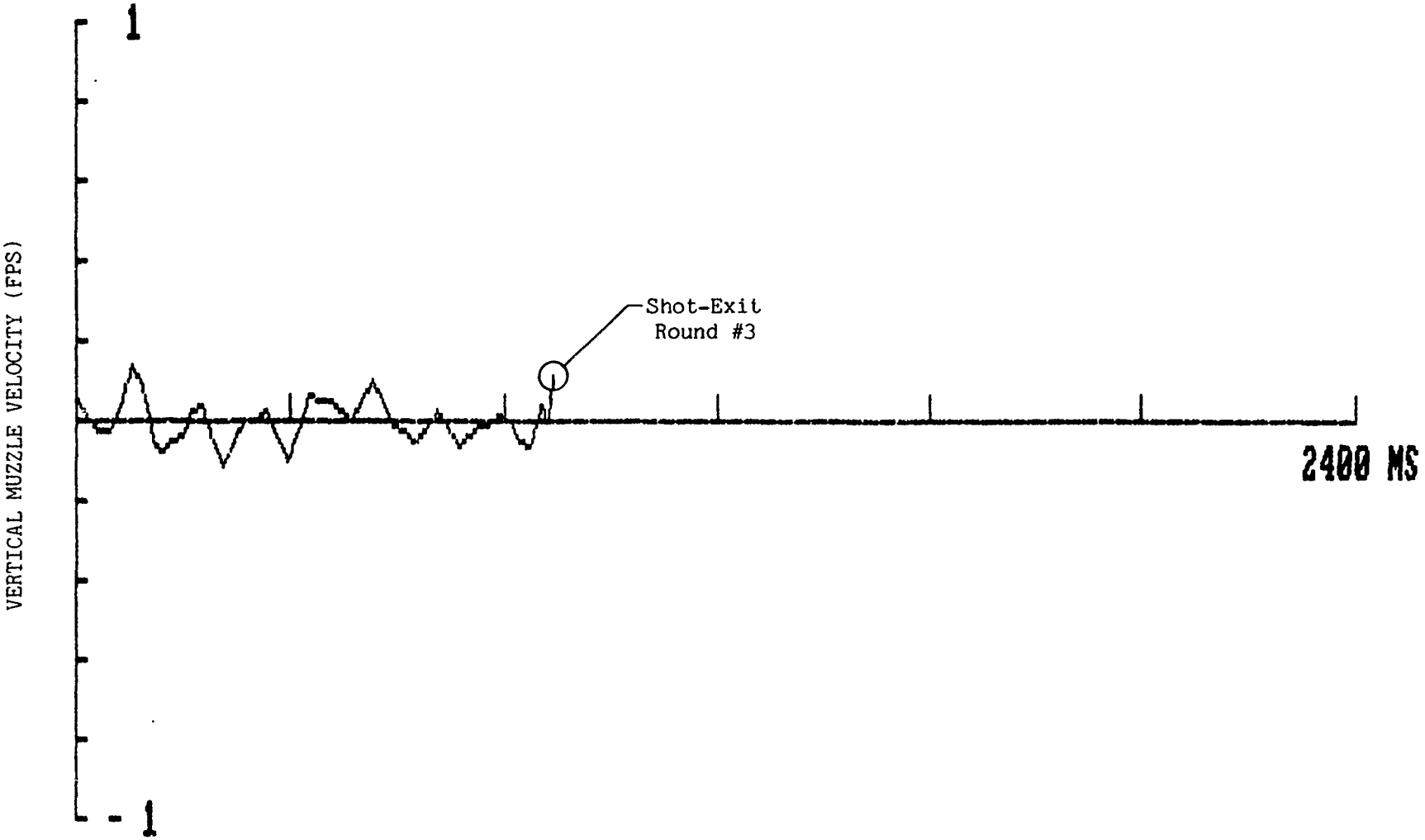

Fig. 21 (Cont'd.)

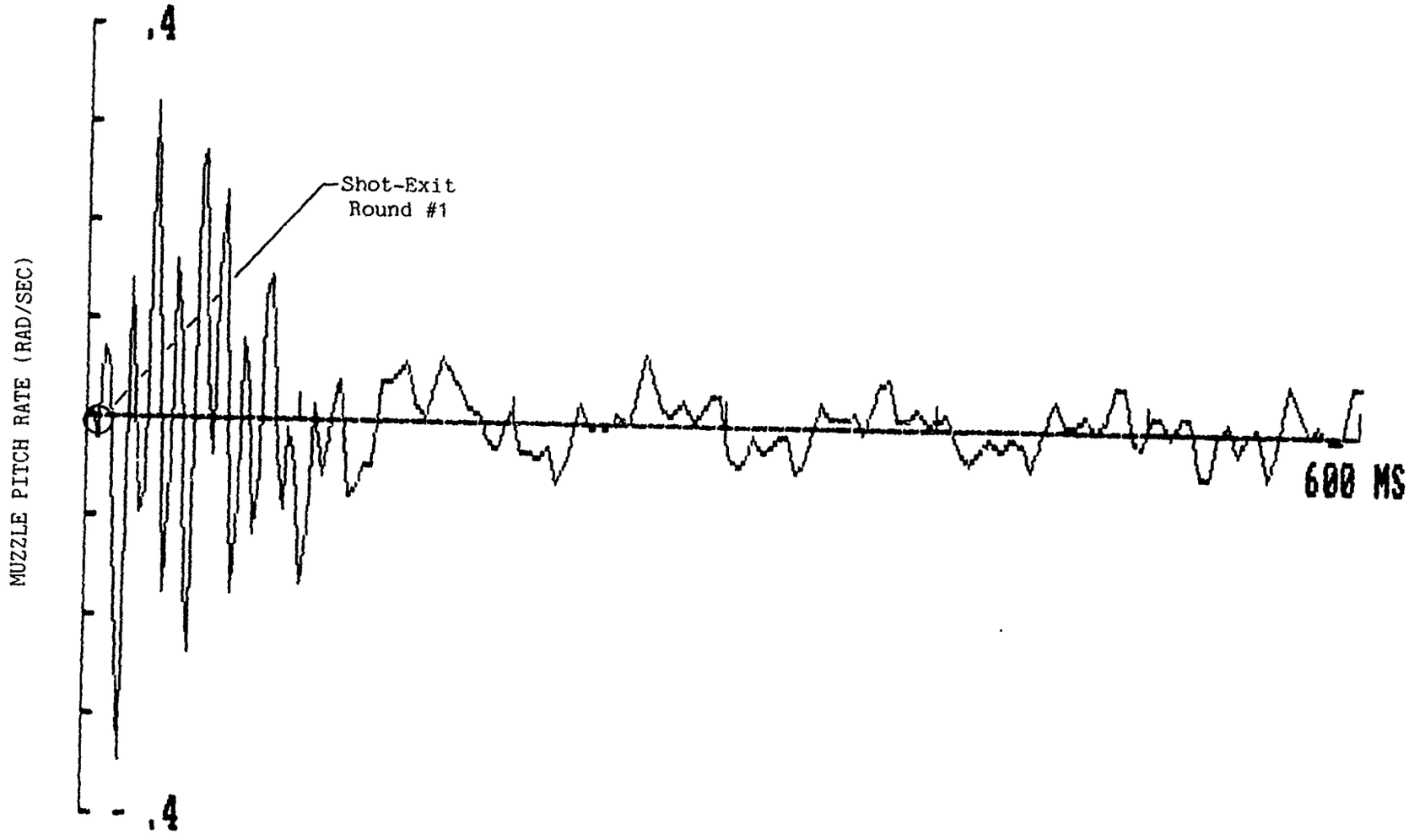

Fig. 22 - Muzzle Pitch Rate for Three-Round Burst With Vertical-Plane "Window"

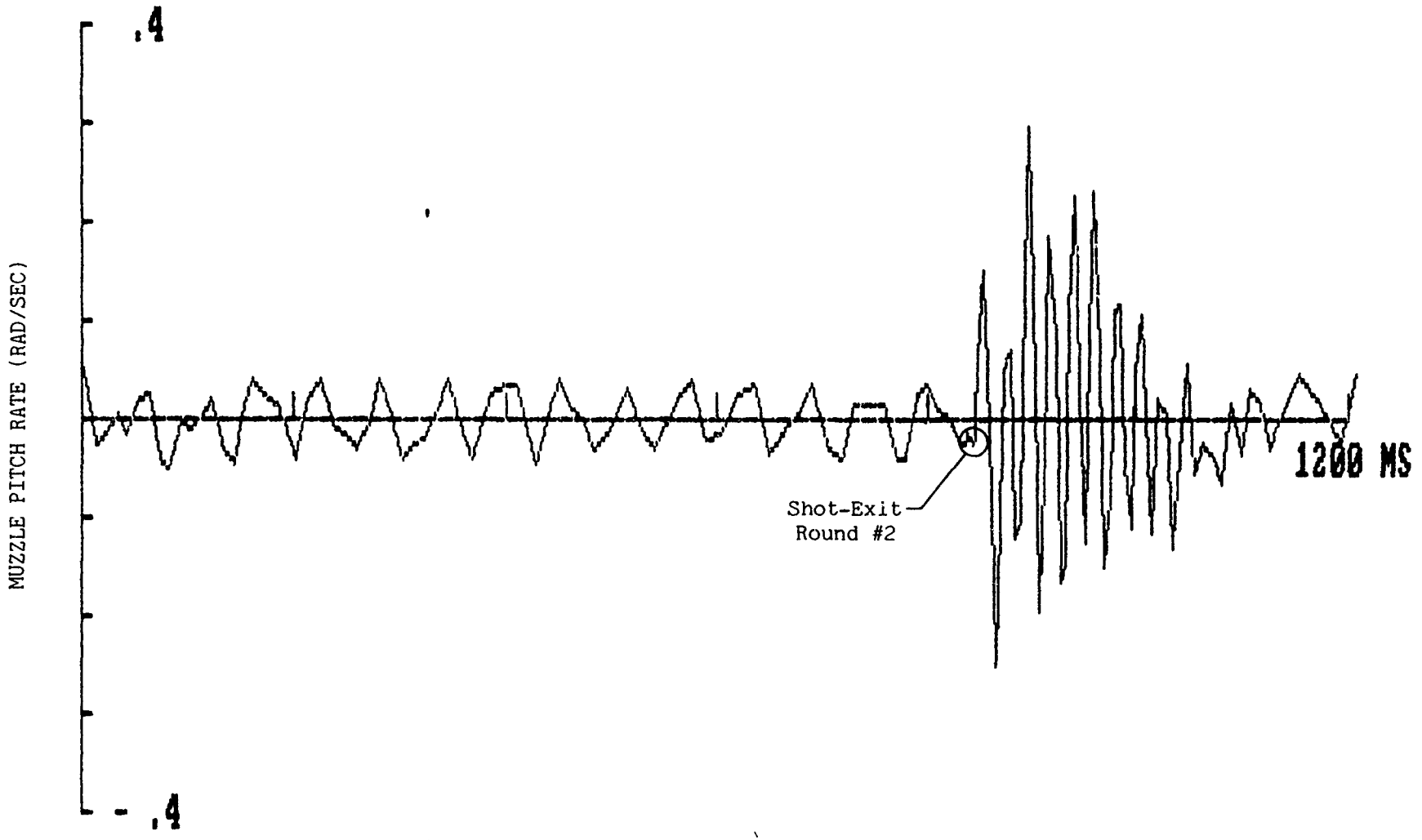

Fig. 22 (Cont'd.)

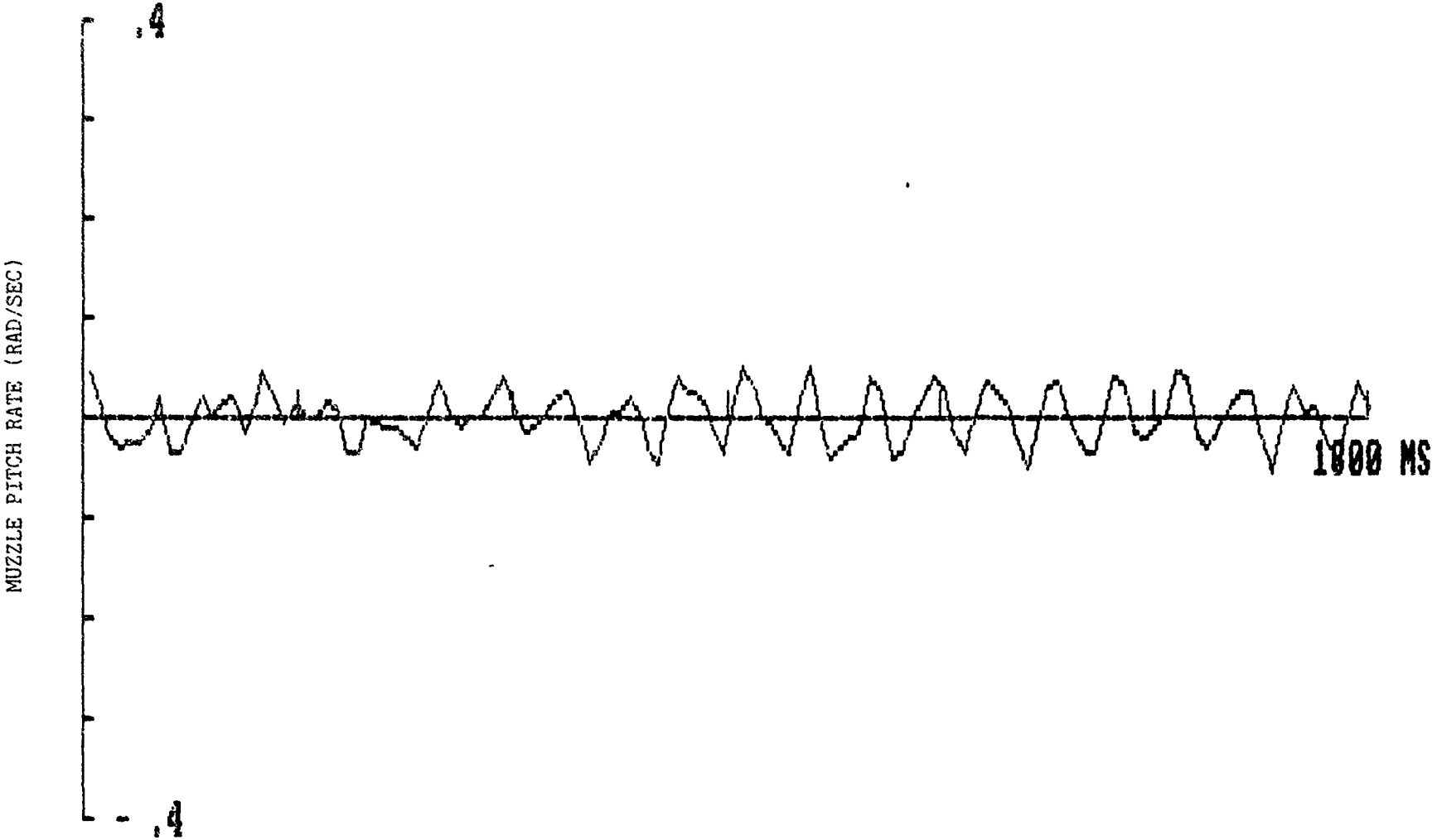

Fig. 22 (Cont'd.)

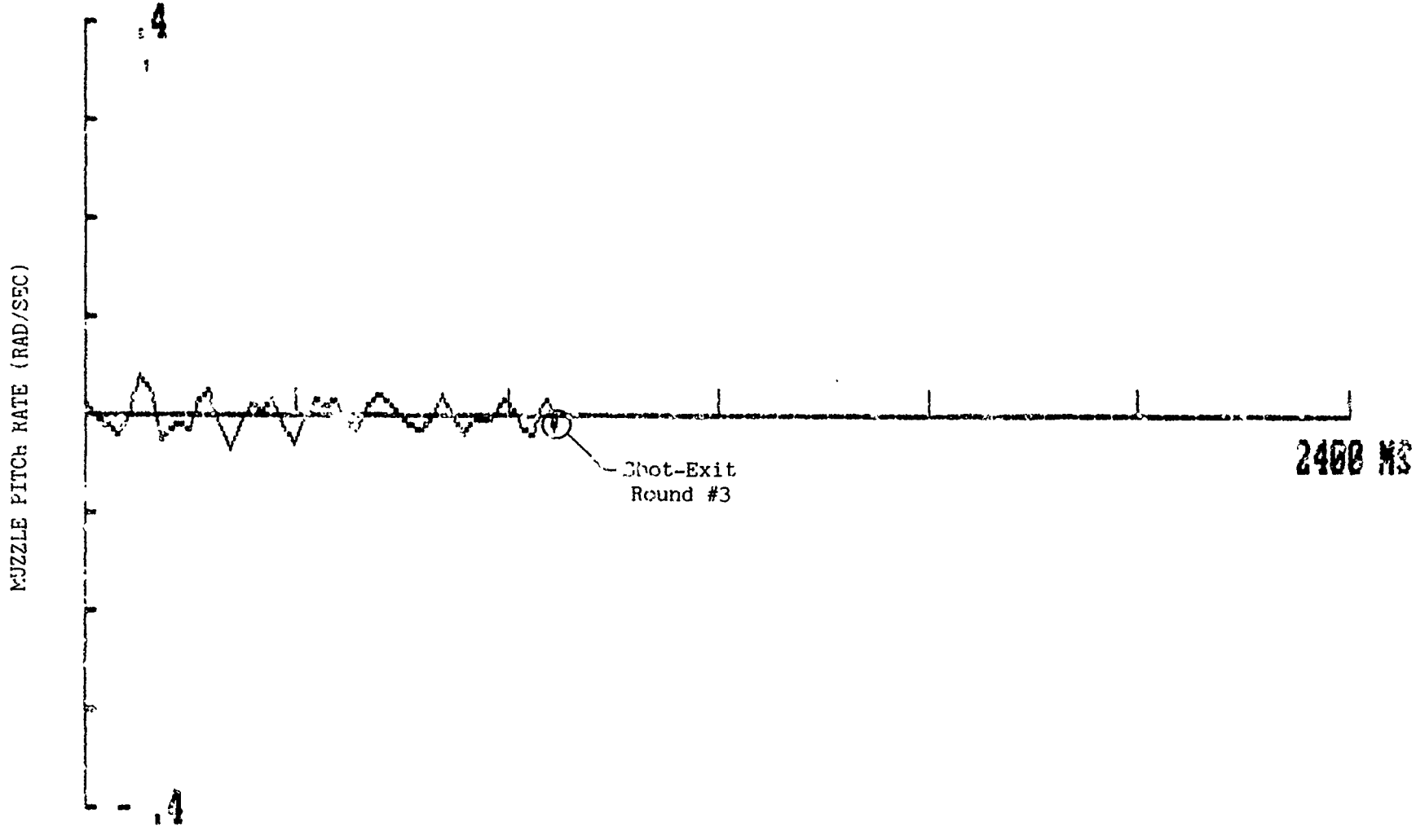

Fig. 22 (Cont'd.)

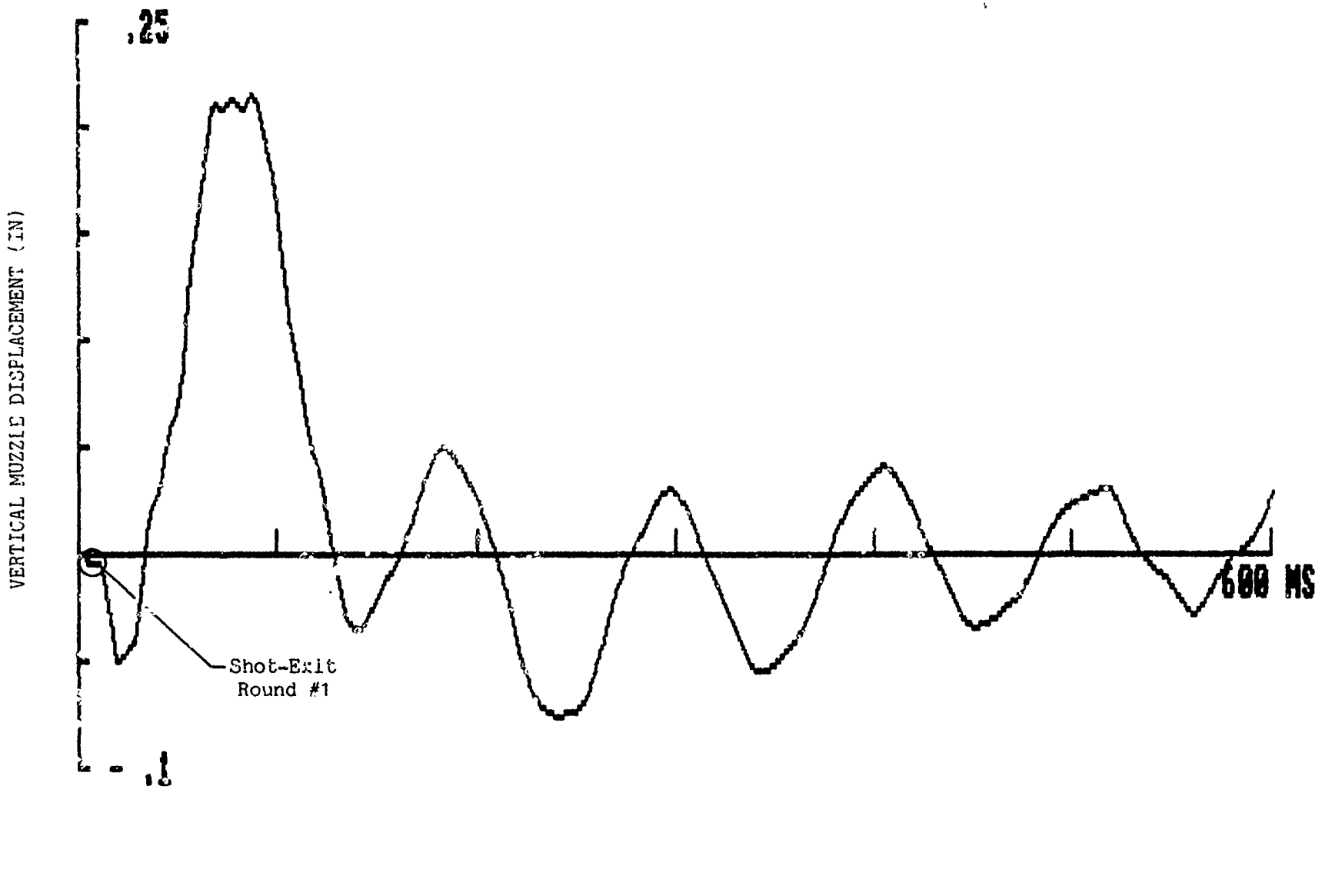

Fig. 23 - Vertical Muzzle Displacement for Three-Round Burst With Combined Vertical and Horizontal-Plane "Windows"

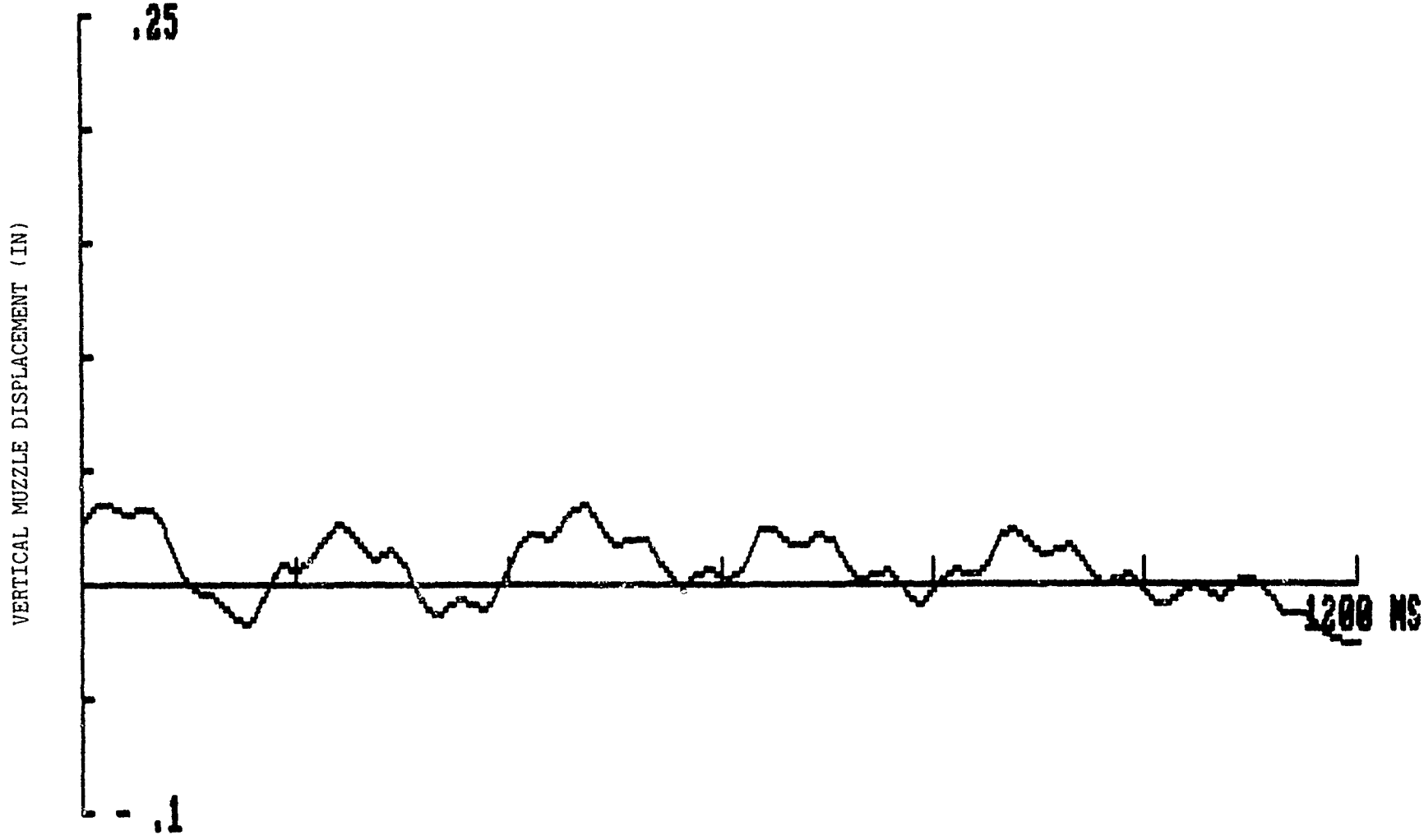

Fig. 23 (Cont'd.)

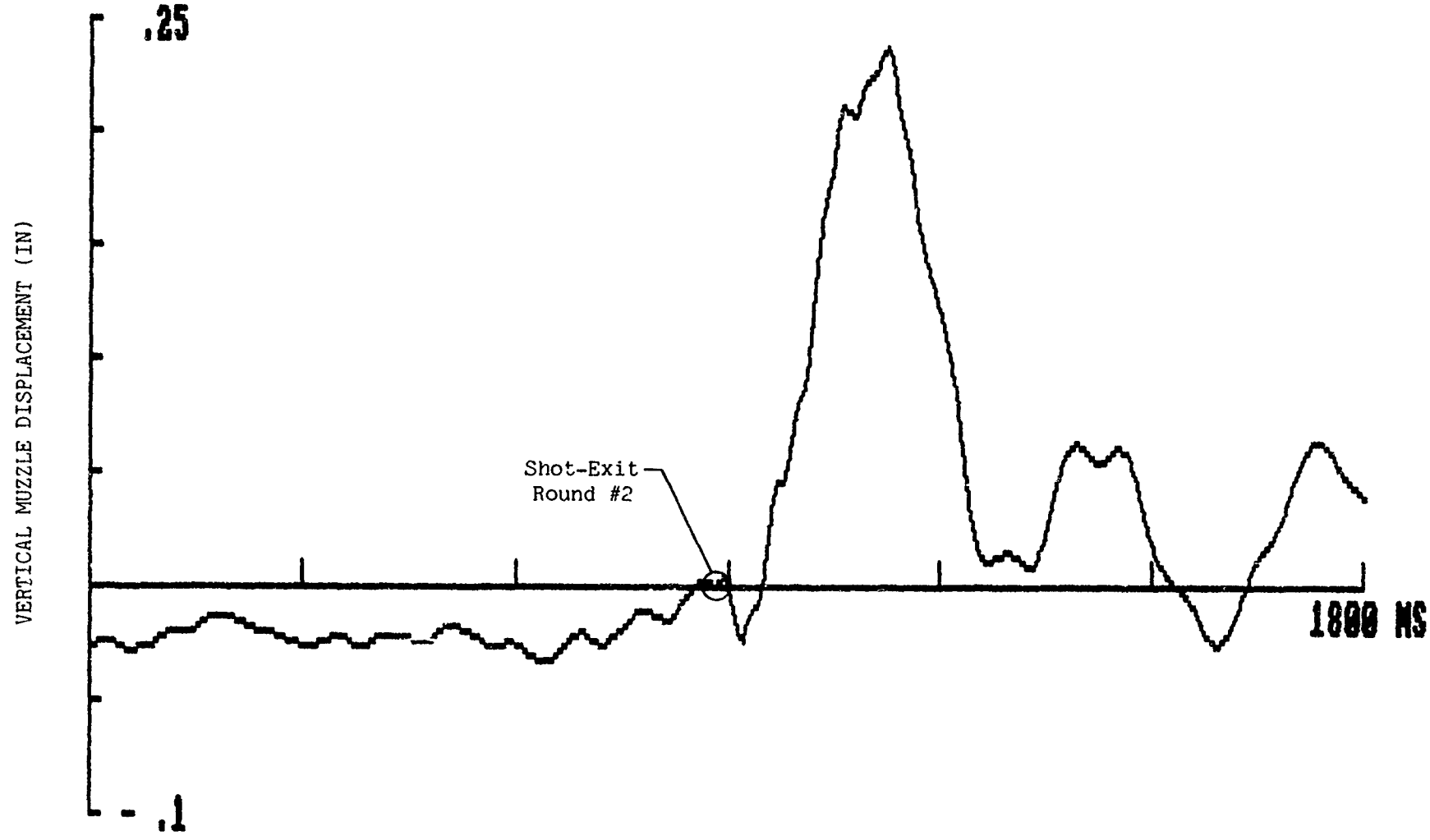
.25
VERTICAL MUZZLE DISPLACEMENT (IN)
Shot-Exit
Round #2
1800 MS
- .1

Fig. 23 (Cont'd.)

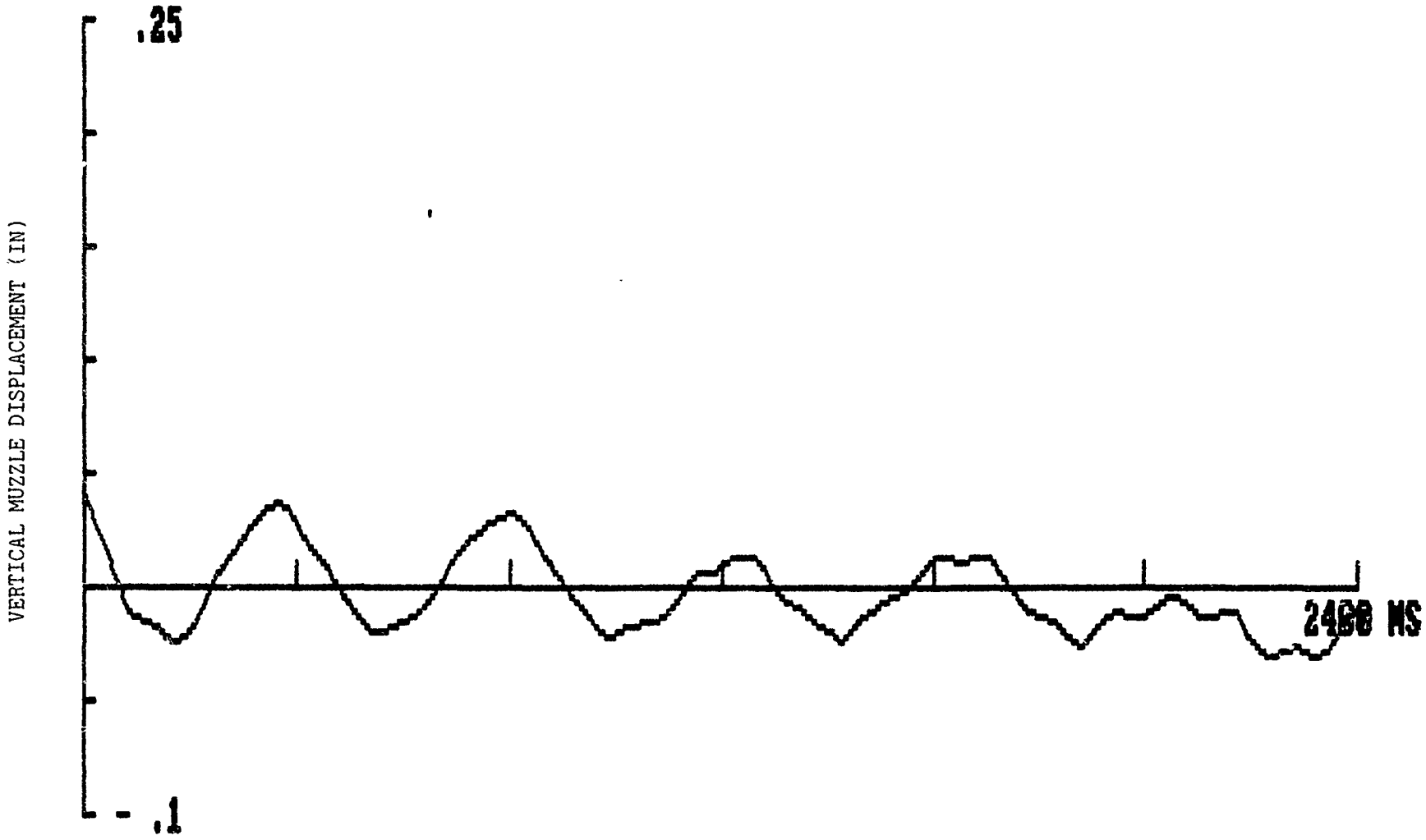

Fig. 23 (Cont'd.)

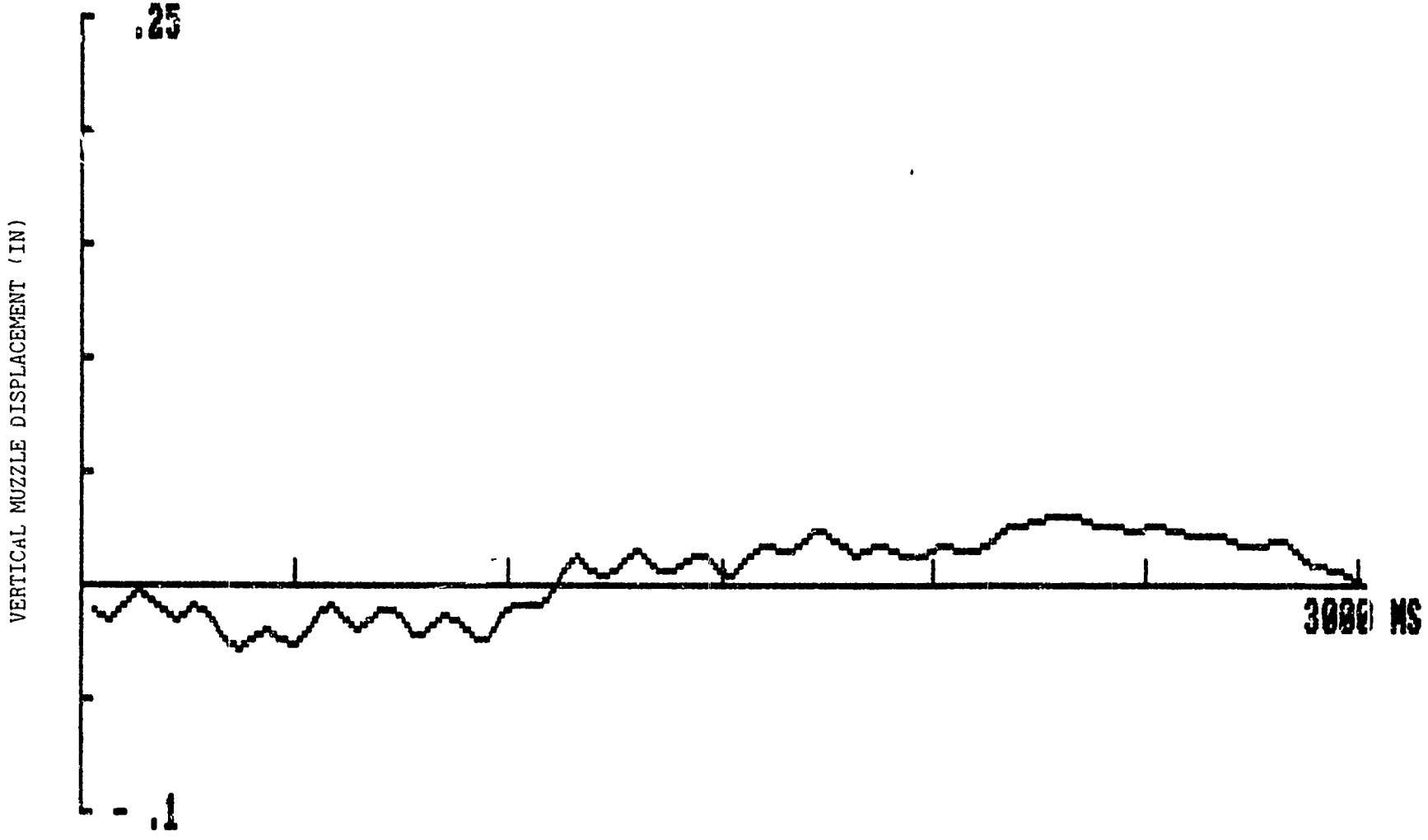

Fig. 23 (Cont'd.)

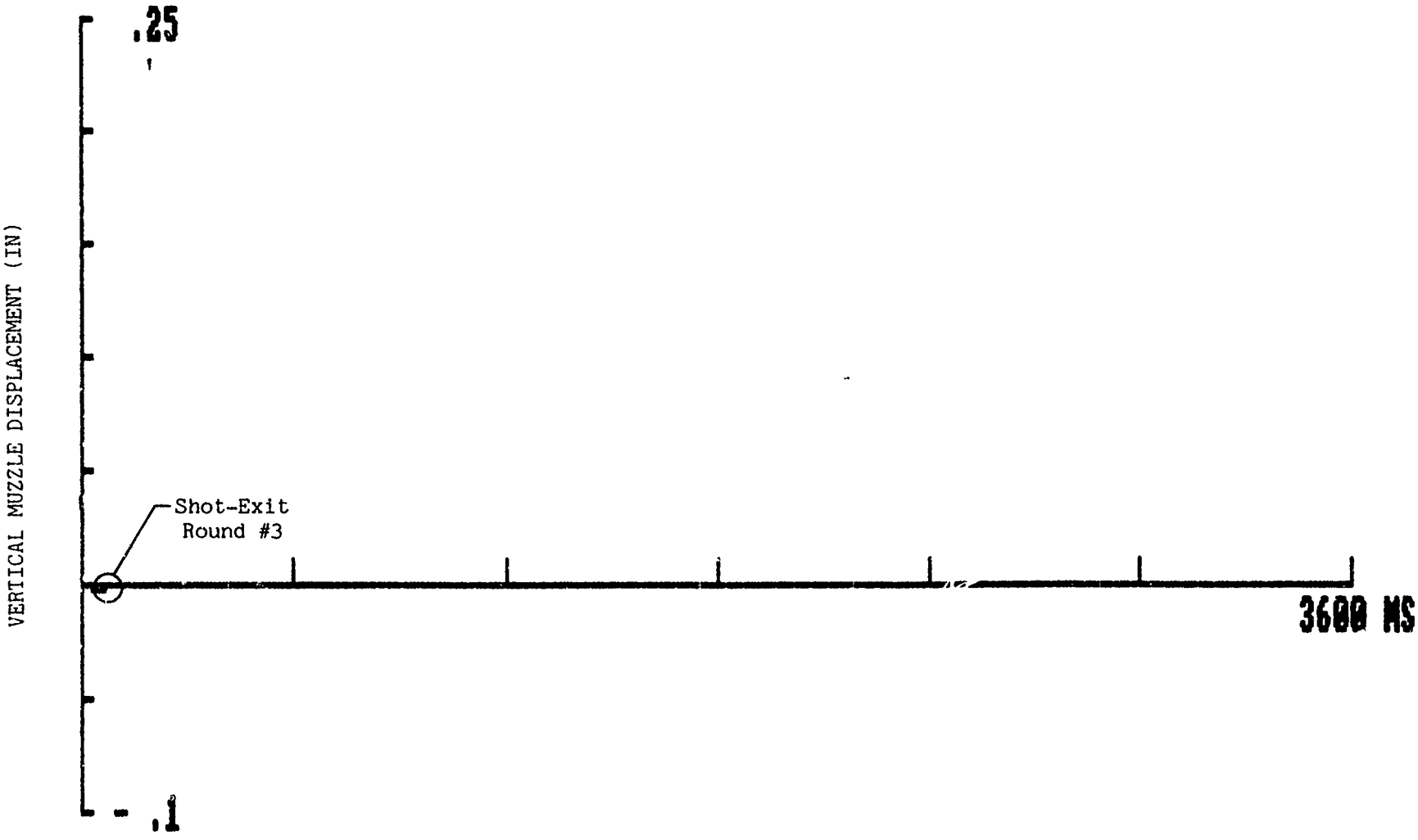
.25
VERTICAL MUZZLE DISPLACEMENT (IN)
Shot-Exit
Round #3
3600 MS
- .1

Fig. 23 (Cont'd.)

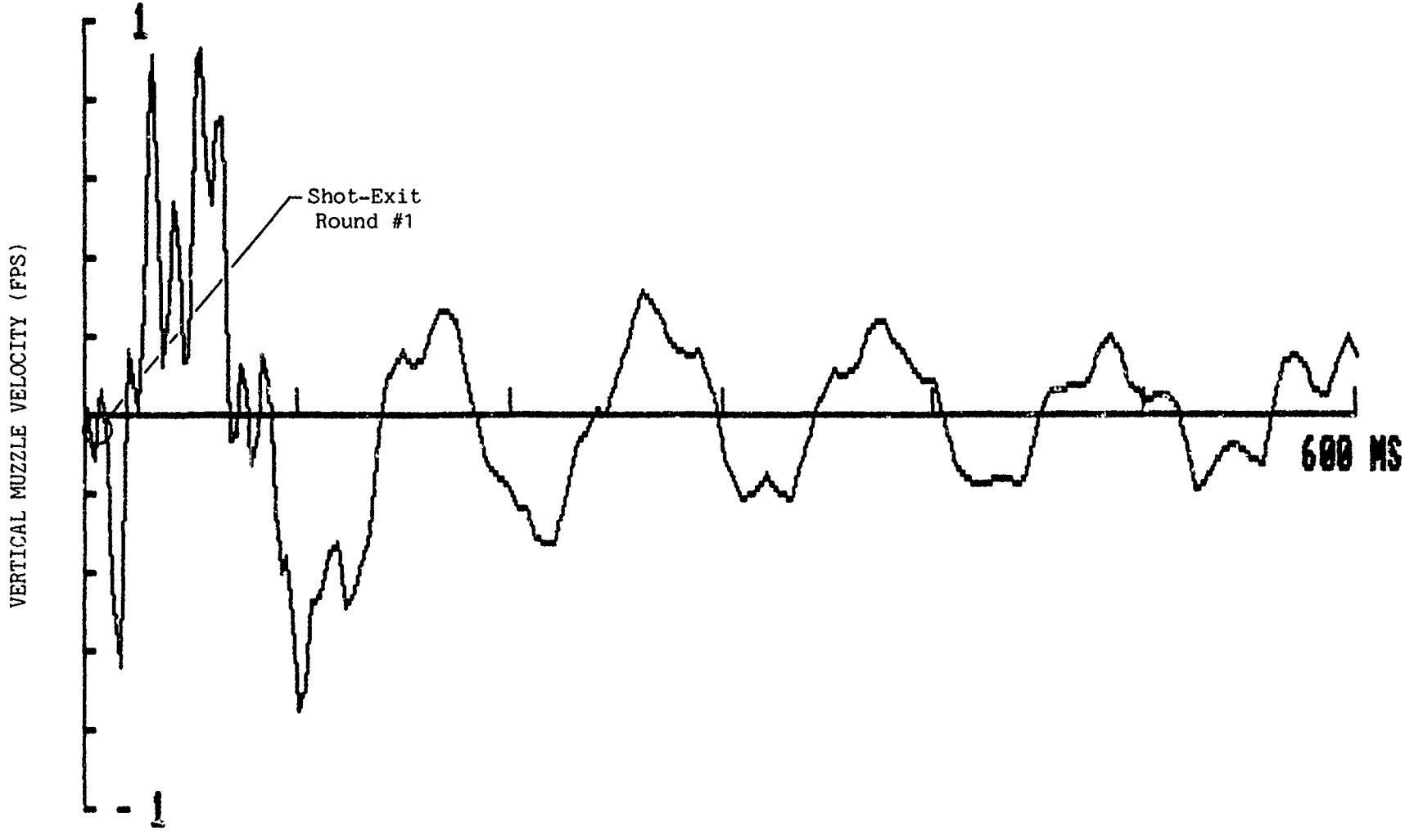

Fig. 24 - Vertical Muzzle Velocity for Three-Round Burst With Combined Vertical and Horizontal-Plane "Windows"

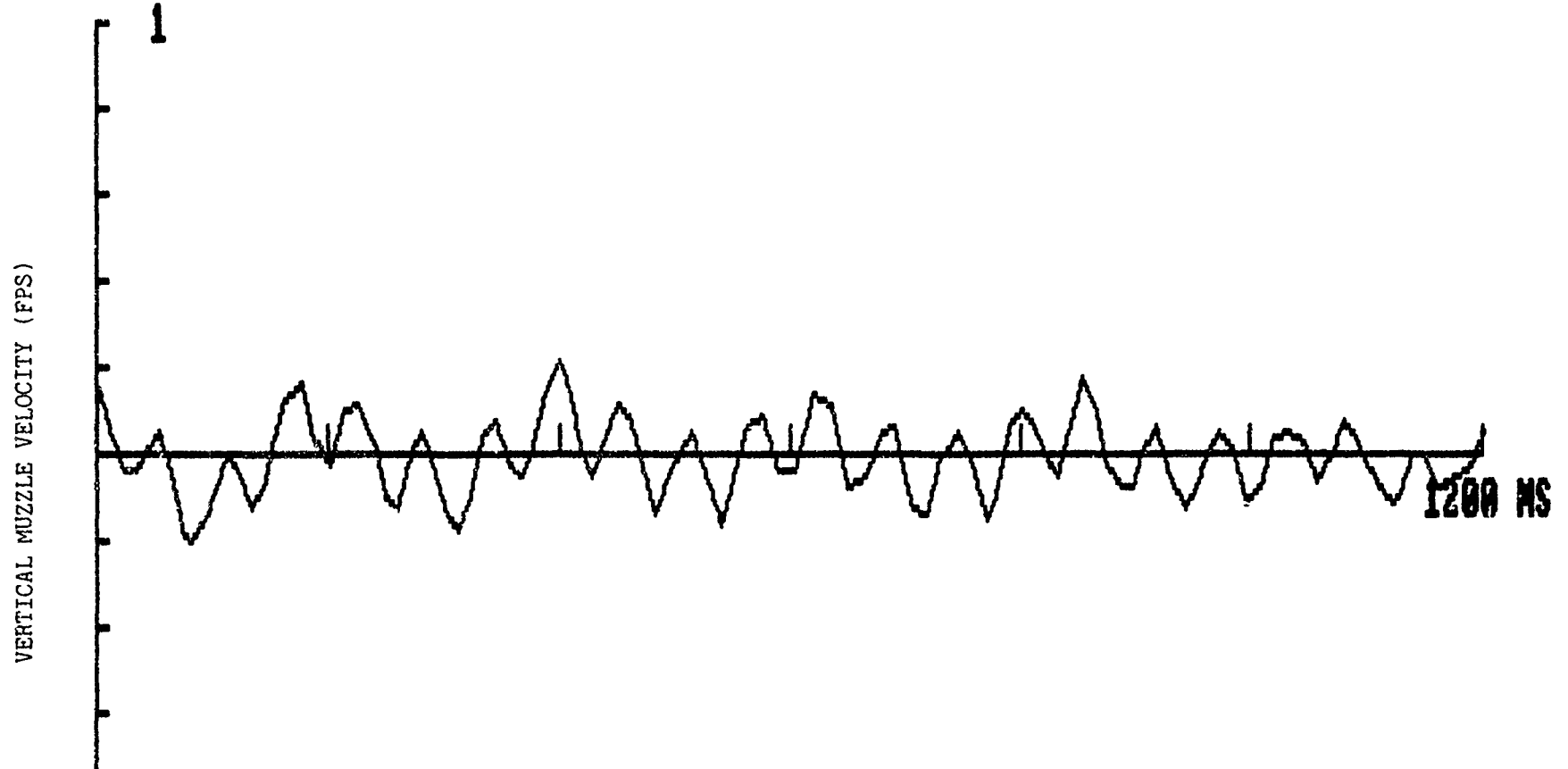

Fig. 24 (Cont'd.)

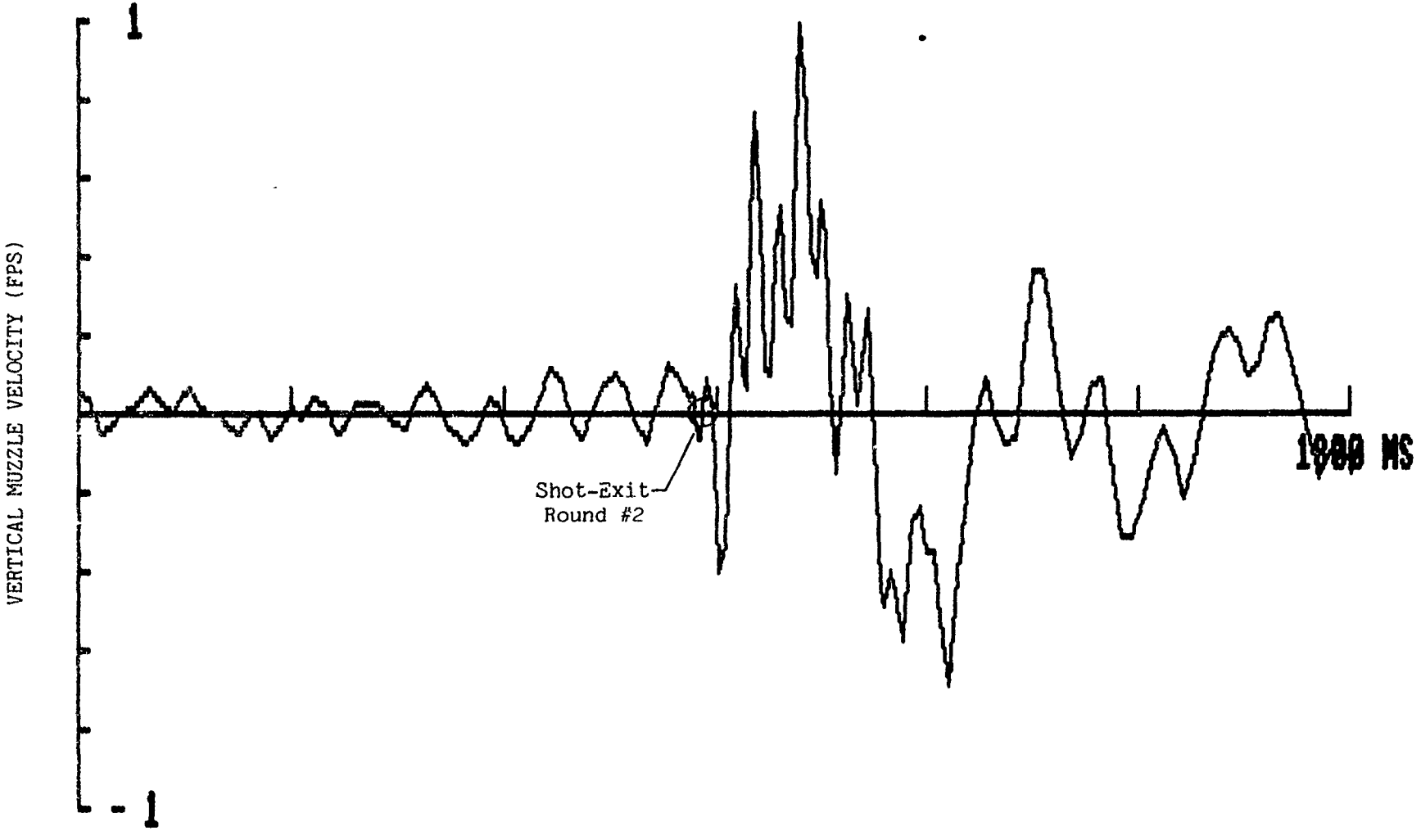

Fig. 24 (Cont'd.)

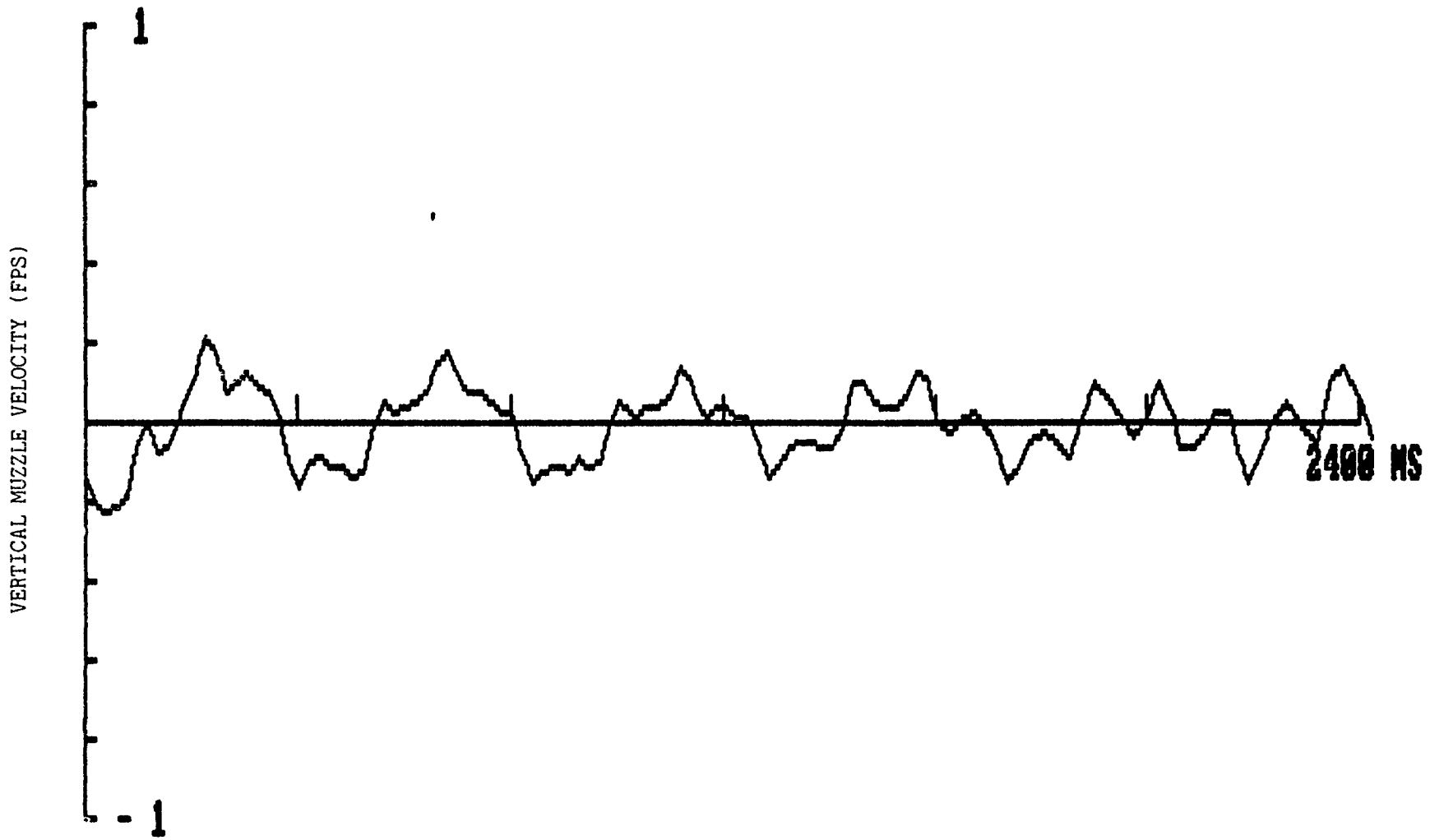

Fig. 24 (Cont'd.)

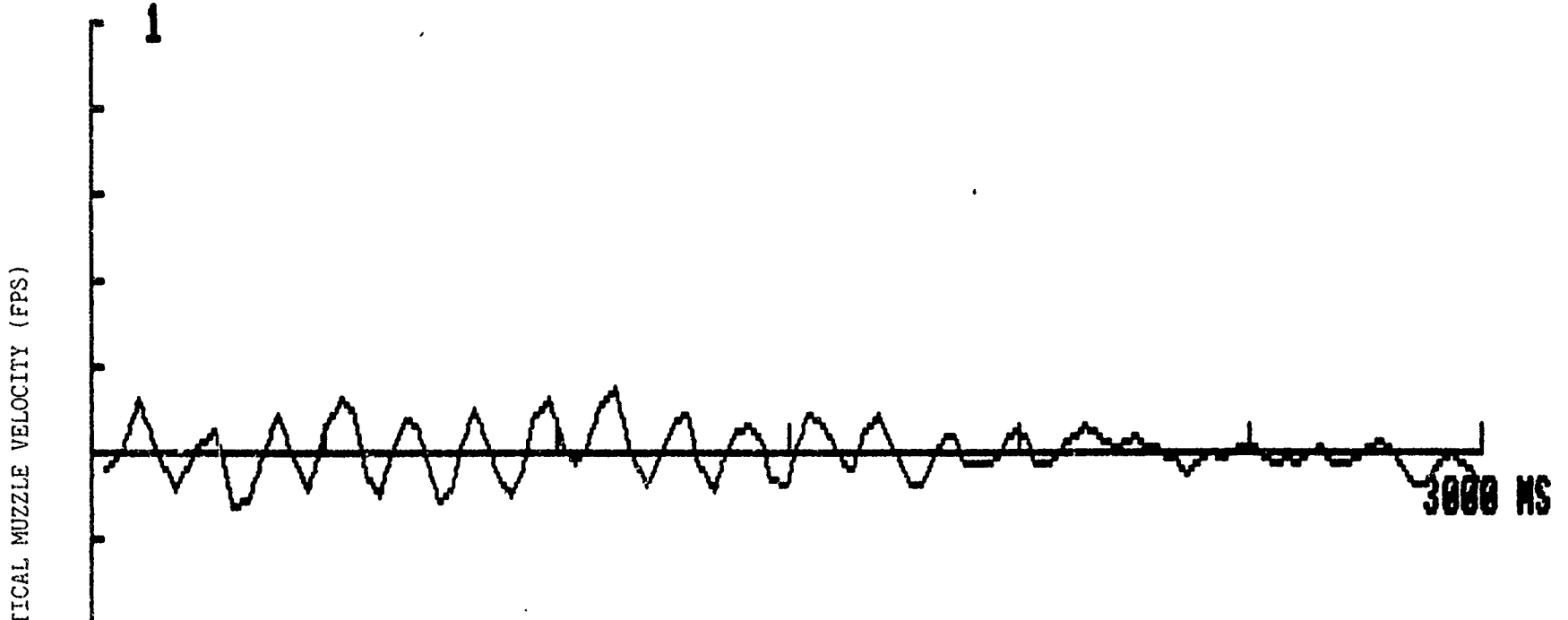

Fig. 24 (Cont'd.)

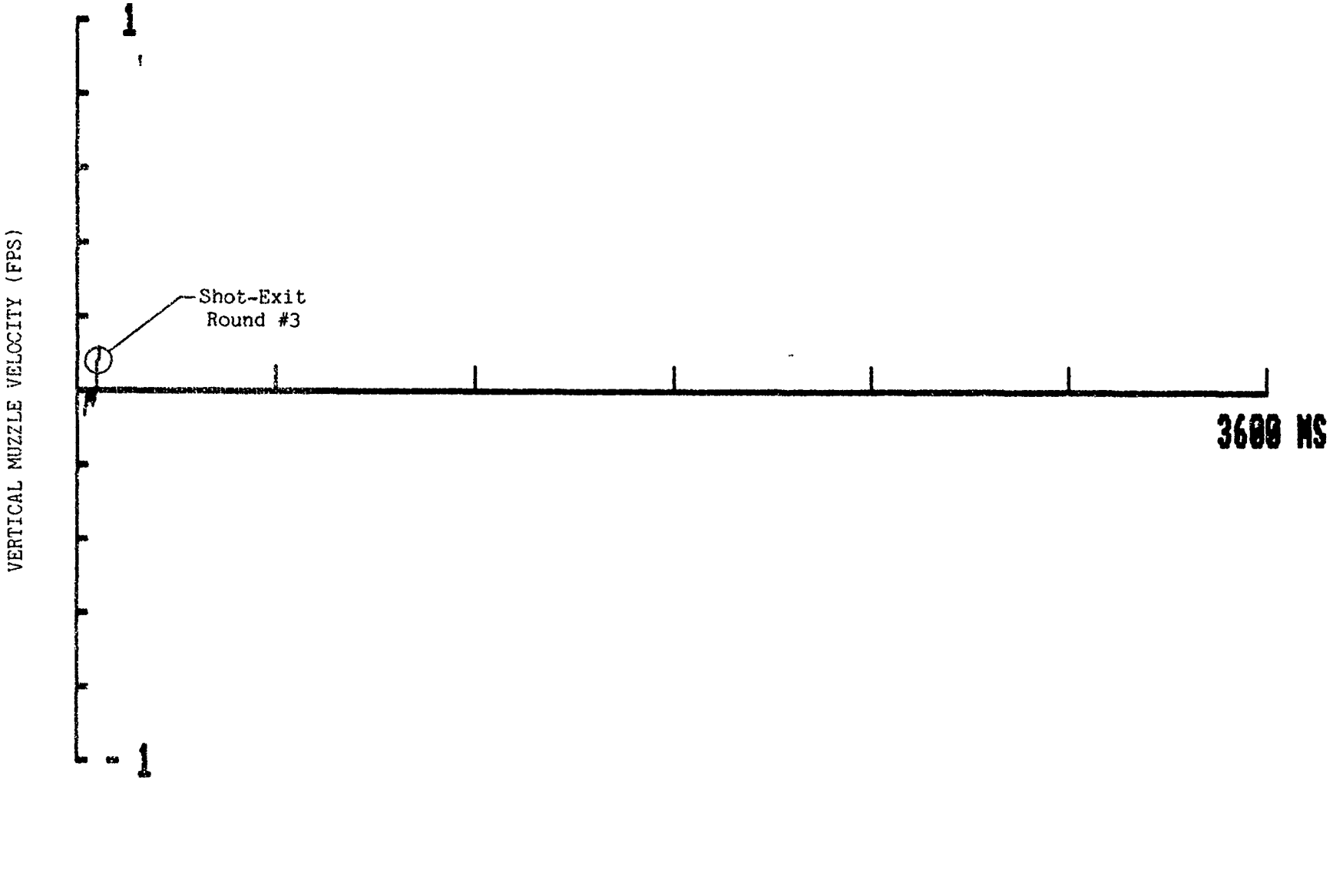

Fig. 24 (Cont'd.)

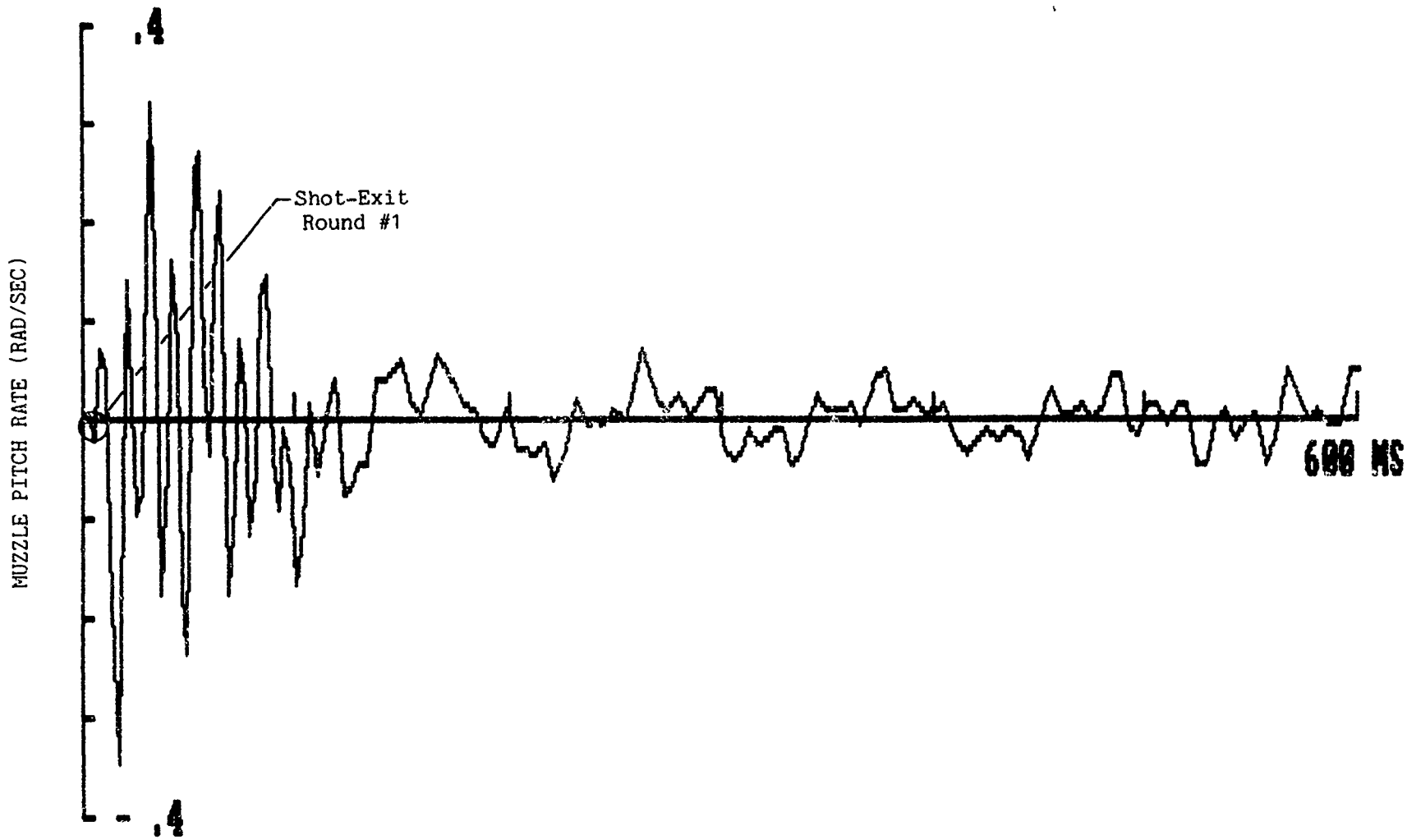

Fig. 25 - Muzzle Pitch Rate for Three-Round Burst With Combined Vertical and Horizontal-Plane "Windows"

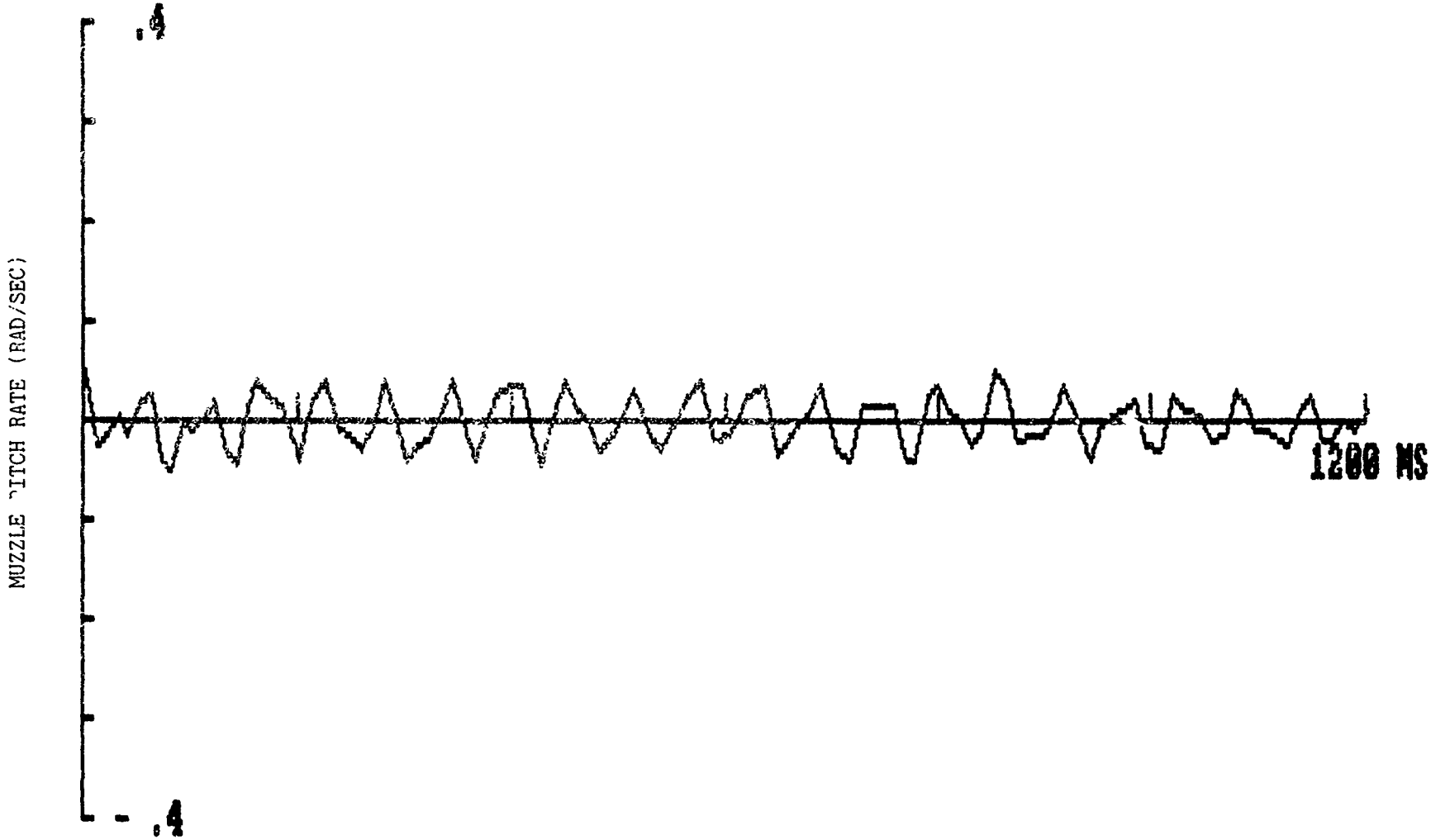

Fig. 25 (Cont'd.)

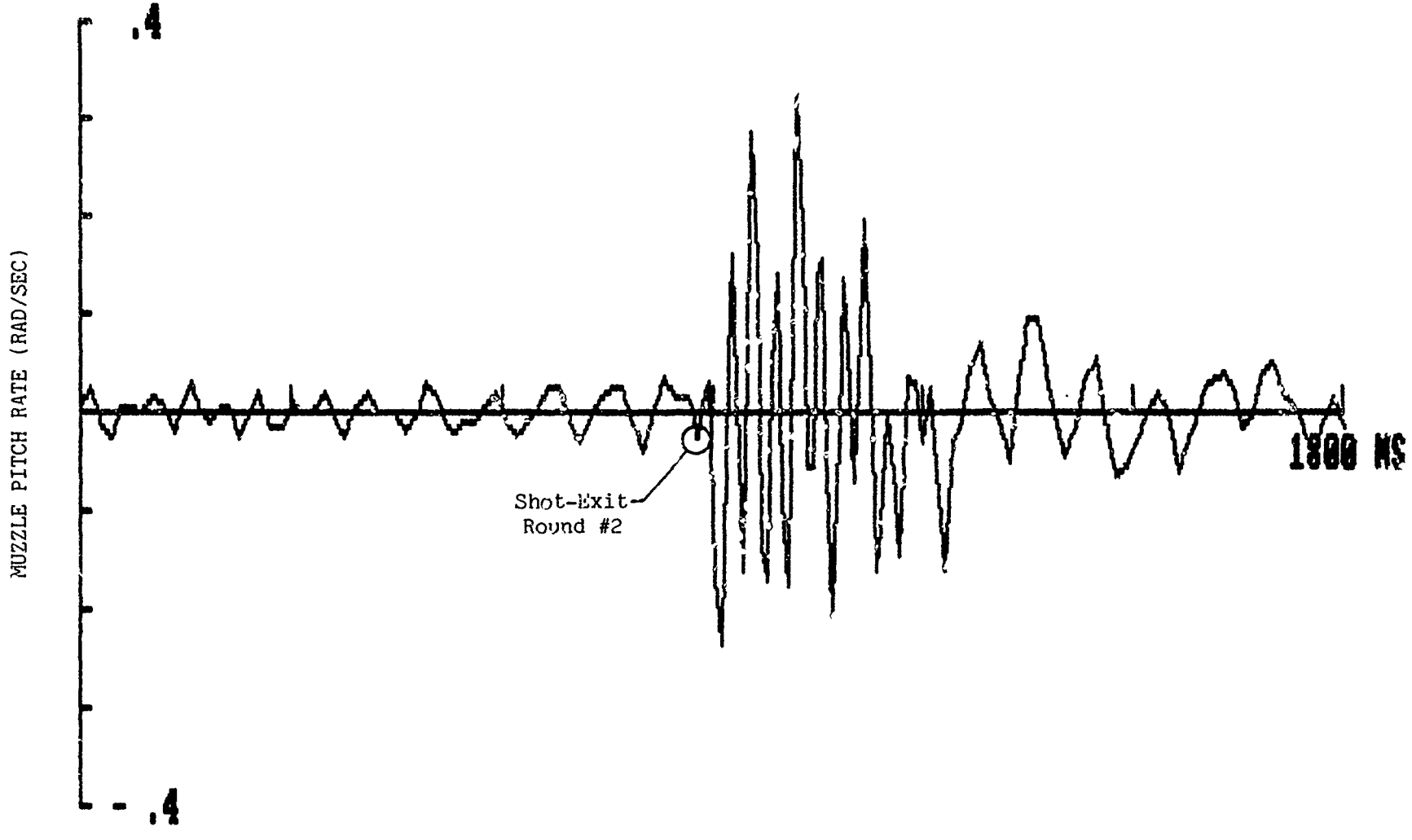

Fig. 25 (Cont'd.)

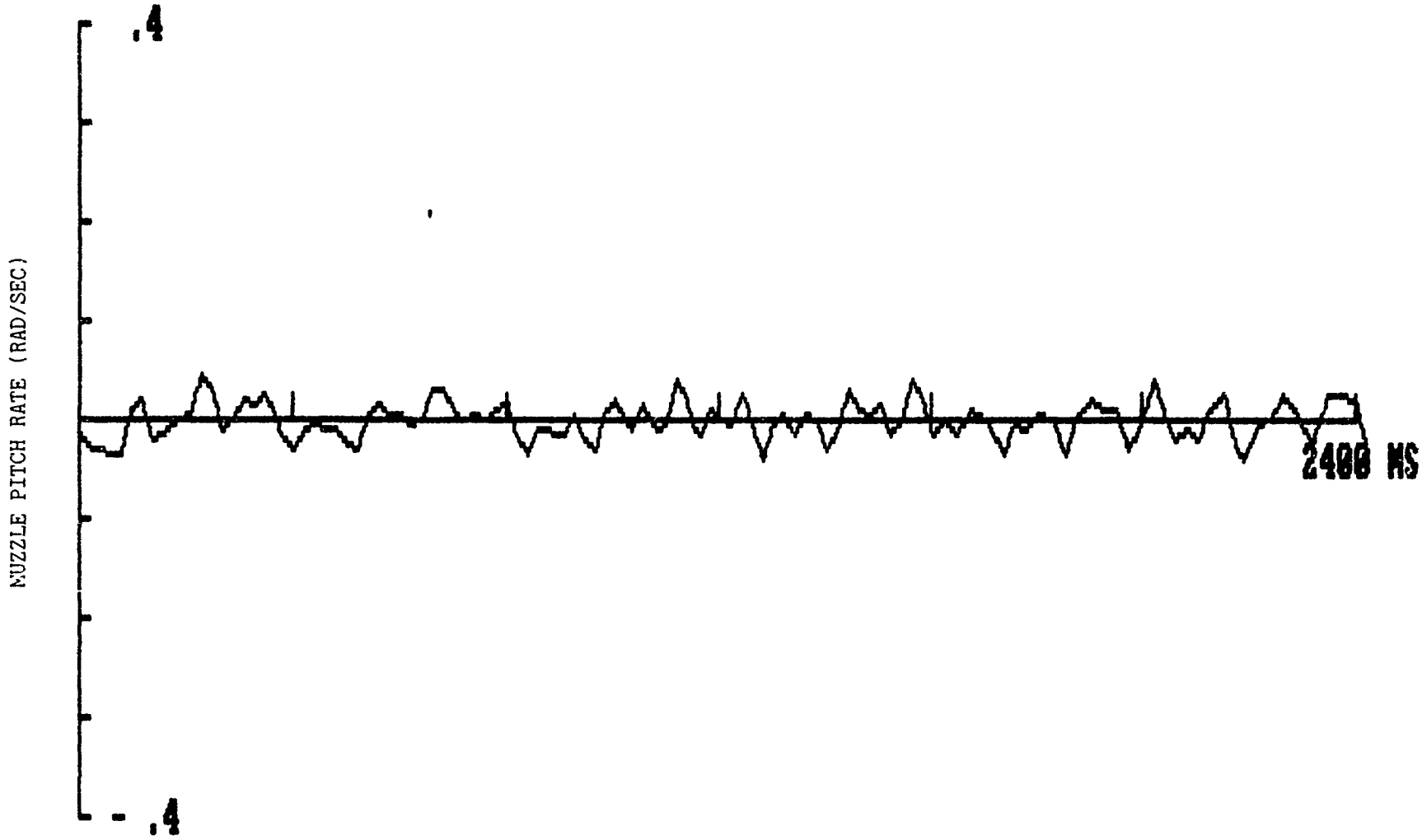

Fig. 25 (Cont'd.)

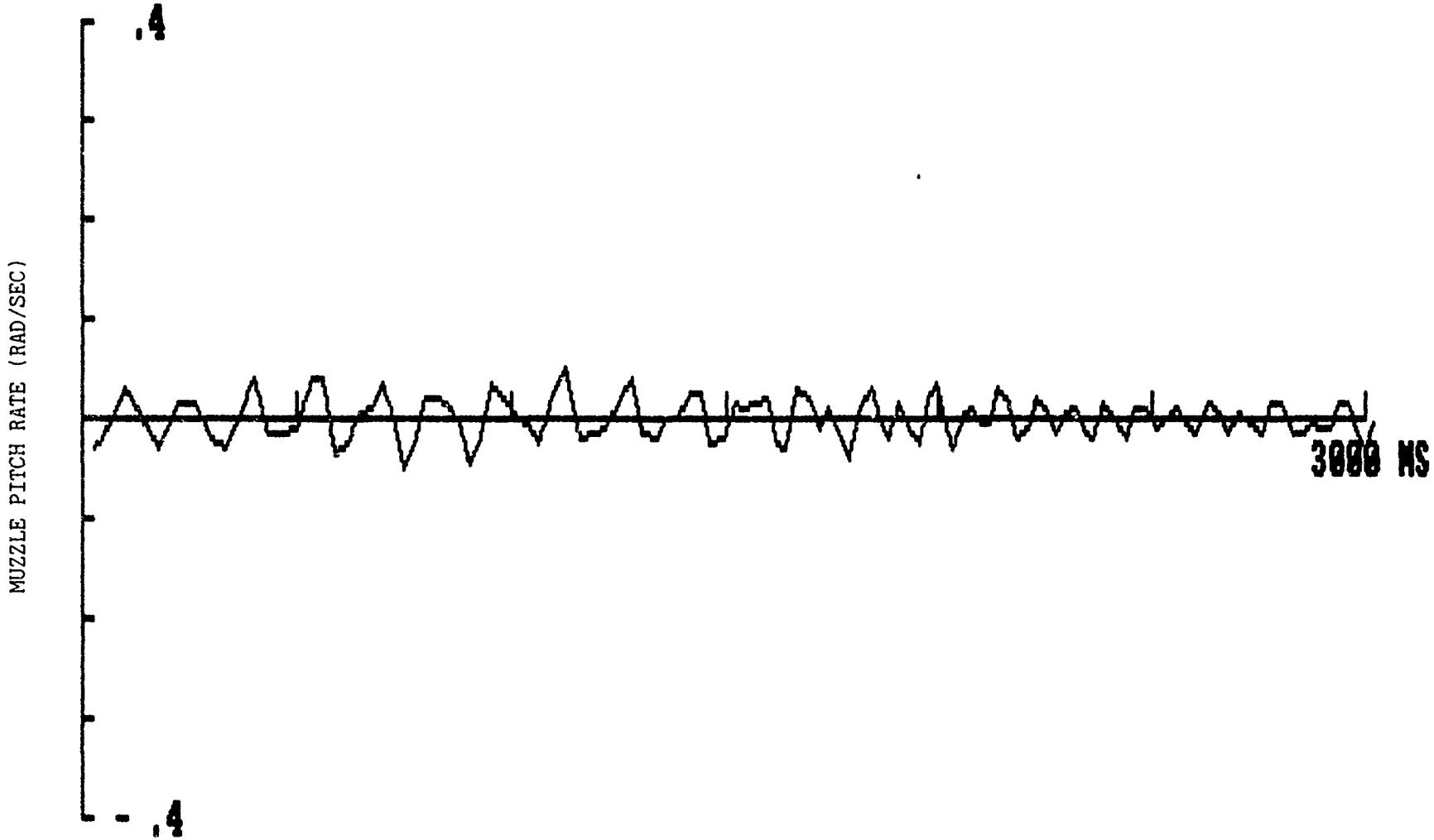

Fig. 25 (Cont'd.)

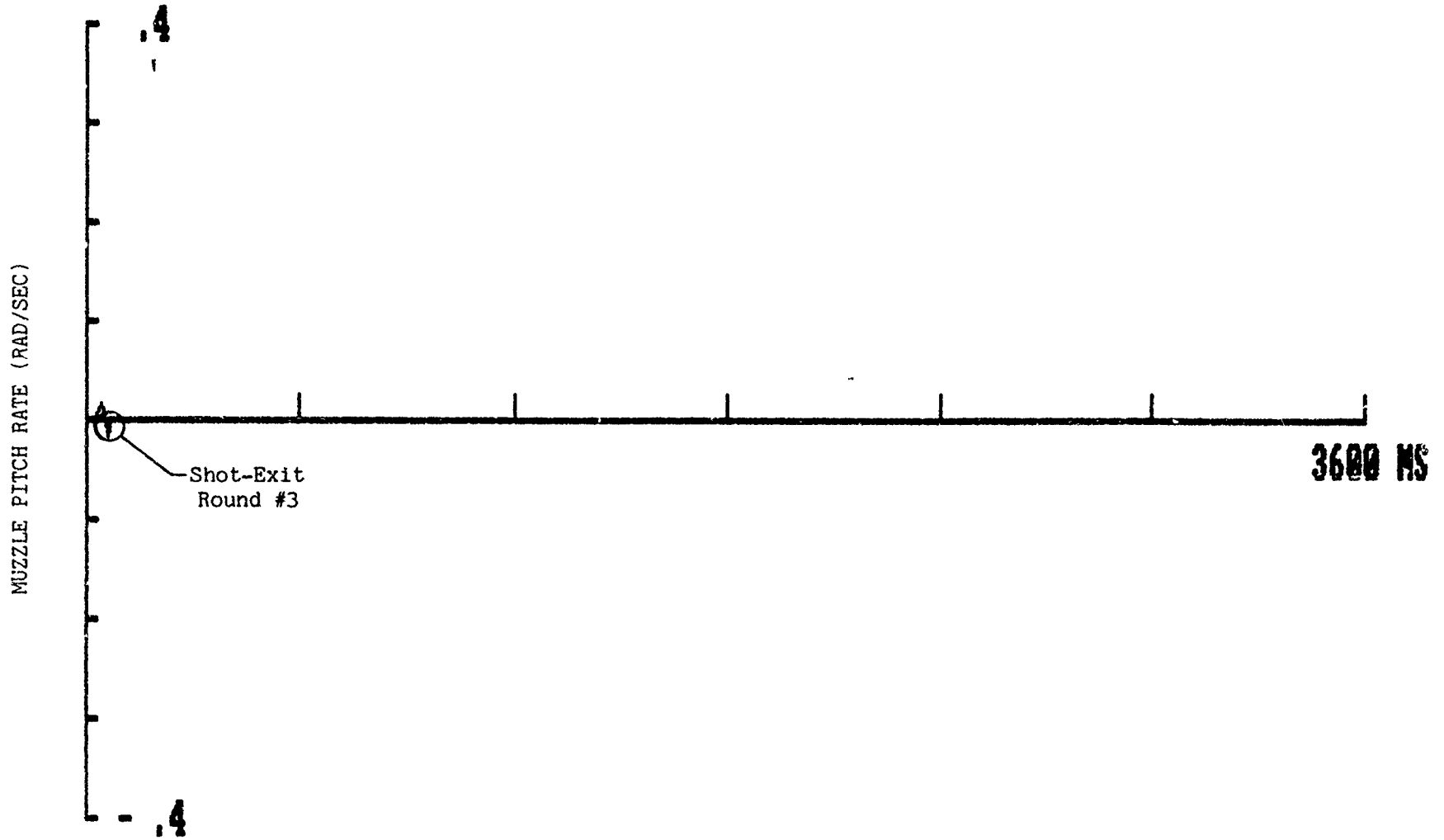

Fig. 25 (Cont'd.)

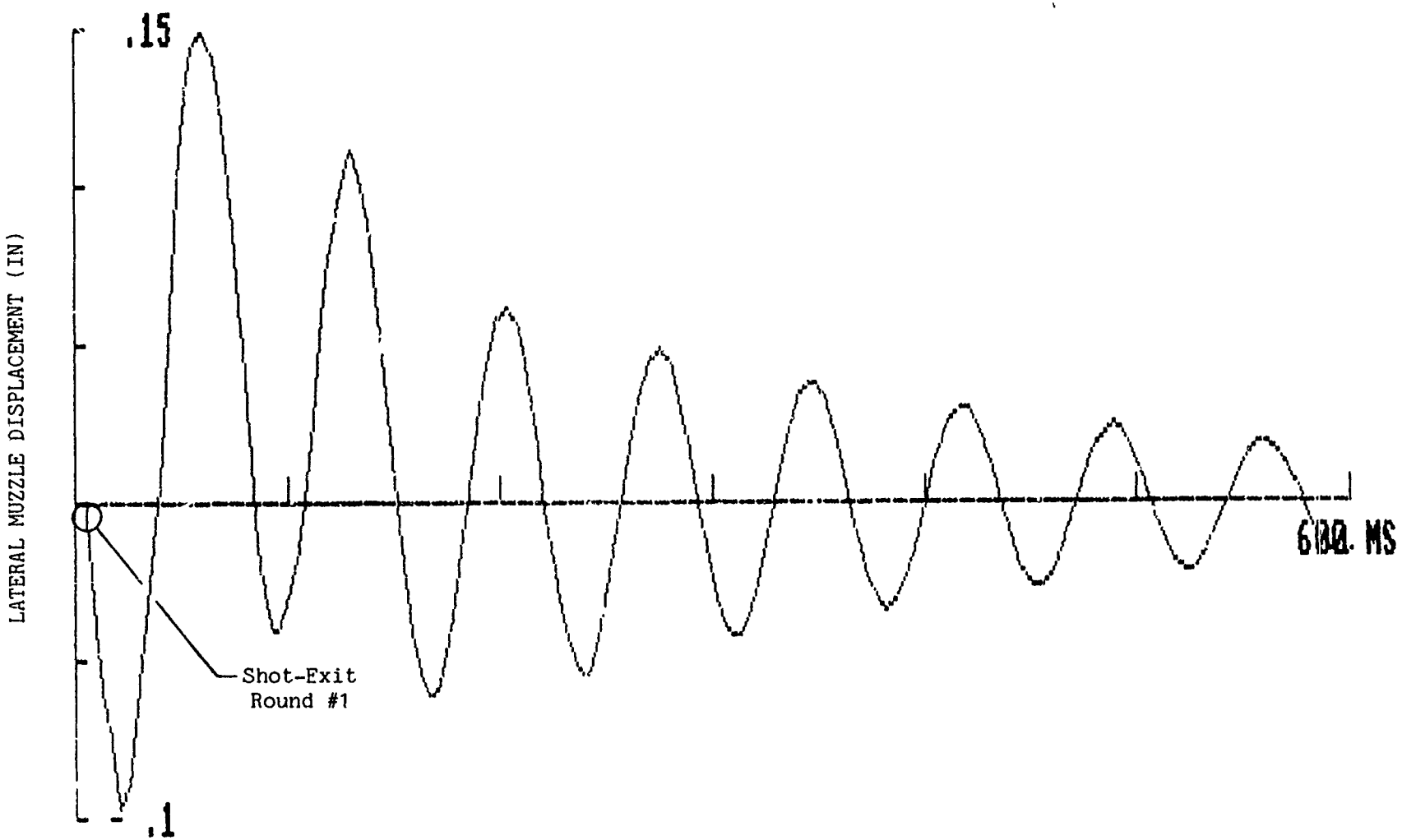

Fig. 26 - Lateral Muzzle Displacement for Three-Round Burst Without Firing Control Signal

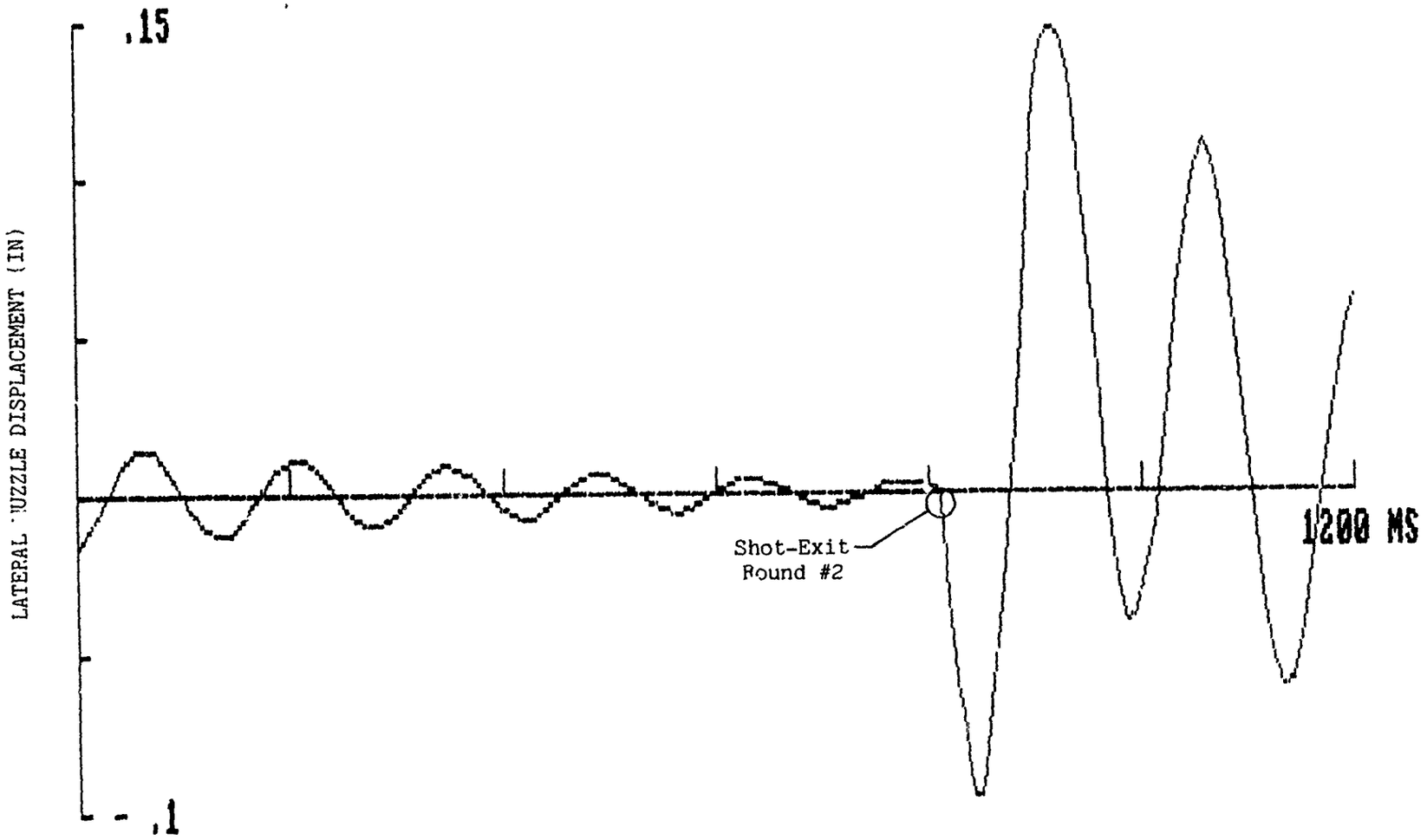
.15
LATERAL MUZZLE DISPLACEMENT (IN)
- .1
Shot-Exit
Round #2
1200 MS

Fig. 26 (Cont'd.)

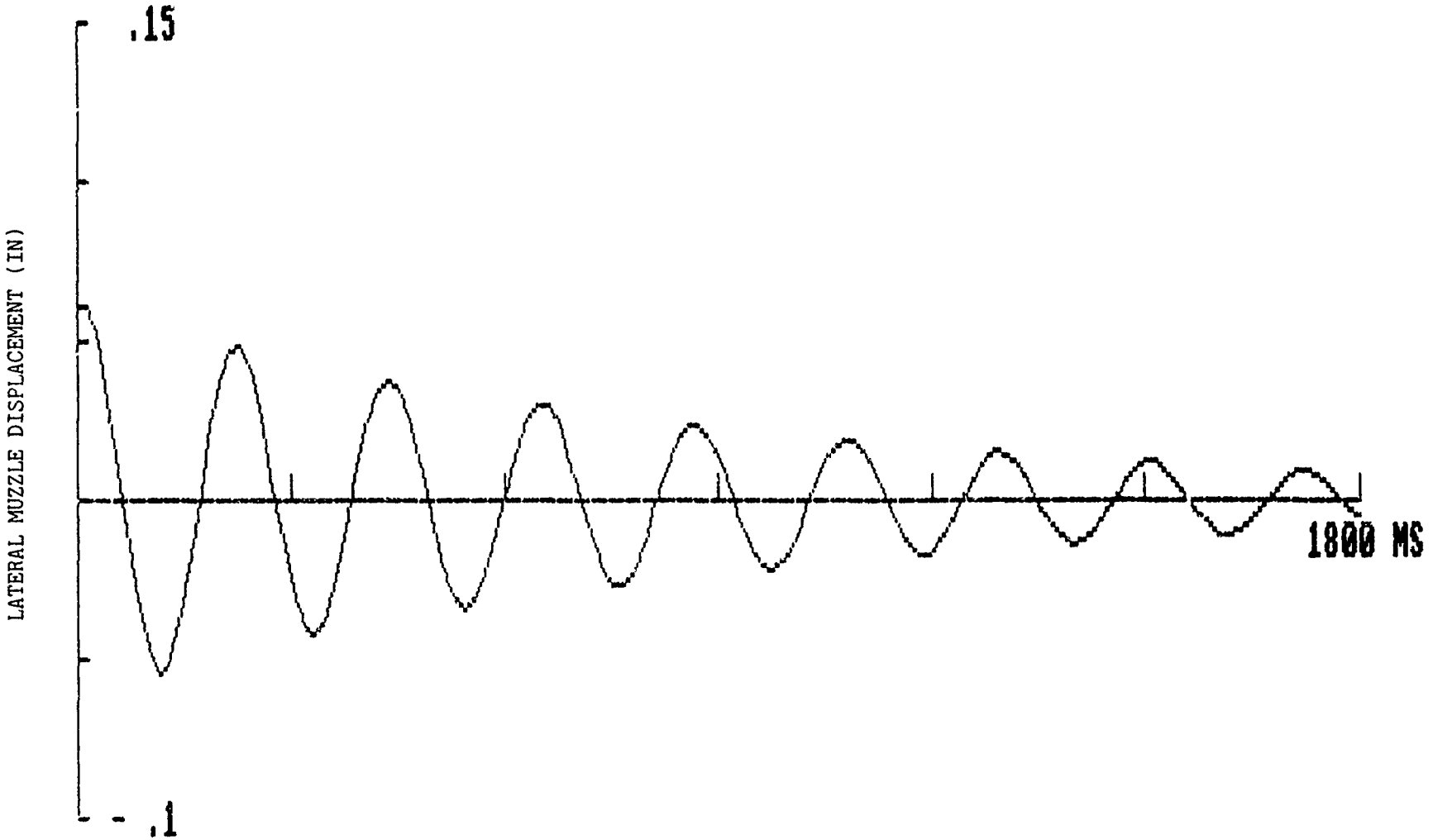

Fig. 26 (Cont'd.)

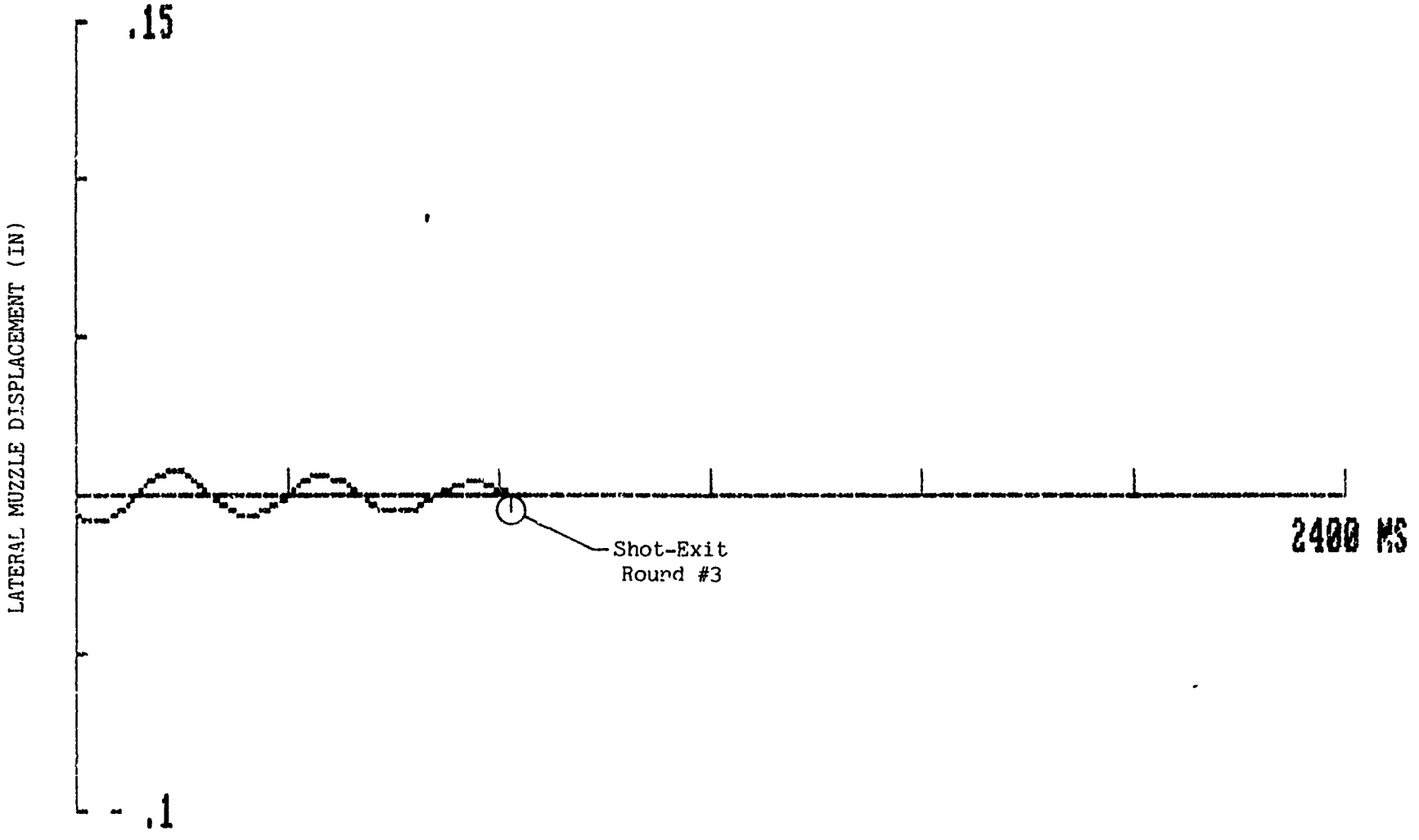
.15
LATERAL MUZZLE DISPLACEMENT (IN)
Shot-Exit
Round #3
2400 MS
- .1

Fig. 26 (Cont'd.)

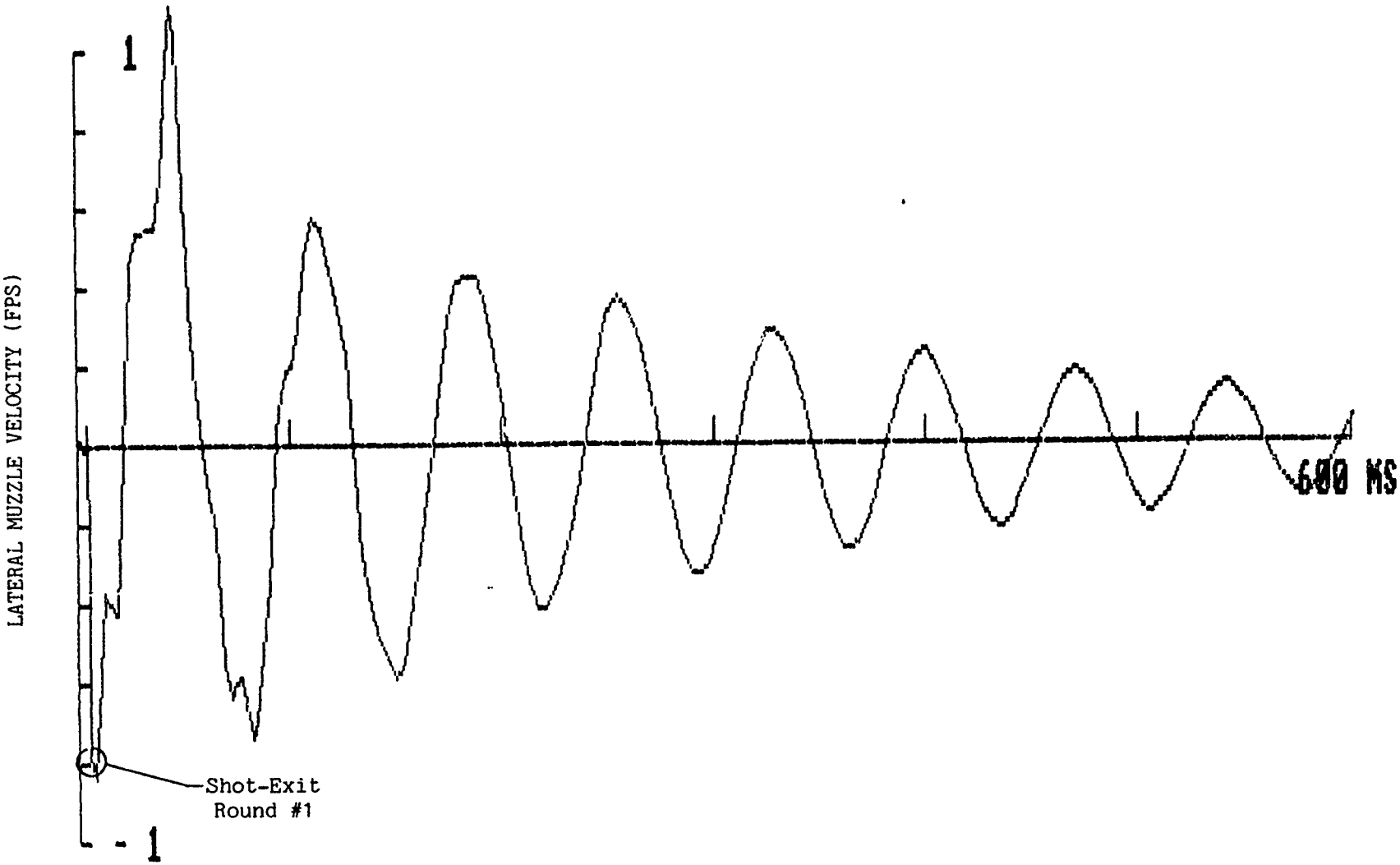

Fig. 27 - Lateral Muzzle Velocity for Three-Round Burst Without Firing Control Signal

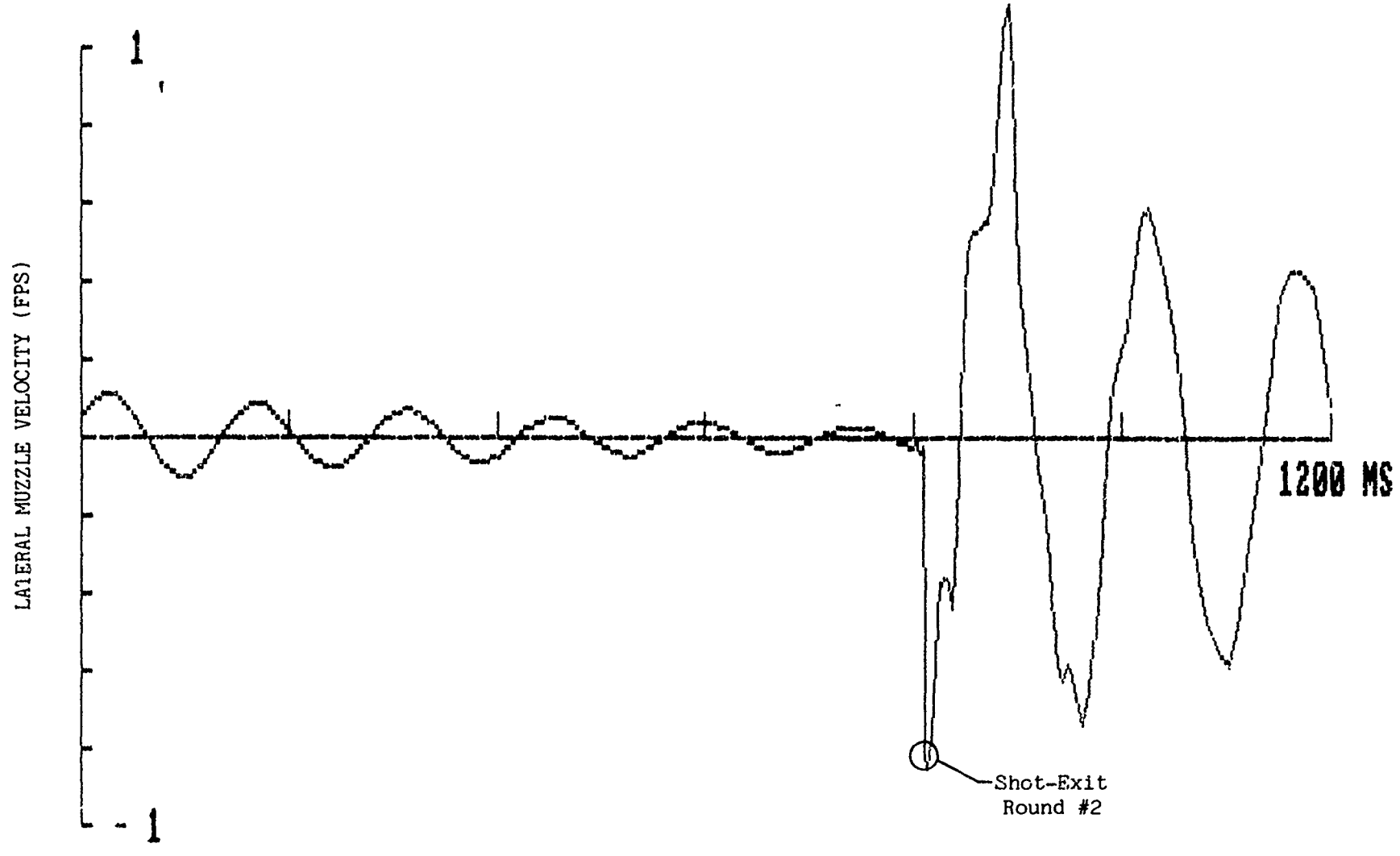

Fig. 27 (Cont'd.)

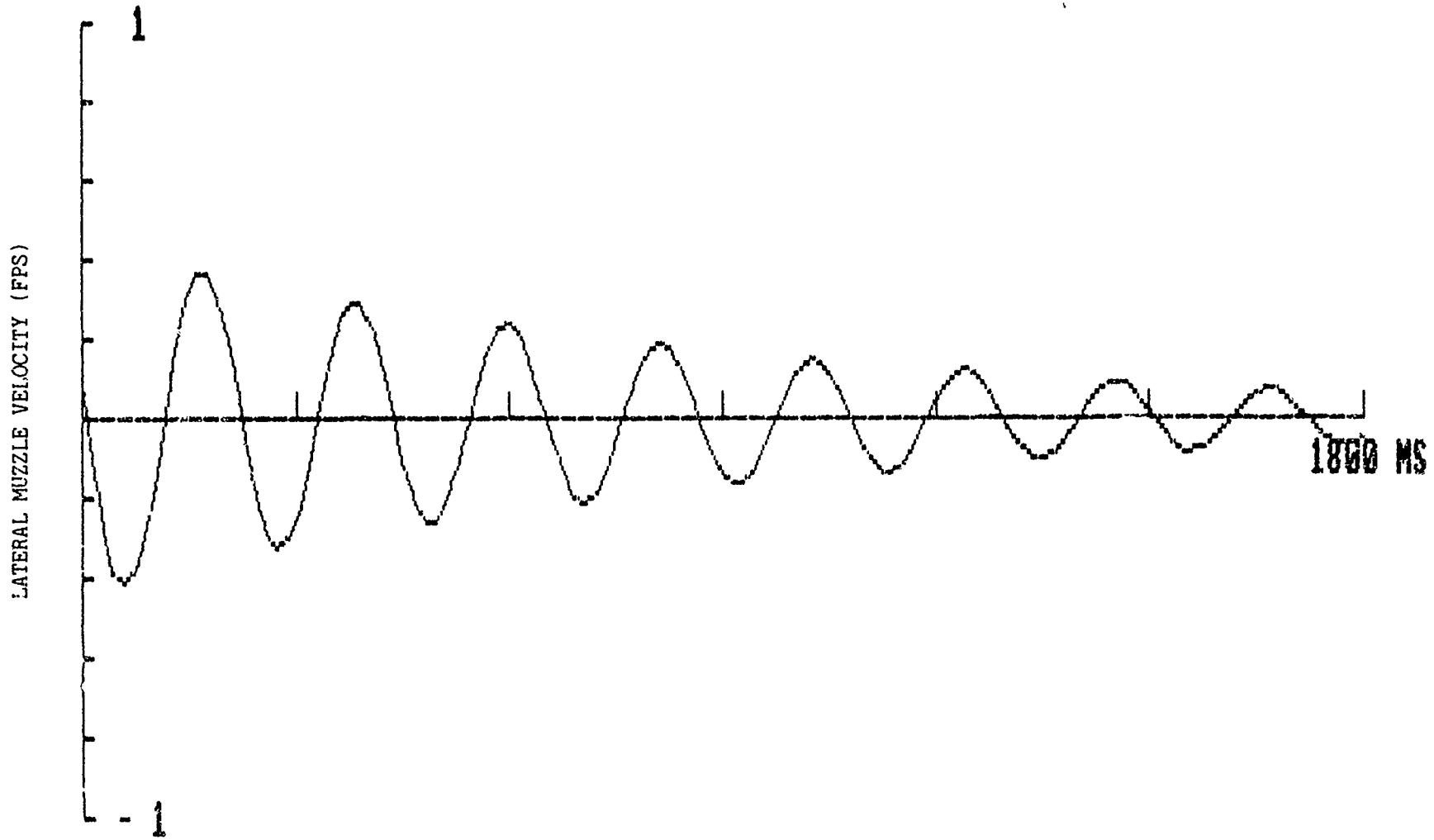

Fig. 27 (Cont'd.)

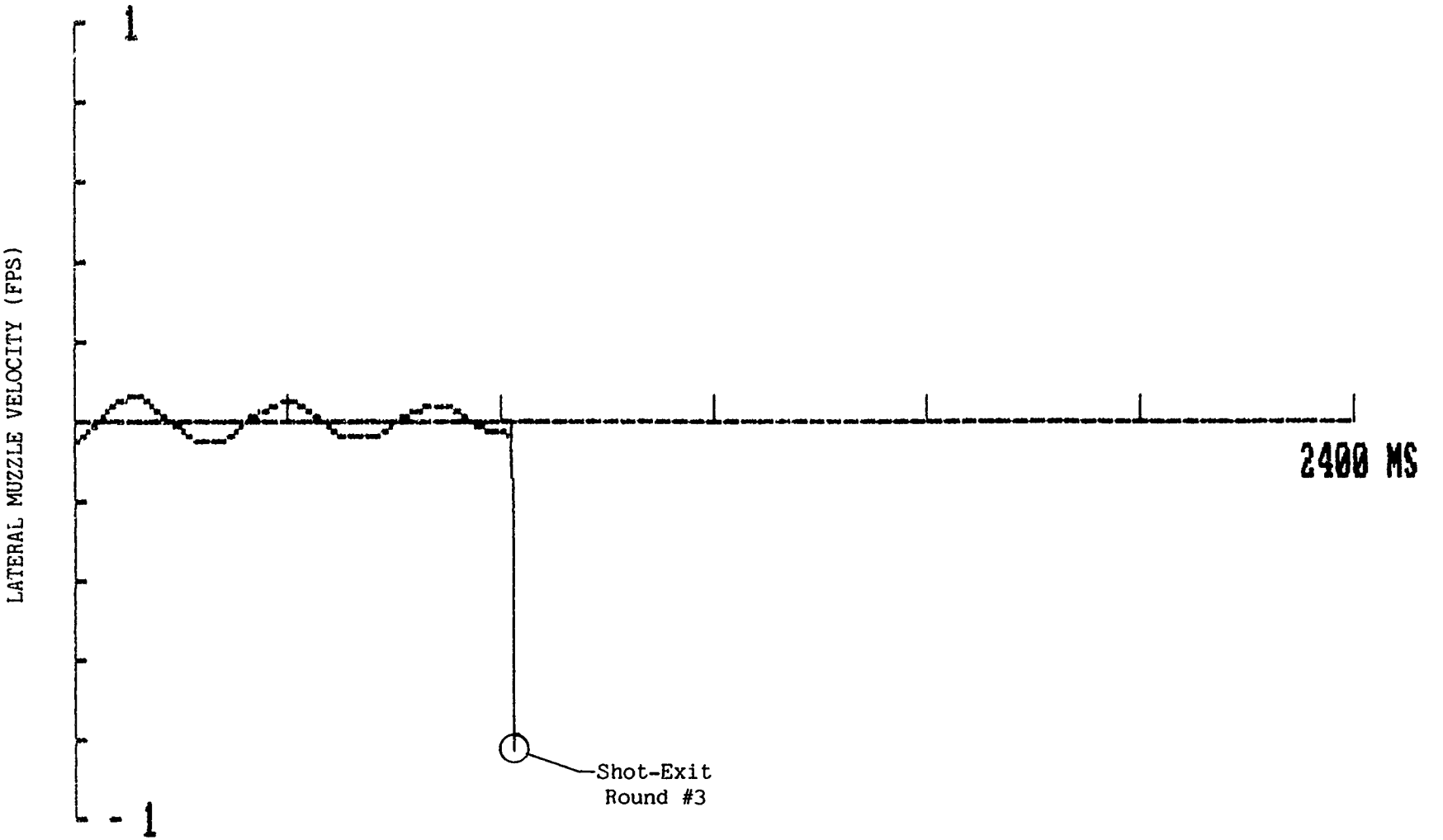

Fig. 27 (Cont'd.)

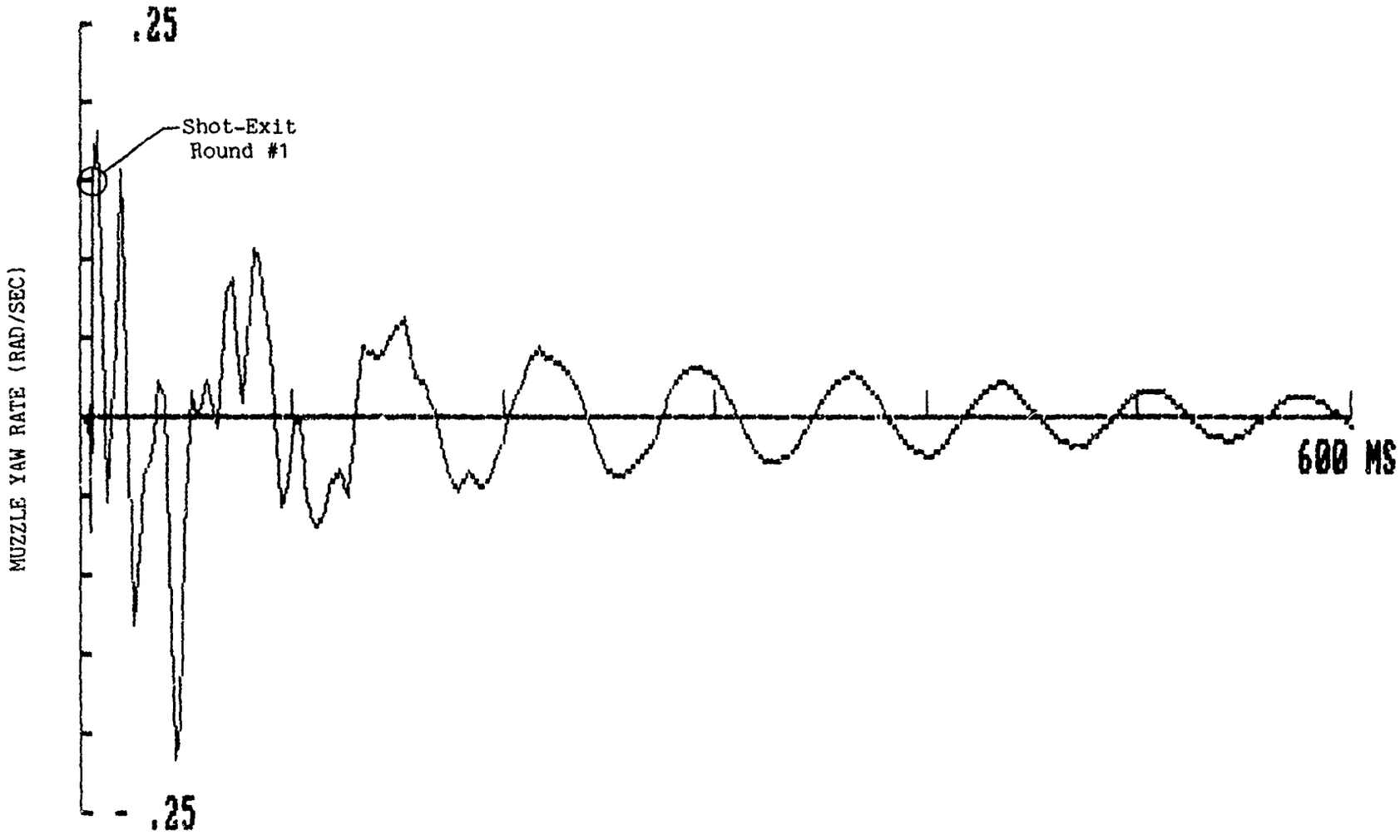

Fig. 28 - Muzzle Yaw Rate for Three-Round Burst Without Firing Control Signal

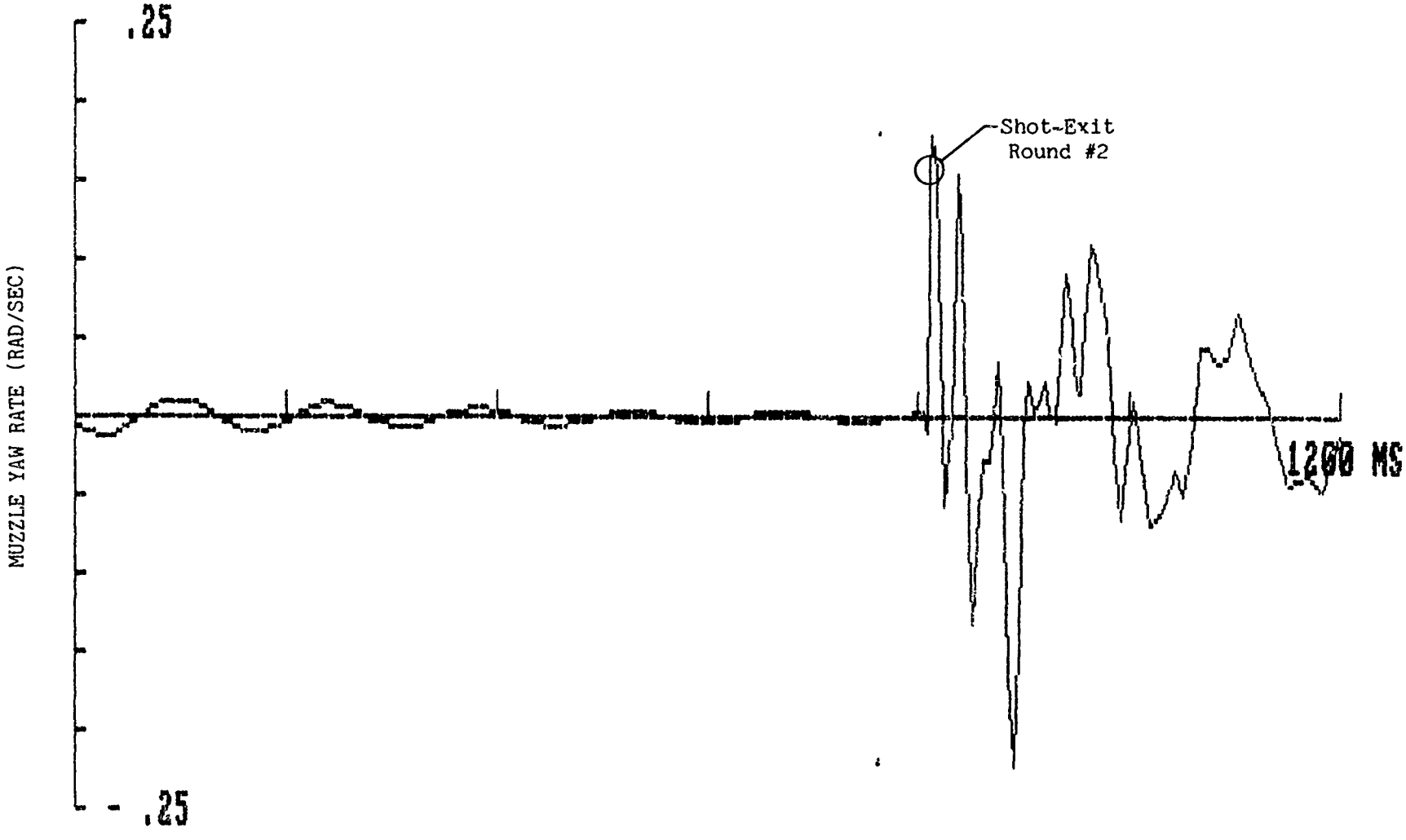

Fig. 28 (Cont'd.)

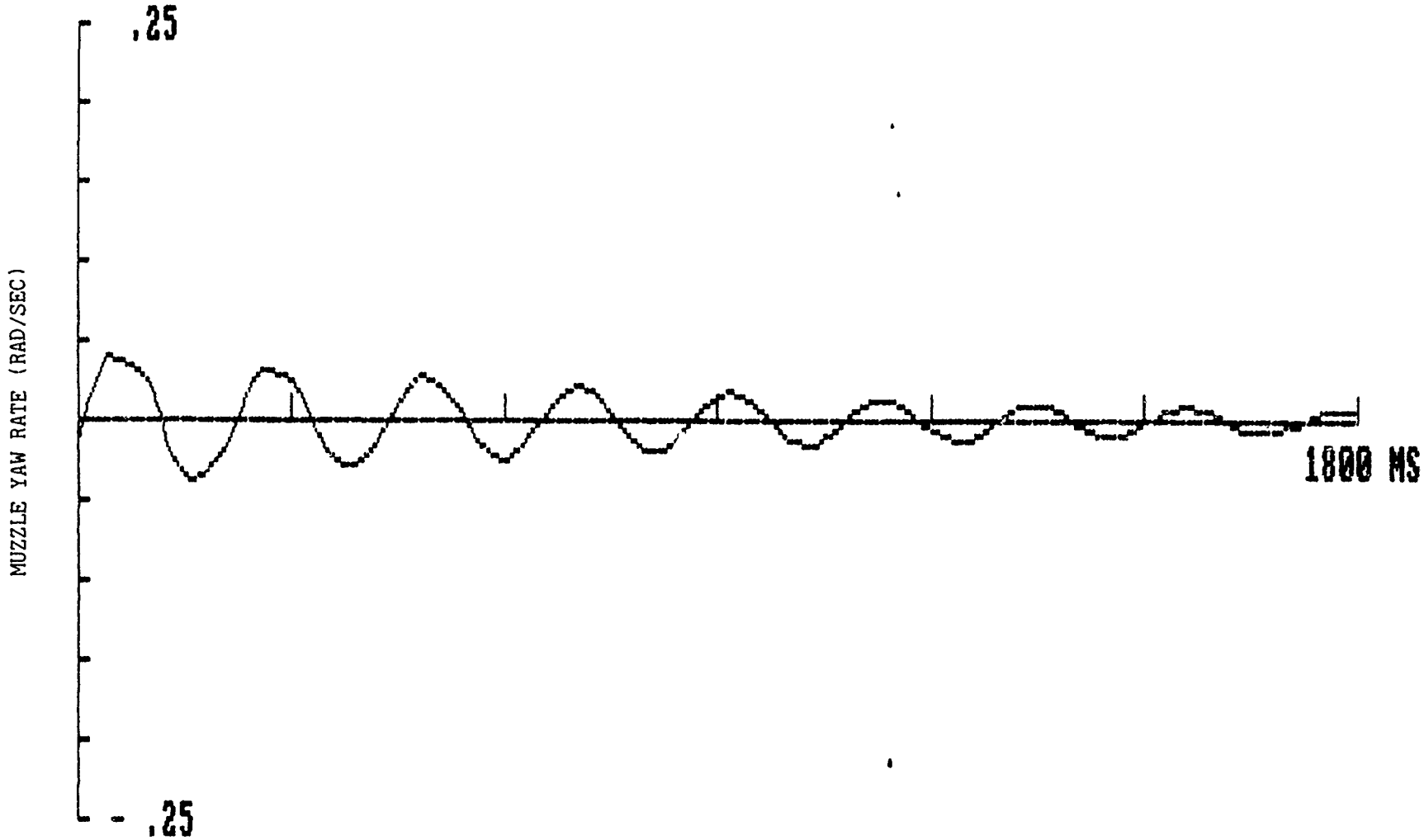

Fig. 28 (Cont'd.)

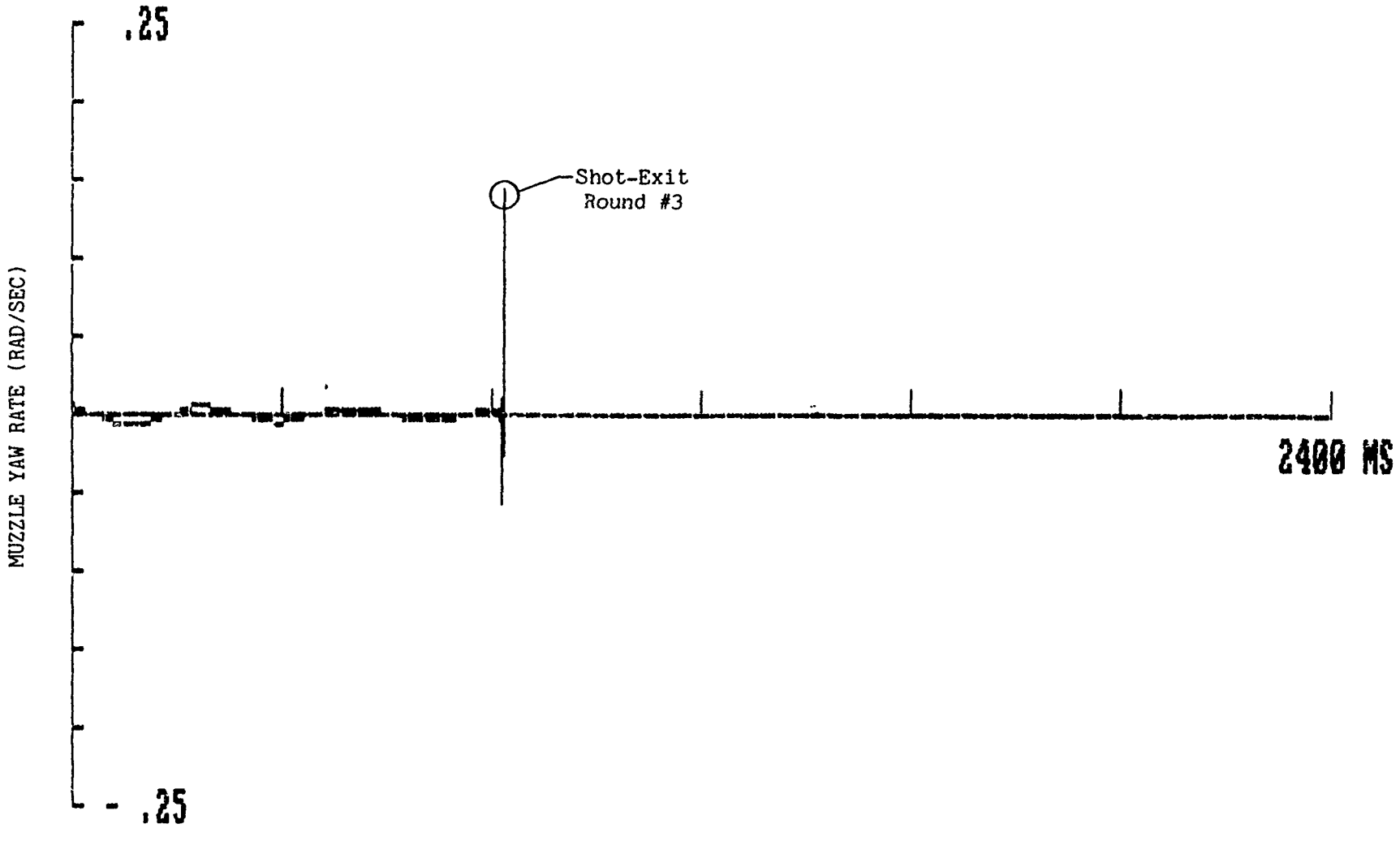

Fig. 28 (Cont'd.)

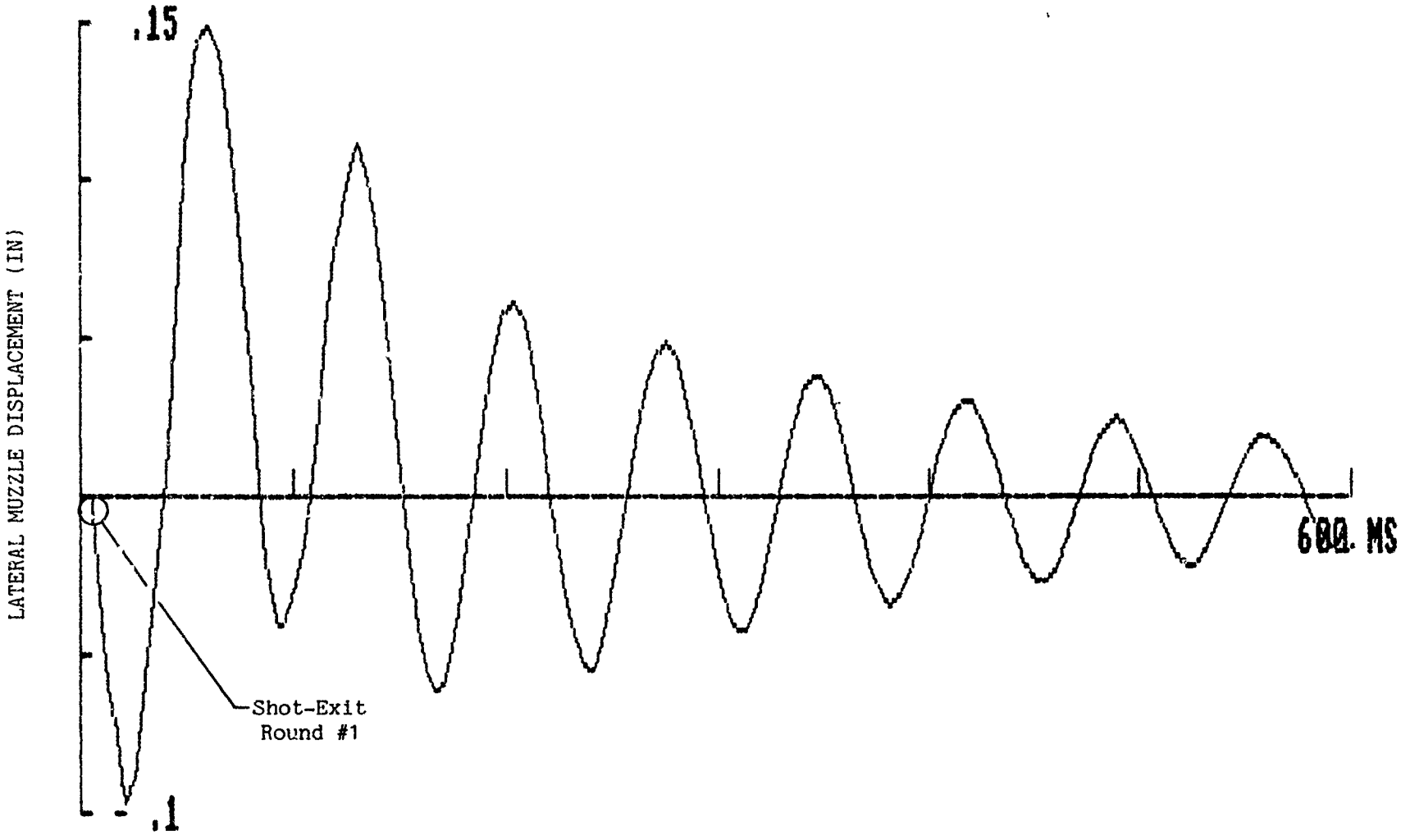

Fig. 29 - Lateral Muzzle Displacement for Three-Round Burst With Vertical-Plane "Window"

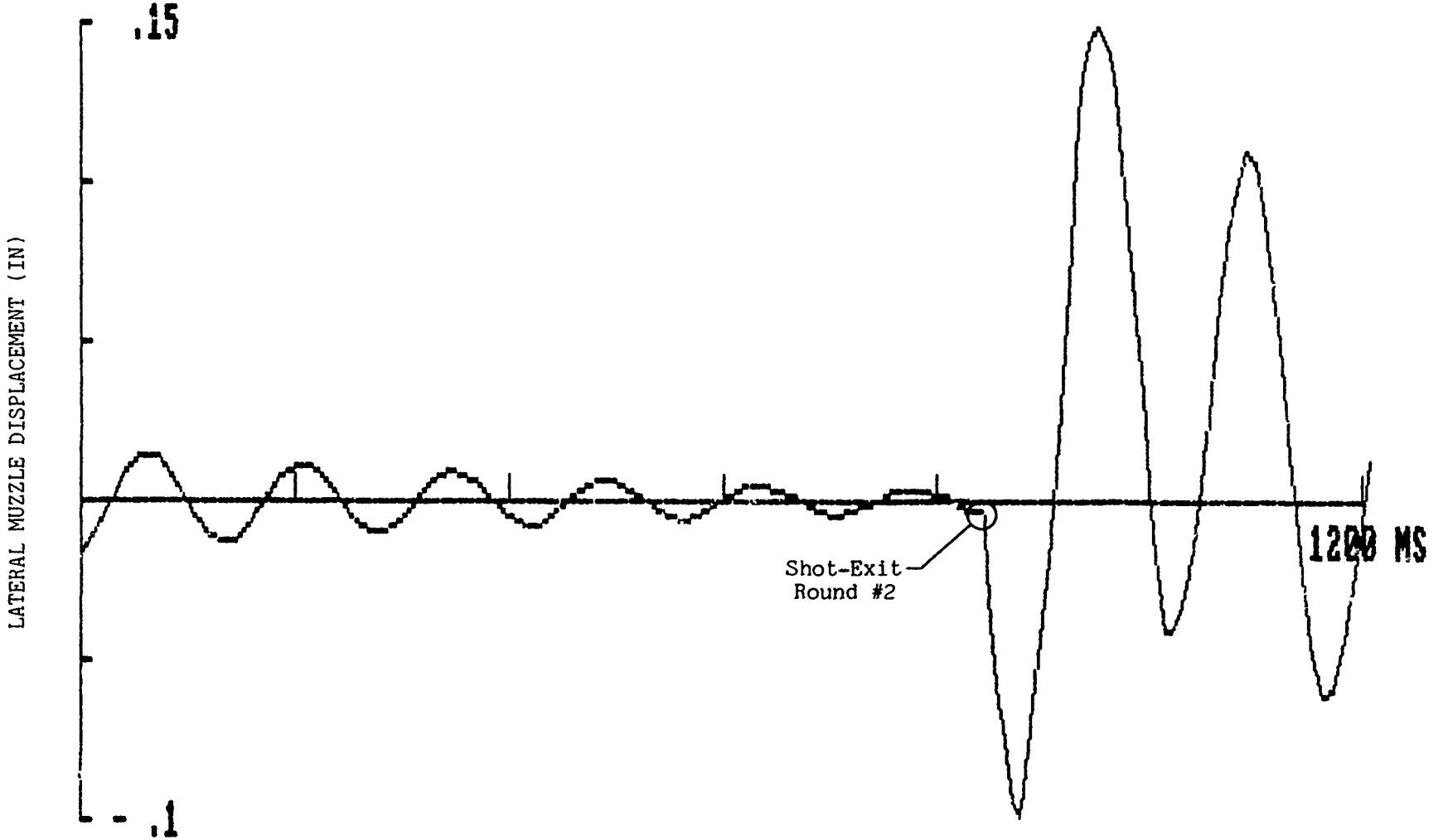
.15
LATERAL MUZZLE DISPLACEMENT (IN)
- .1
Shot-Exit
Round #2
1200 MS

Fig. 29 (Cont'd.)

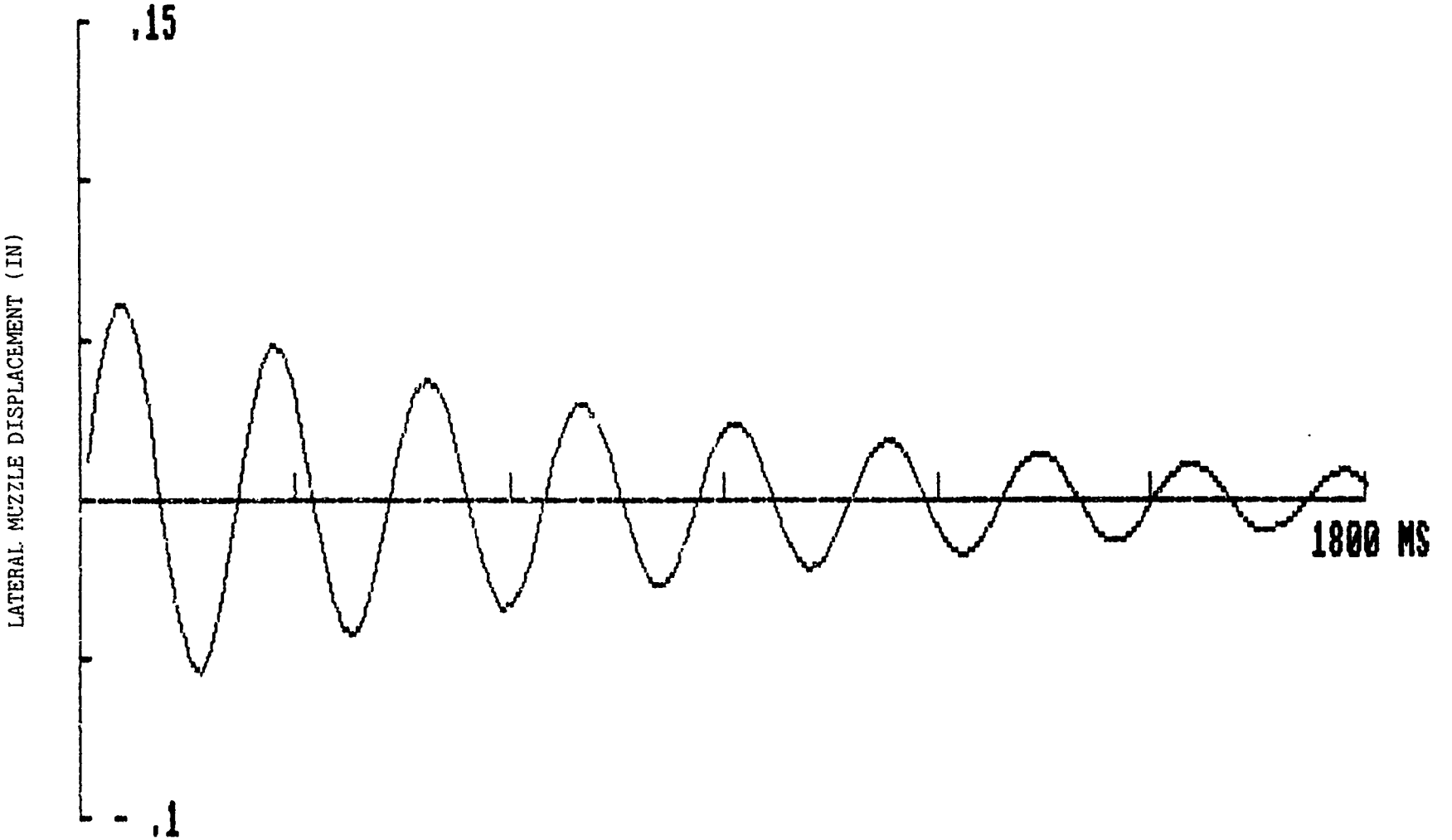

Fig. 29 (Cont'd.)

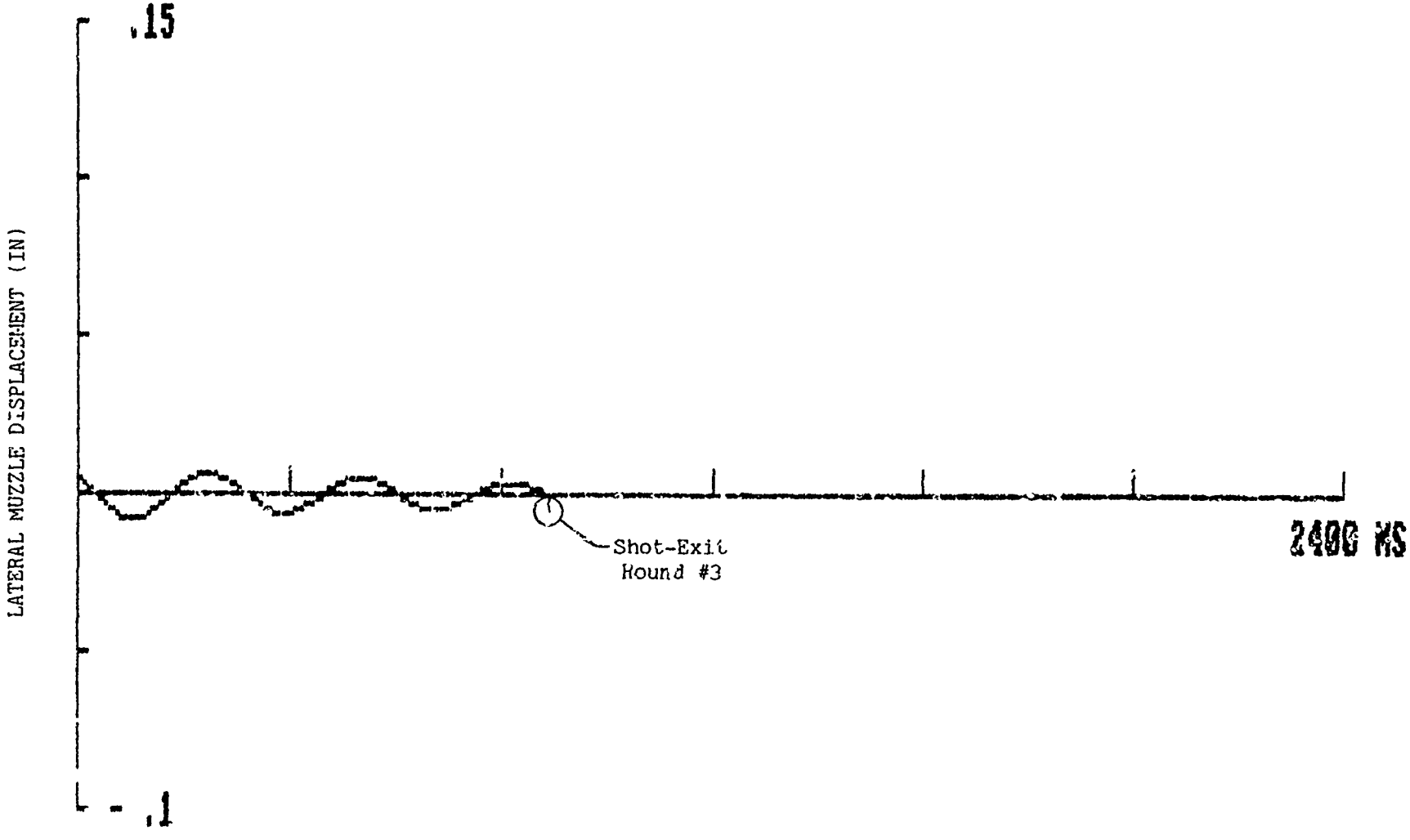
.15
LATERAL MUZZLE DISPLACEMENT (IN)
- .1
Shot-Exit
Round #3
2400 MS

Fig. 29 (Cont'd.)

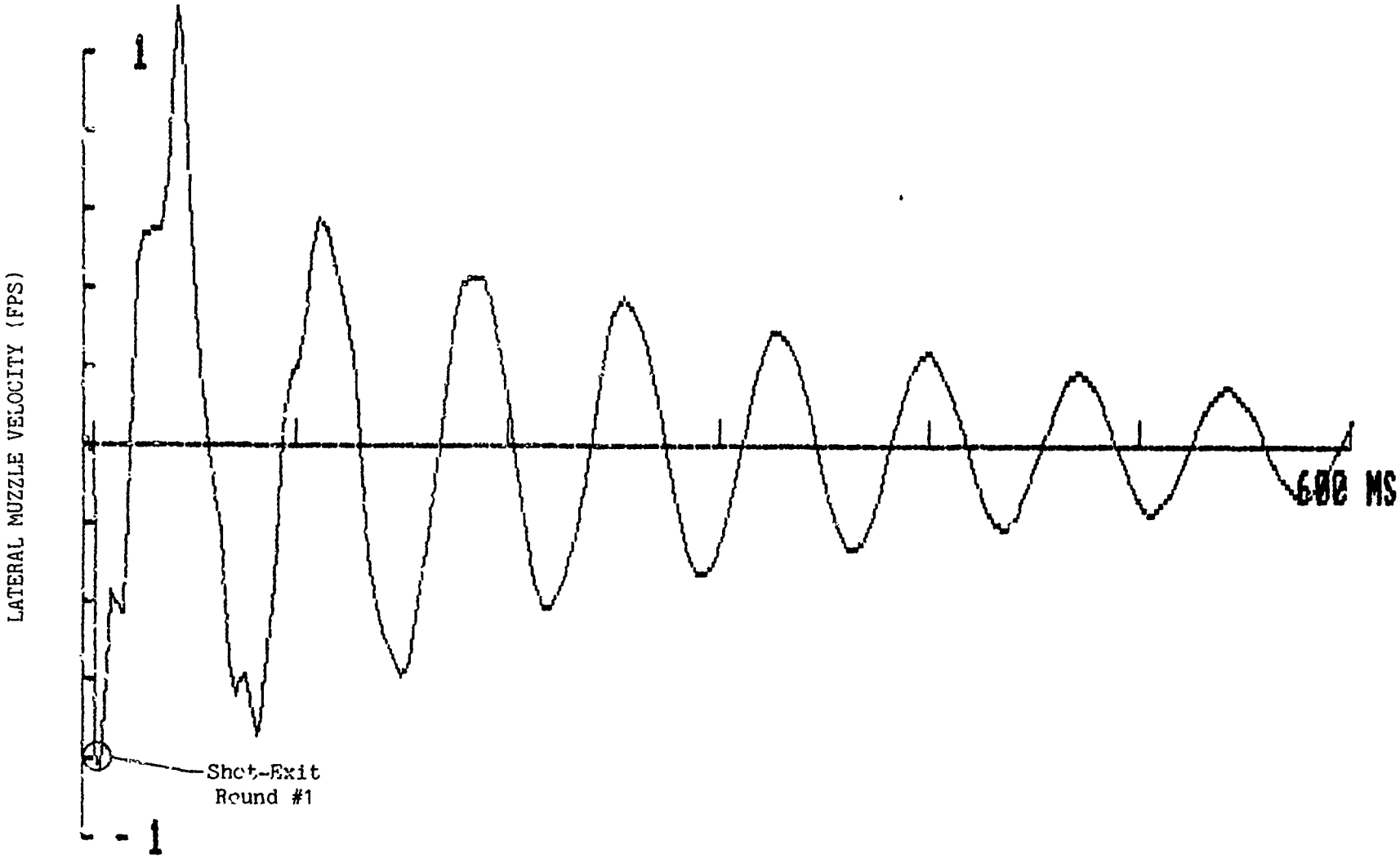

Fig. 30 - Lateral Muzzle Velocity for Three-Round Burst With Vertical-Plane "Window"

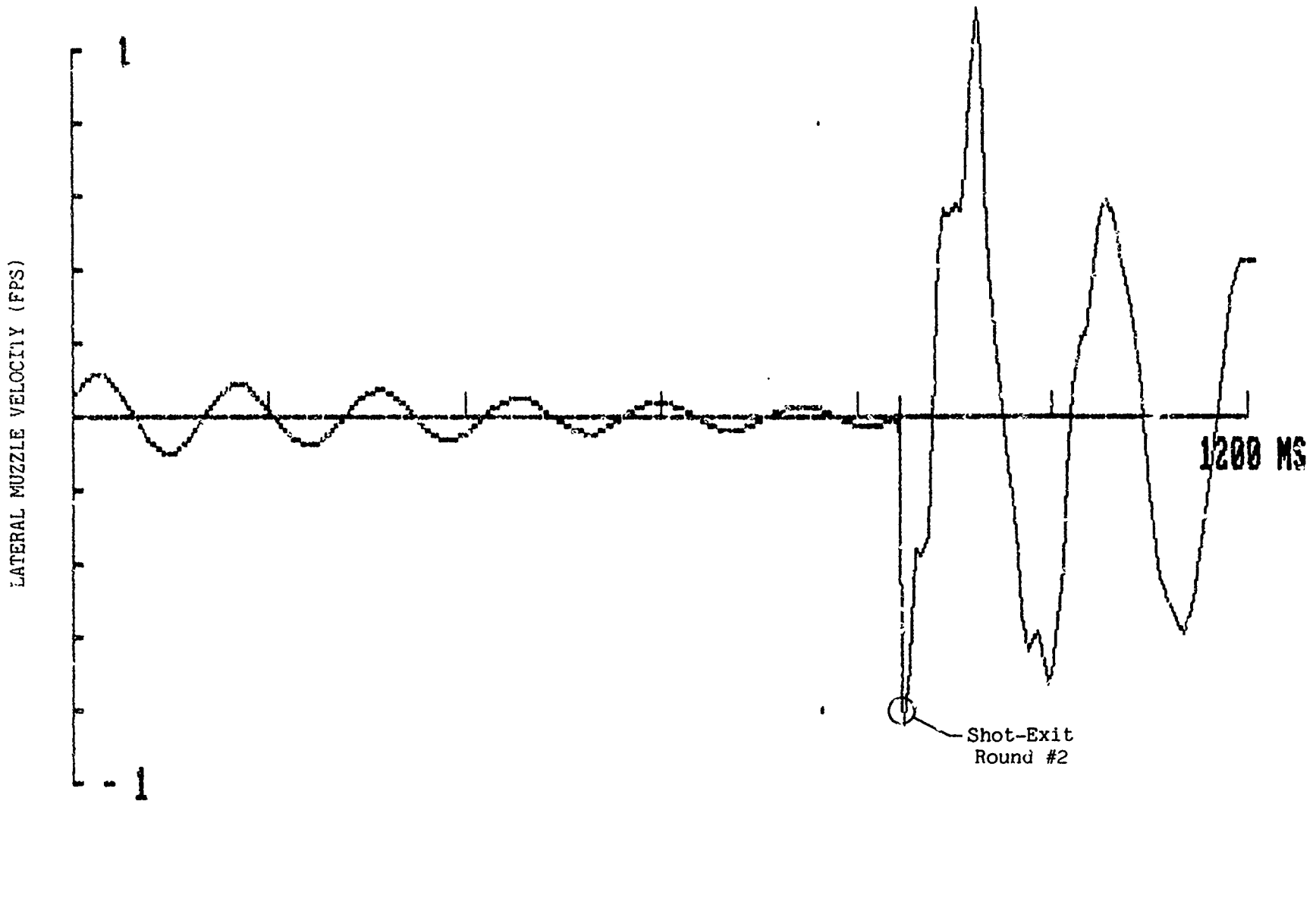

Fig. 30 (Cont'd.)

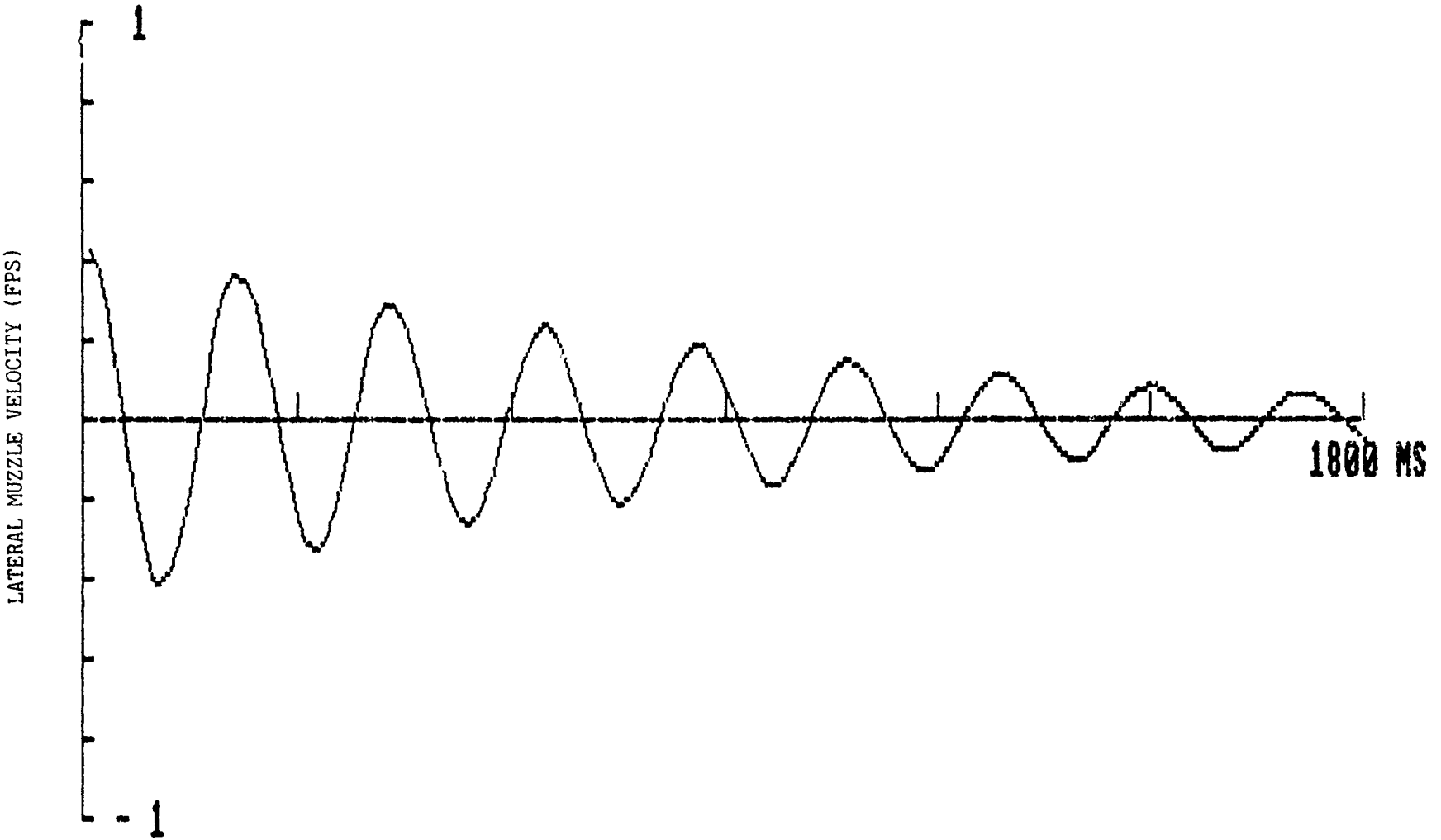

Fig. 30 (Cont'd.)

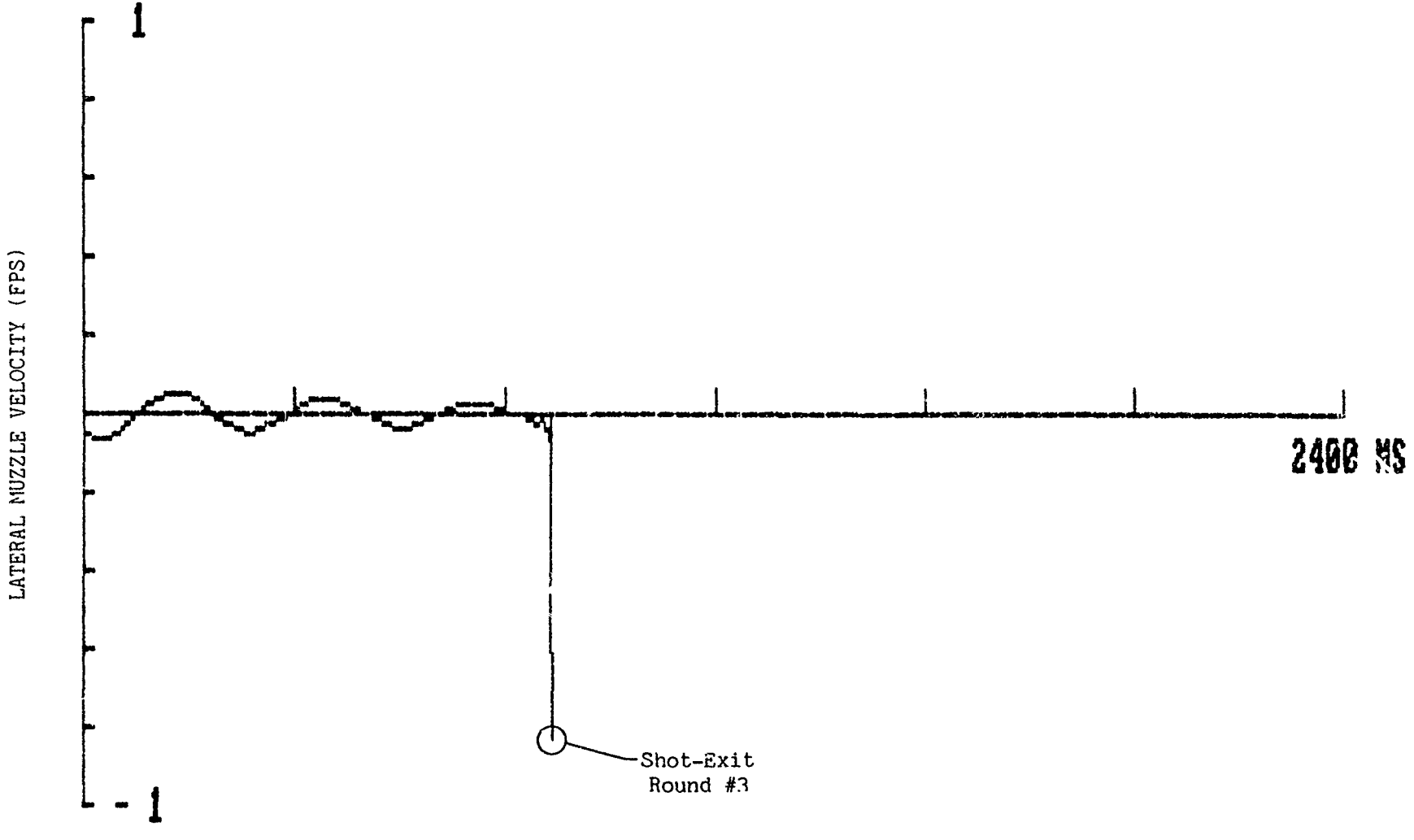

Fig. 30 (Cont'd.)

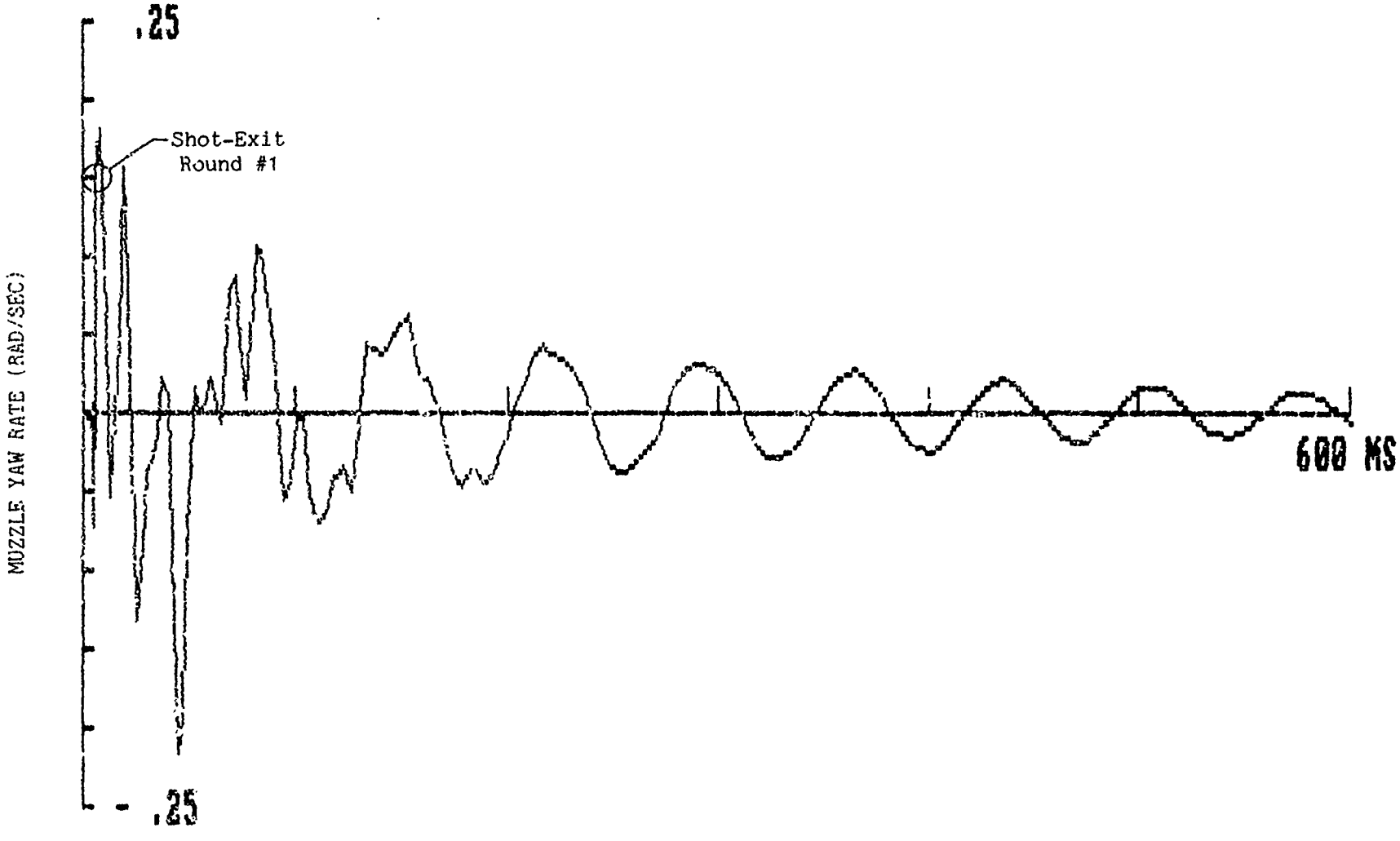

Fig. 31 - Muzzle Yaw Rate for Three-Round Burst With Vertical-Plane "Window"

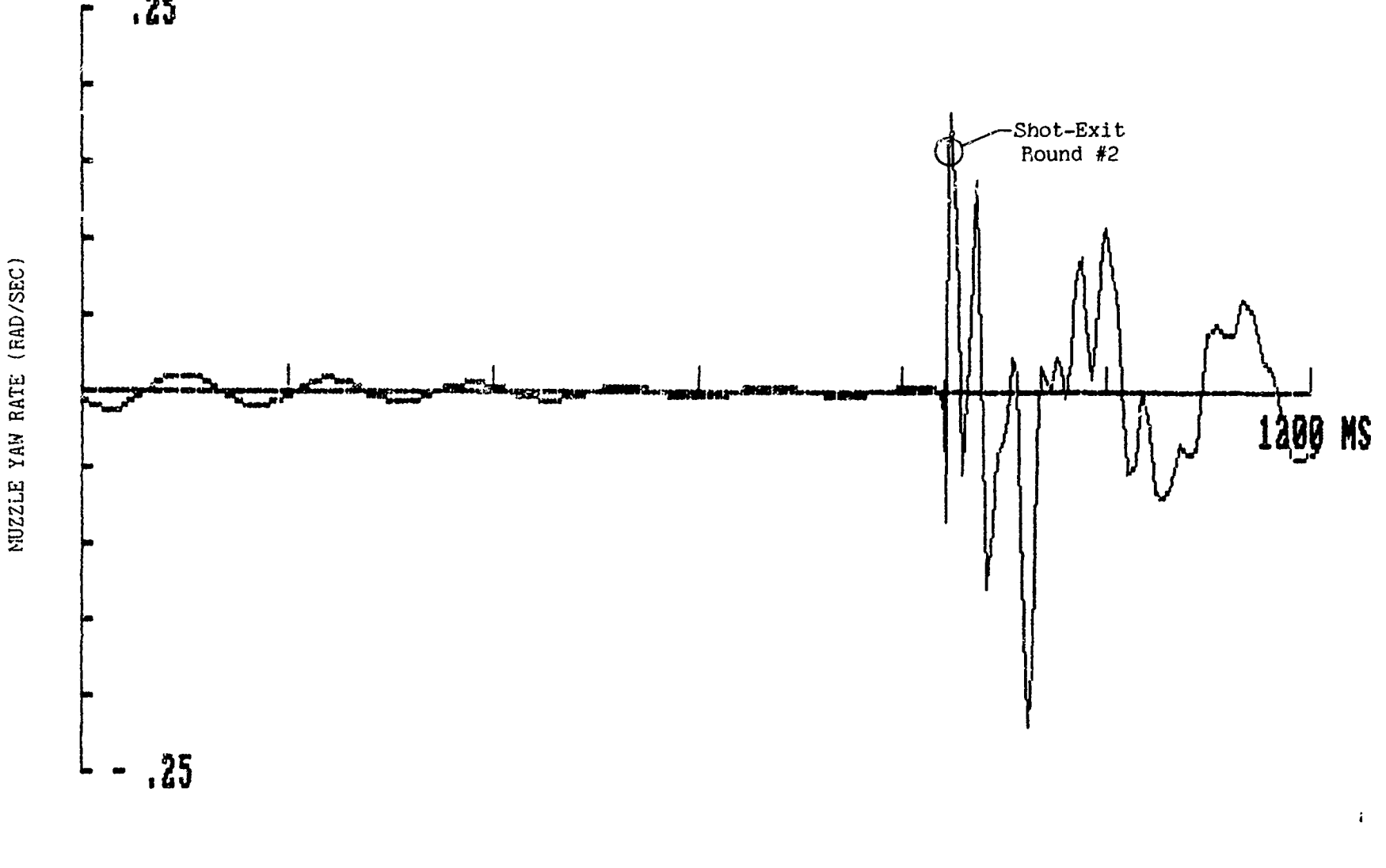

Fig. 31 (Cont'd.)

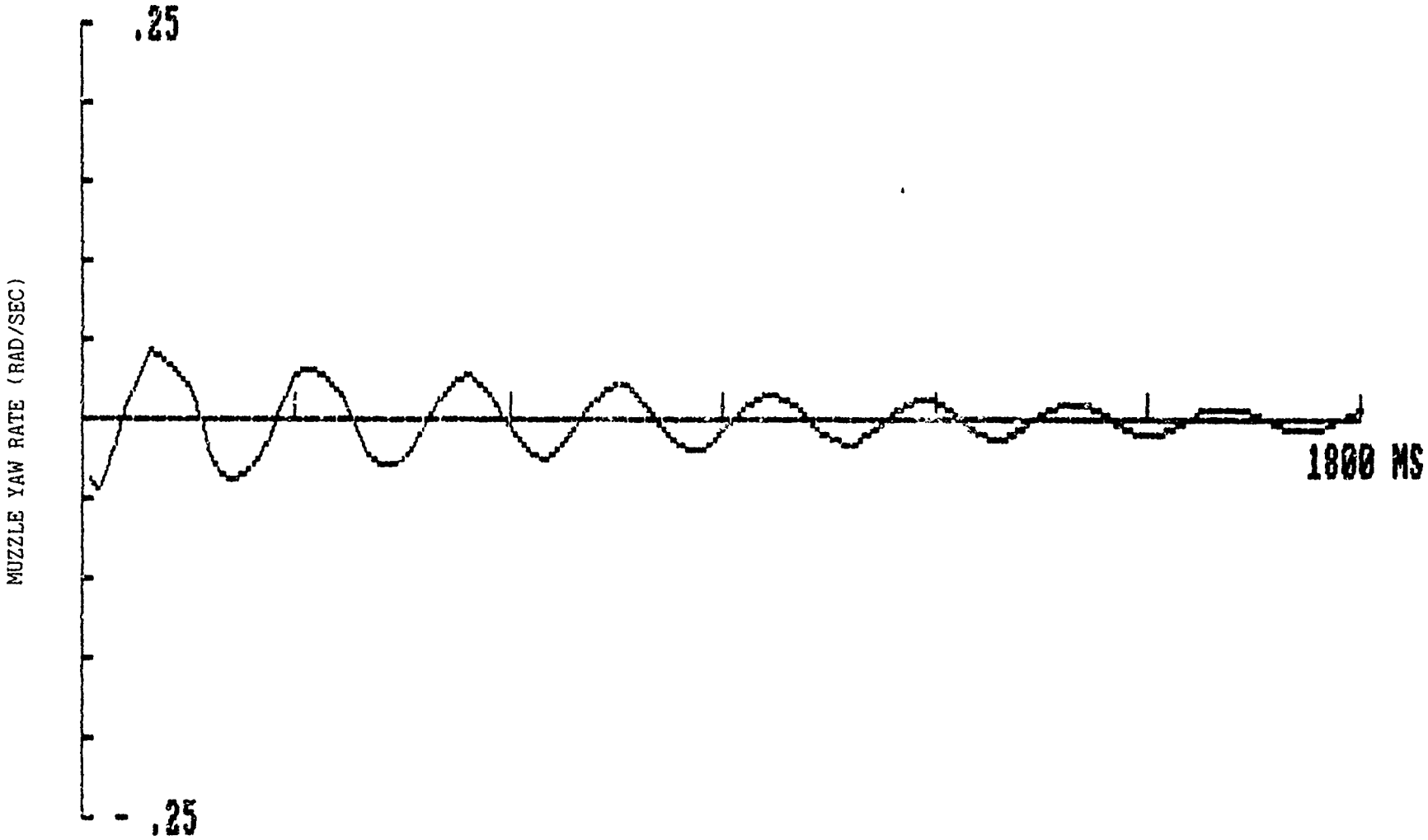

Fig. 31 (Cont'd.)

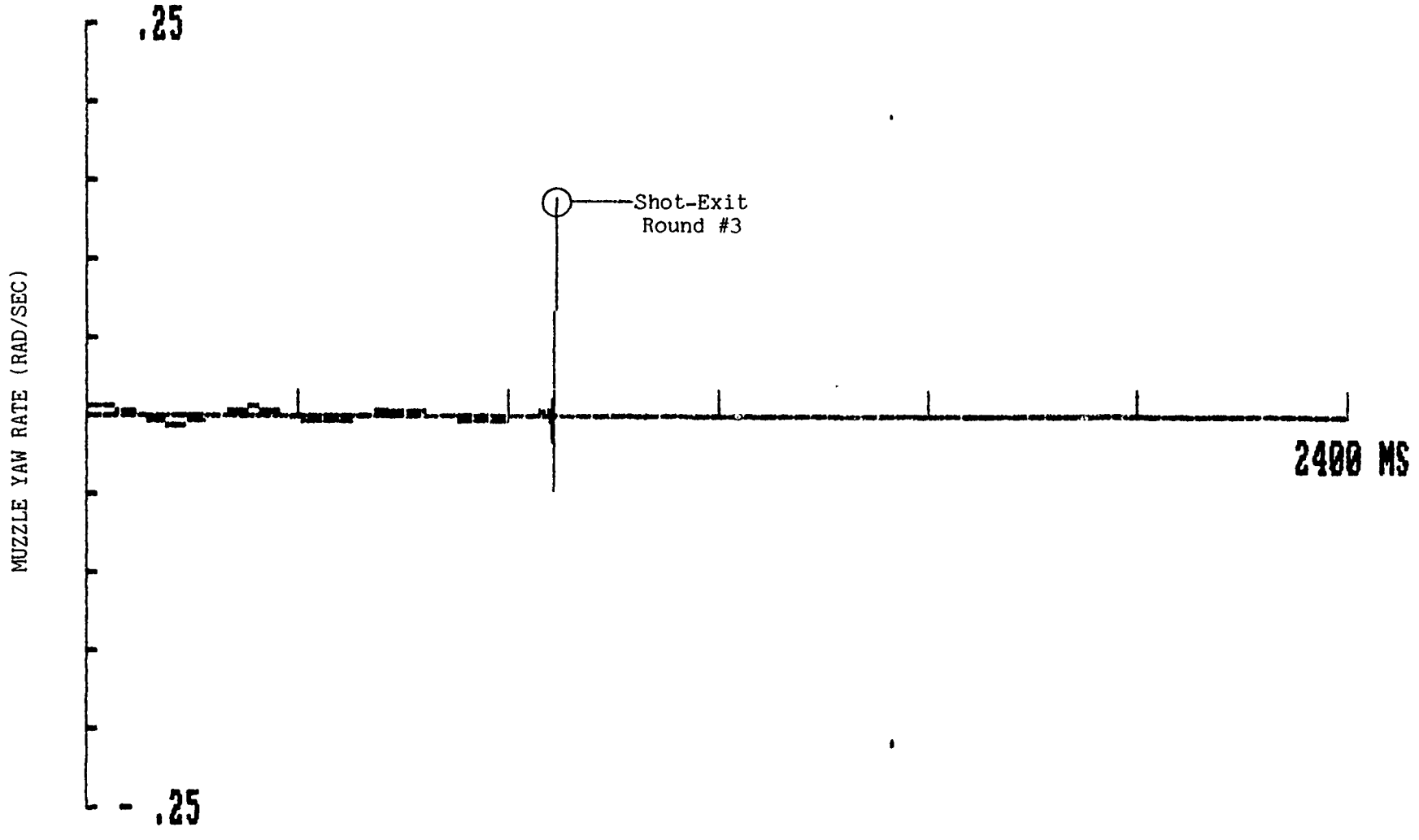

Fig. 31 (Cont'd.)

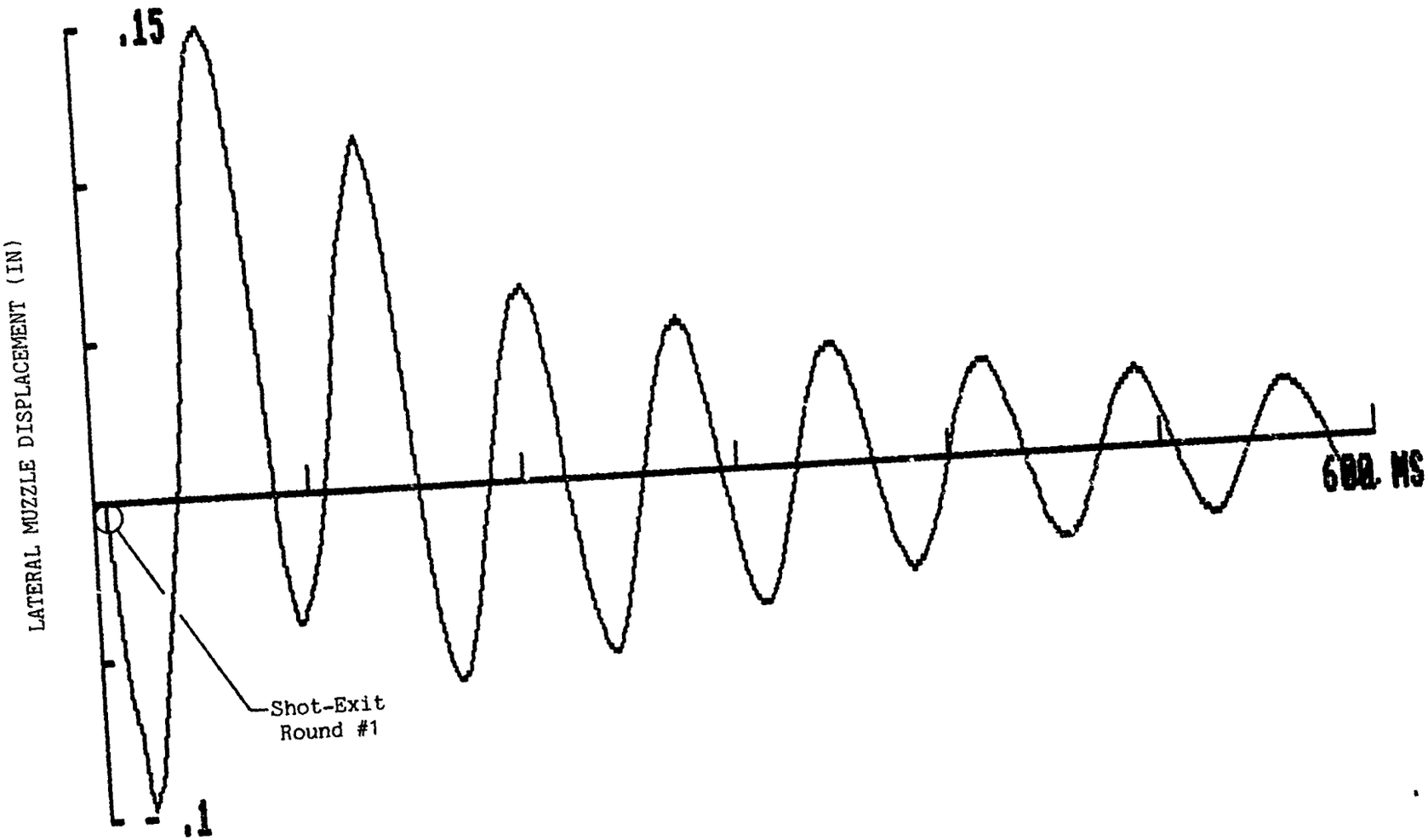

Fig. 32 - Lateral Muzzle Displacement for Three-Round Burst With Combined Vertical and Horizontal-Plane "Windows"

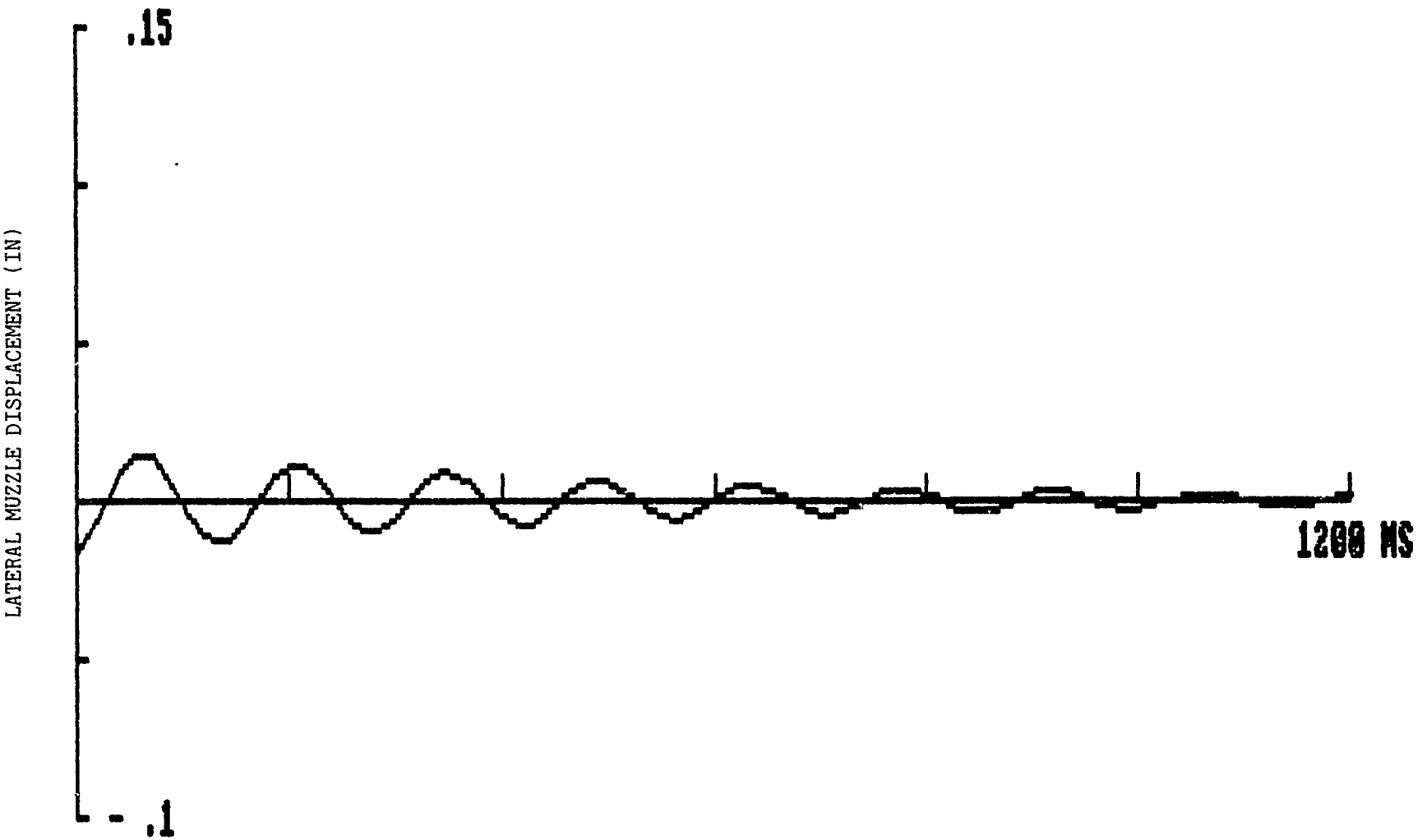

Fig. 32 (Cont'd.)

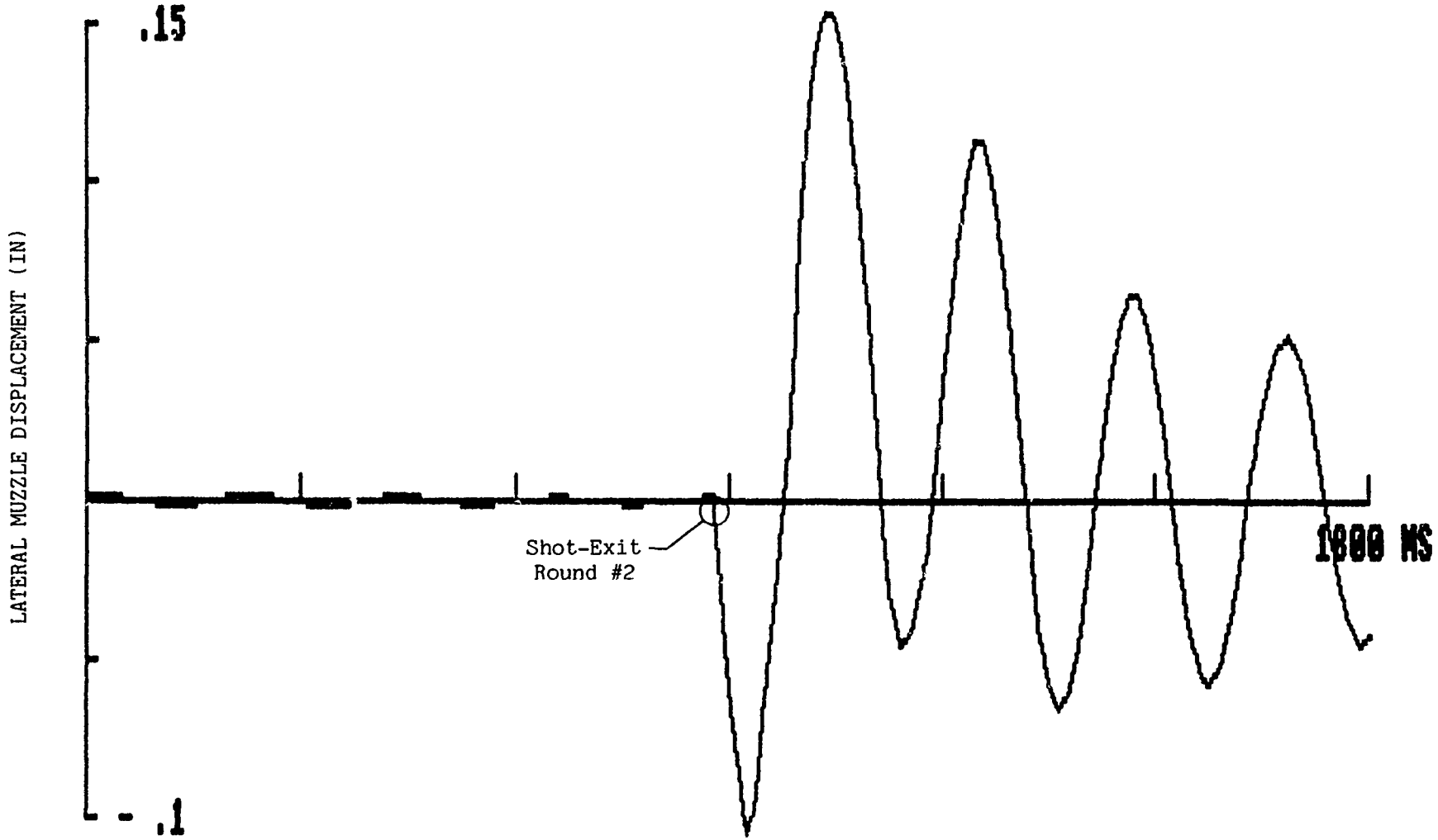
.15
LATERAL MUZZLE DISPLACEMENT (IN)
- .1
Shot-Exit
Round #2
1000 MS

Fig. 32 (Cont'd.)

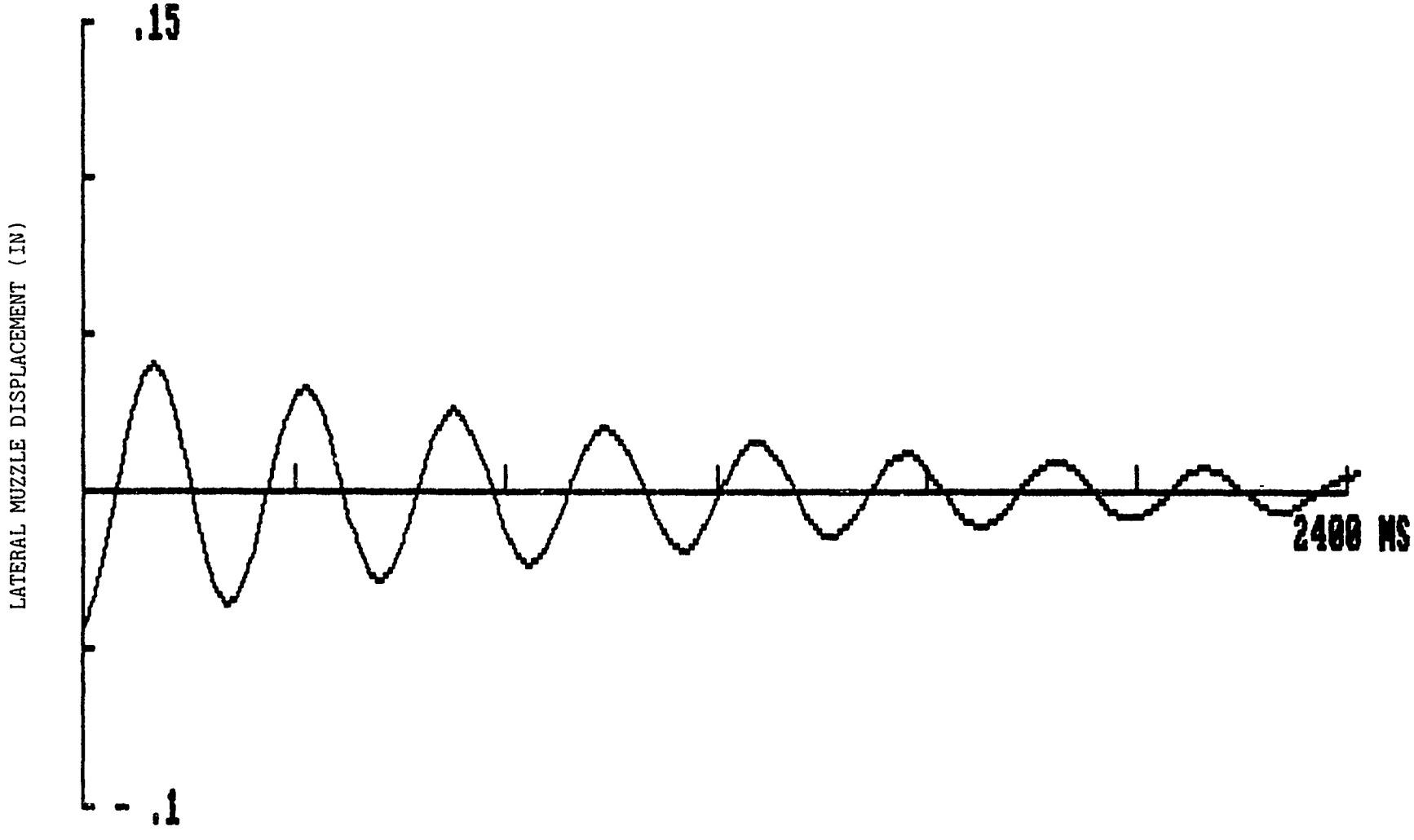

Fig. 32 (Cont'd.)

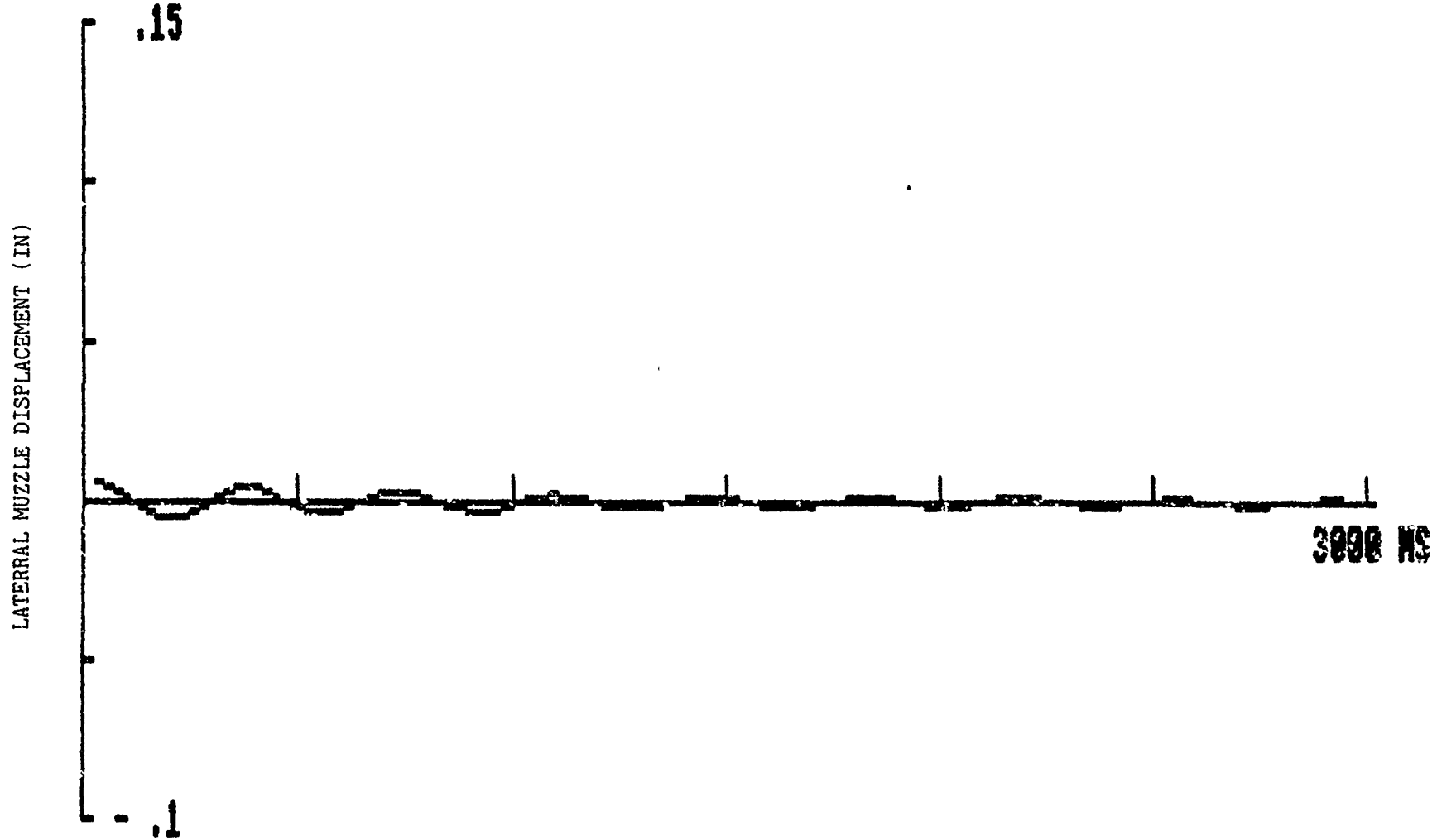

Fig. 32 (Cont'd.)

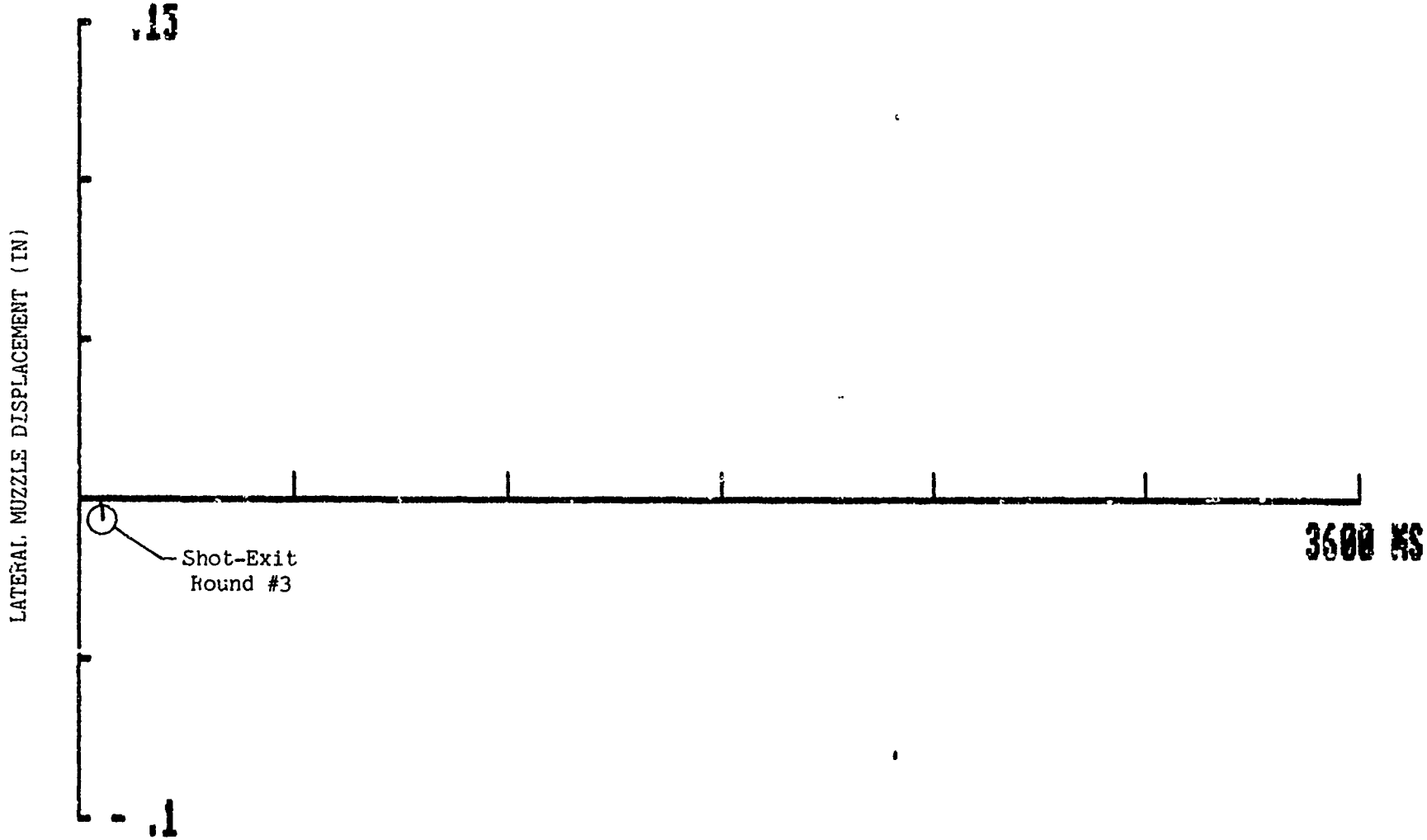
.15
LATERAL MUZZLE DISPLACEMENT (IN)
Shot-Exit
Round #3
3600 MS
- .1

Fig. 32 (Cont'd.)

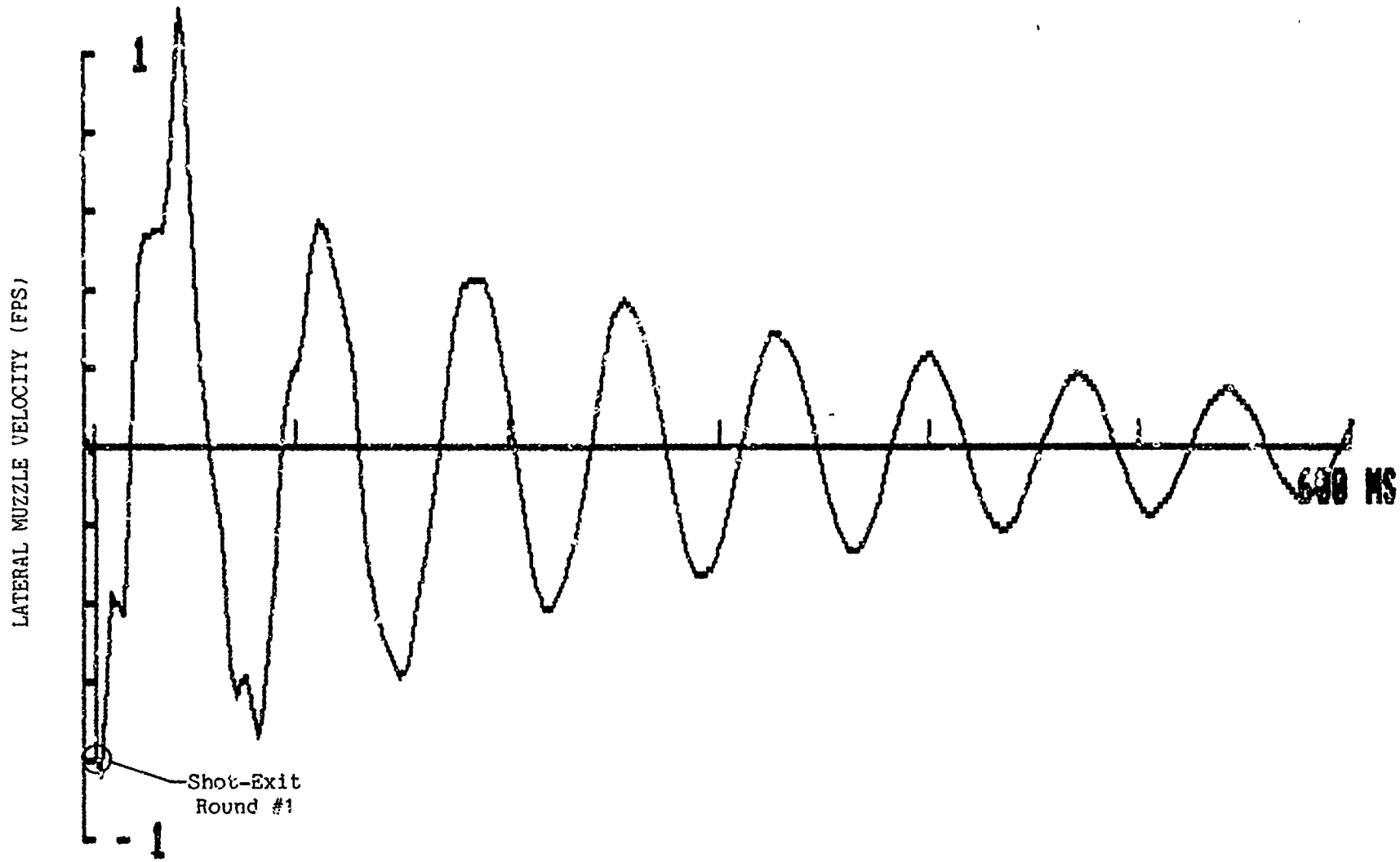

Fig. 33 - Lateral Muzzle Velocity for Three-Round Burst With Combined Vertical and Horizontal-Plane "Windows"

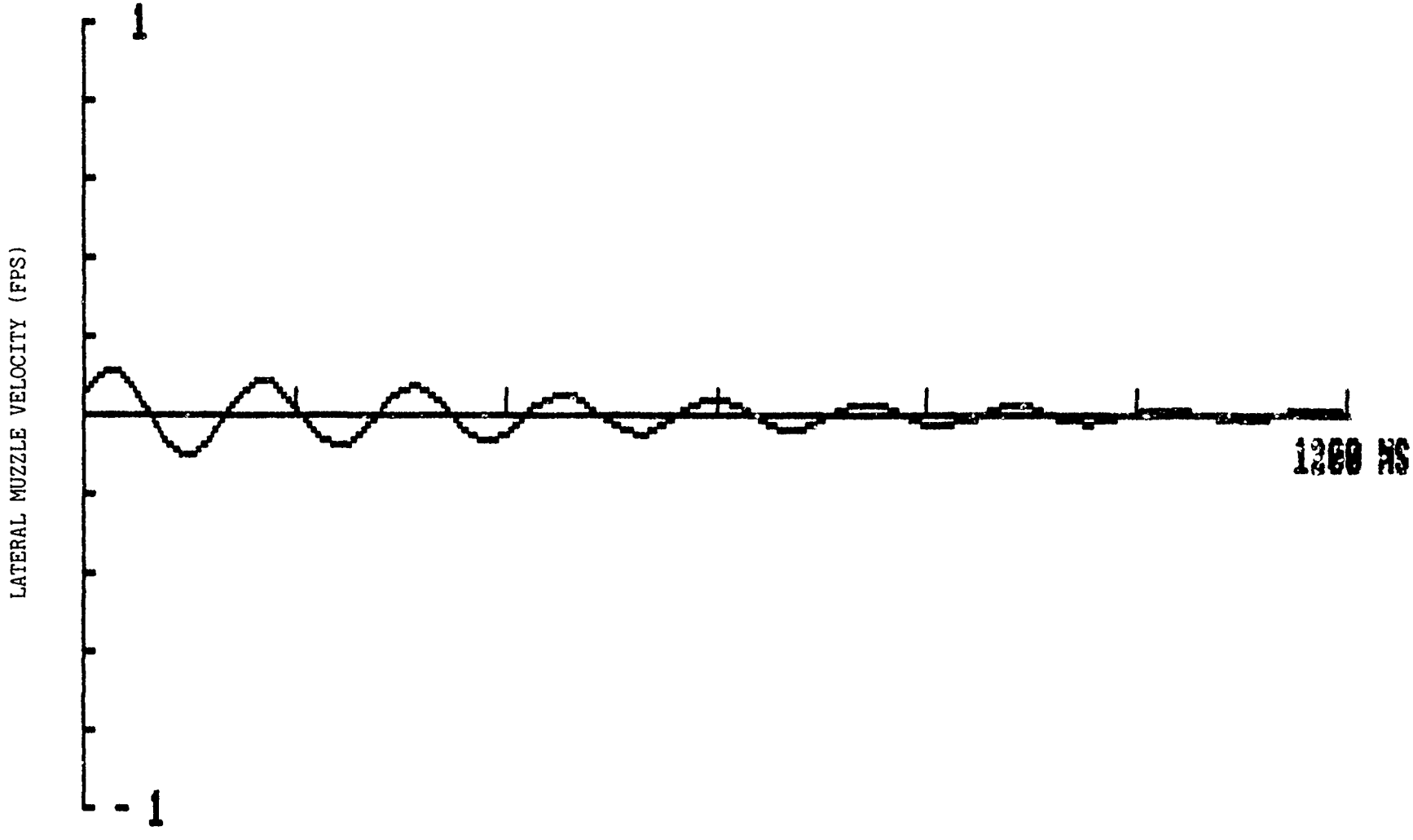

Fig. 33 (Cont'd.)

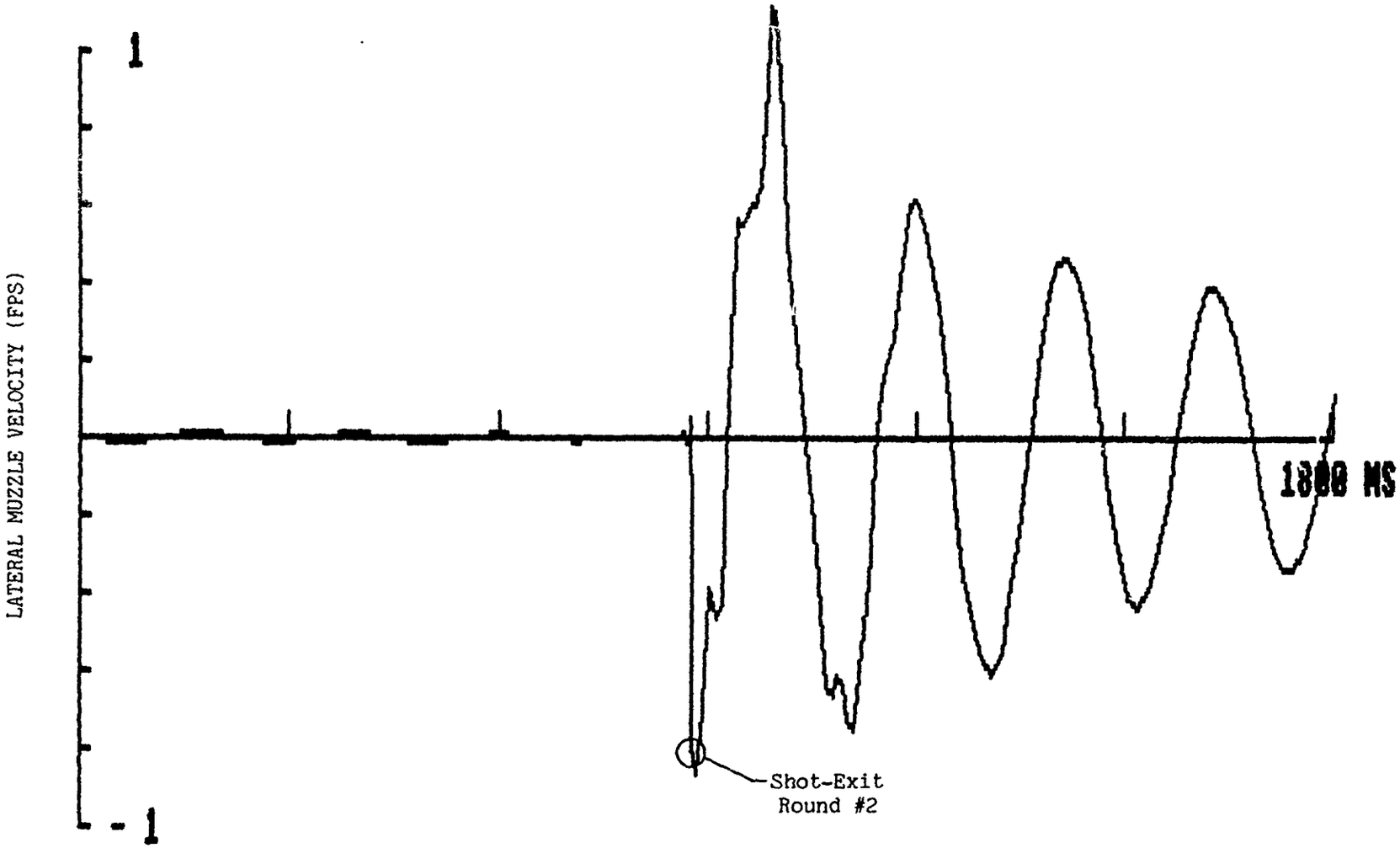

Fig. 33 (Cont'd.)

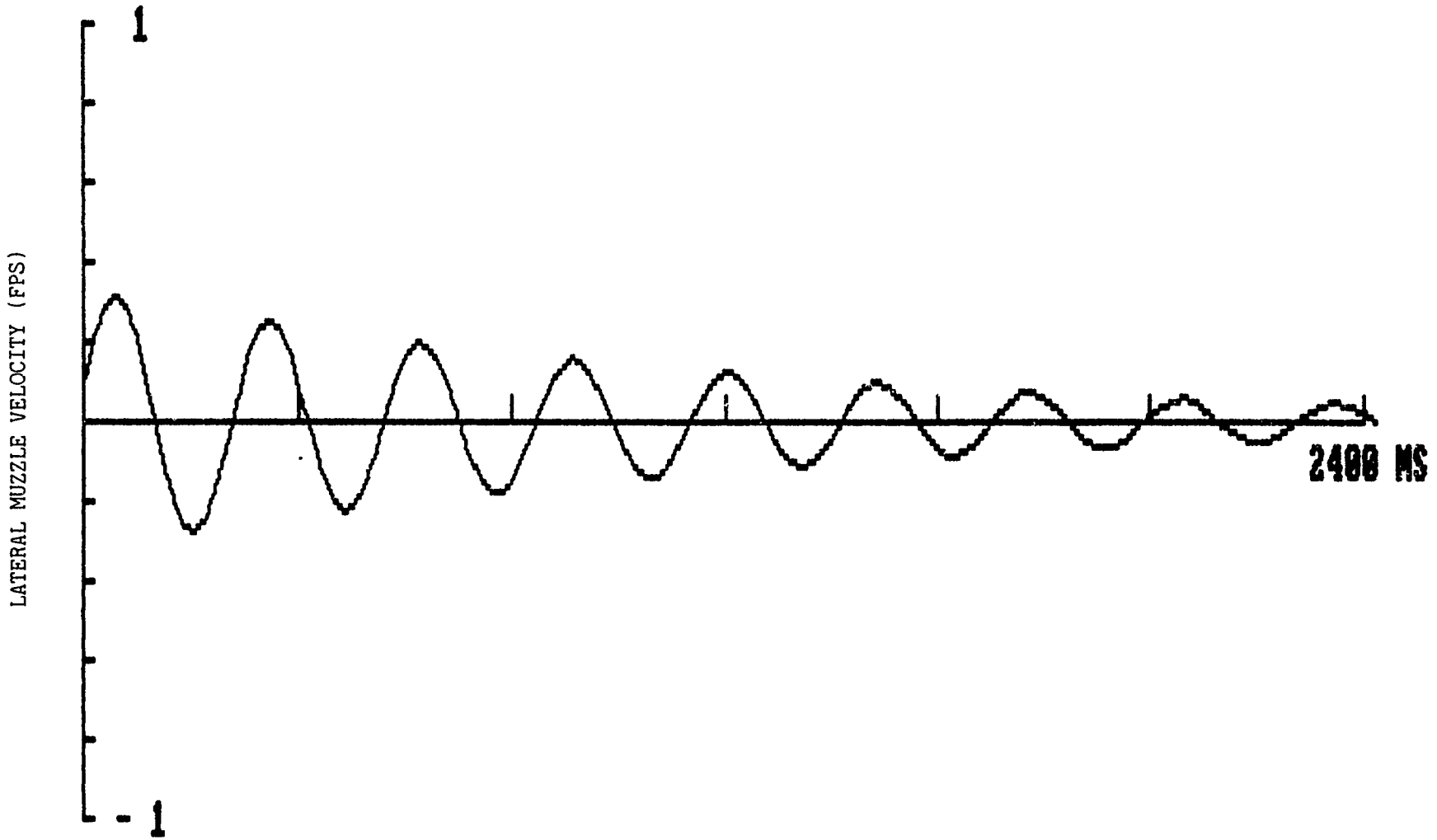

Fig. 33 (Cont'd.)

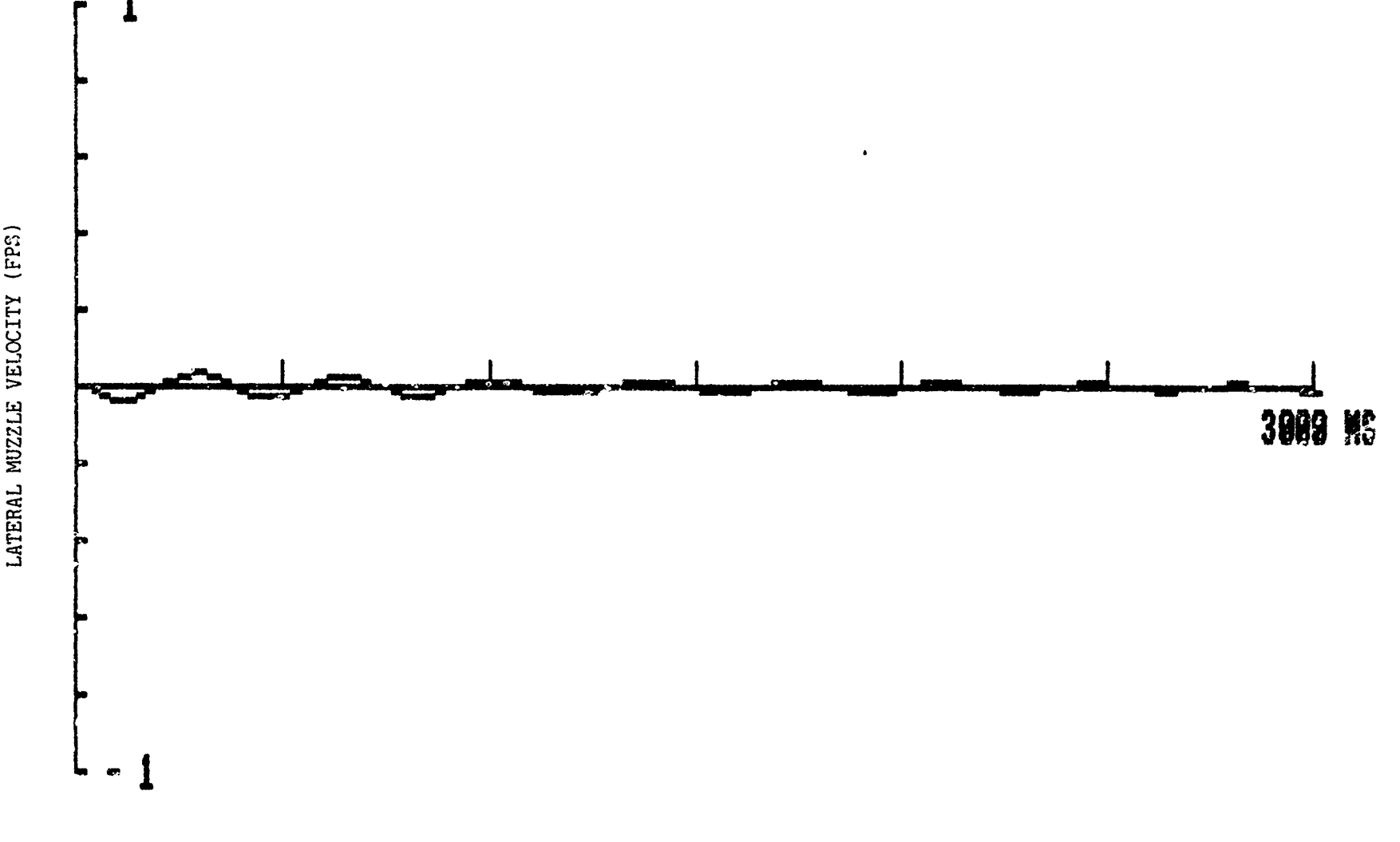

Fig. 33 (Cont'd.)

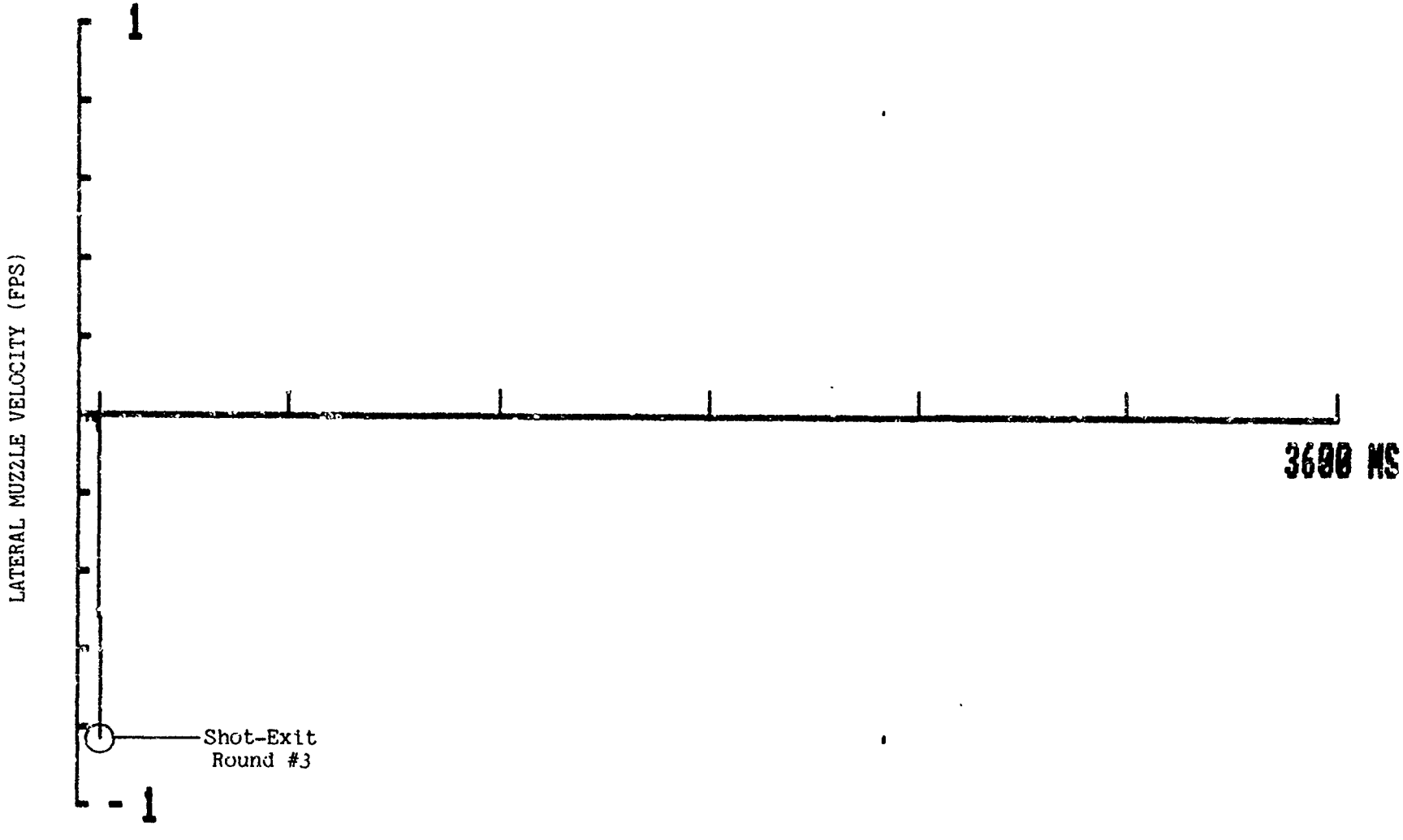

Fig. 33 (Cont'd.)

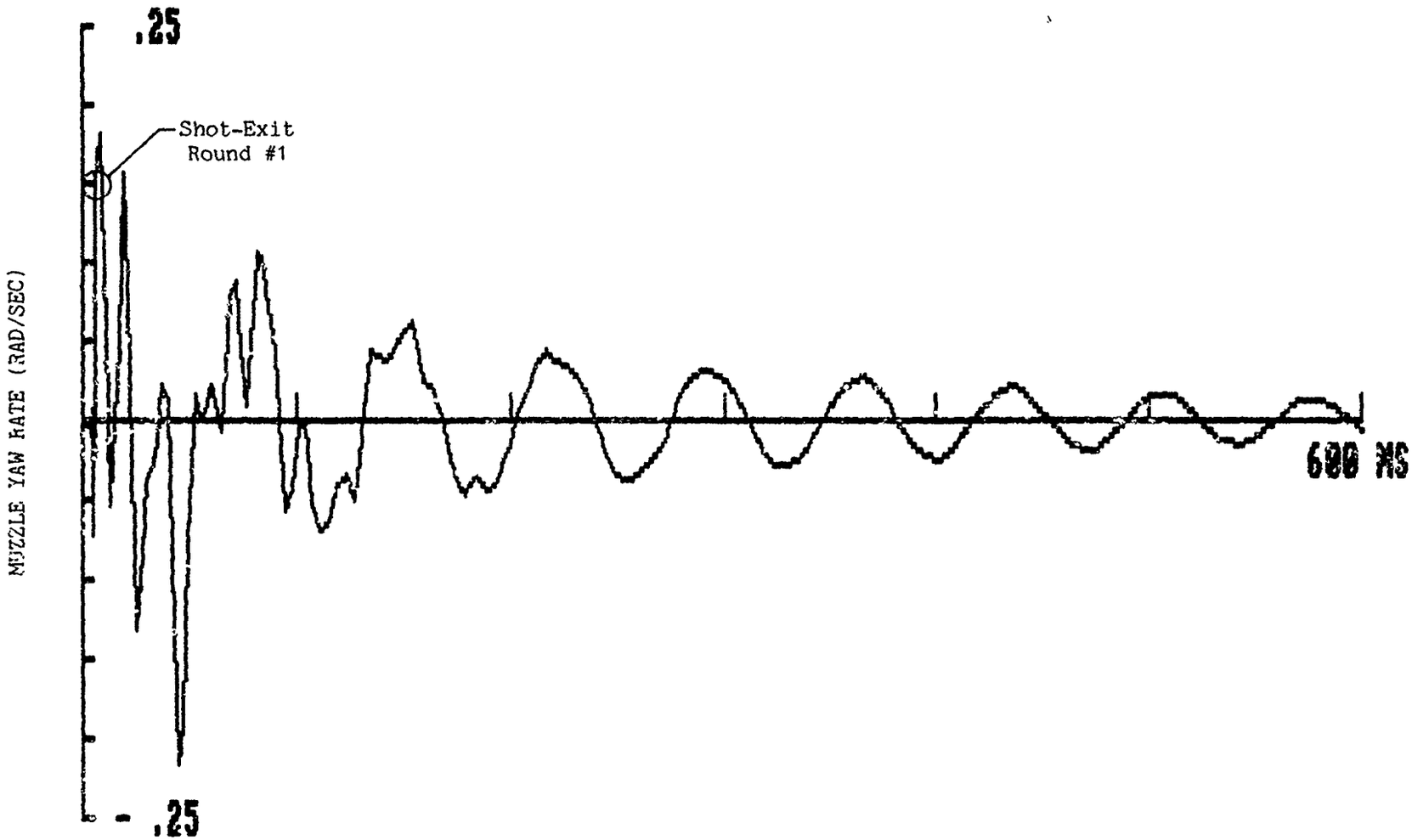

Fig. 34 - Muzzle Yaw Rate for Three-Round Burst With Combined Vertical and Horizontal-Plane "Windows"

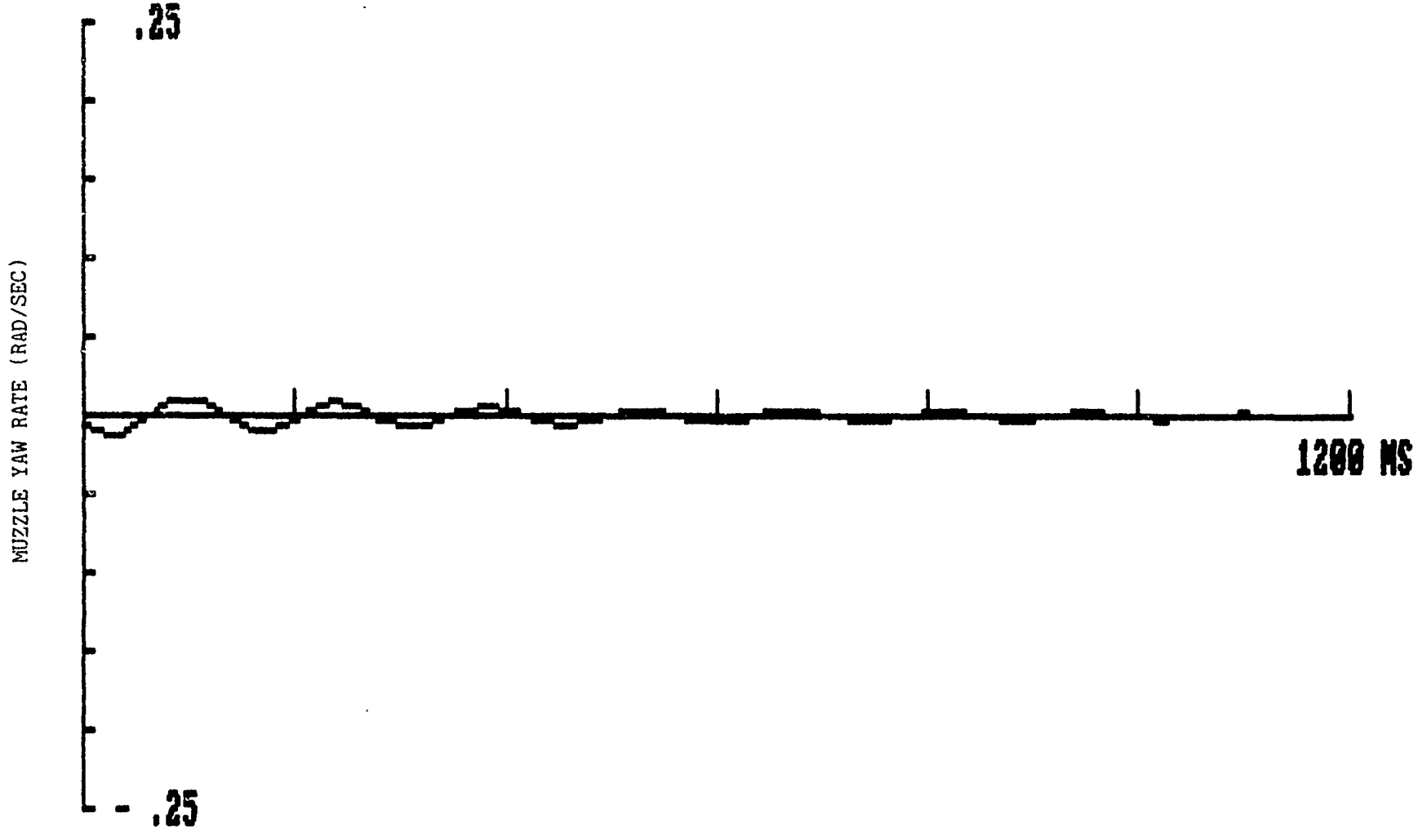

Fig. 34 (Cont'd.)

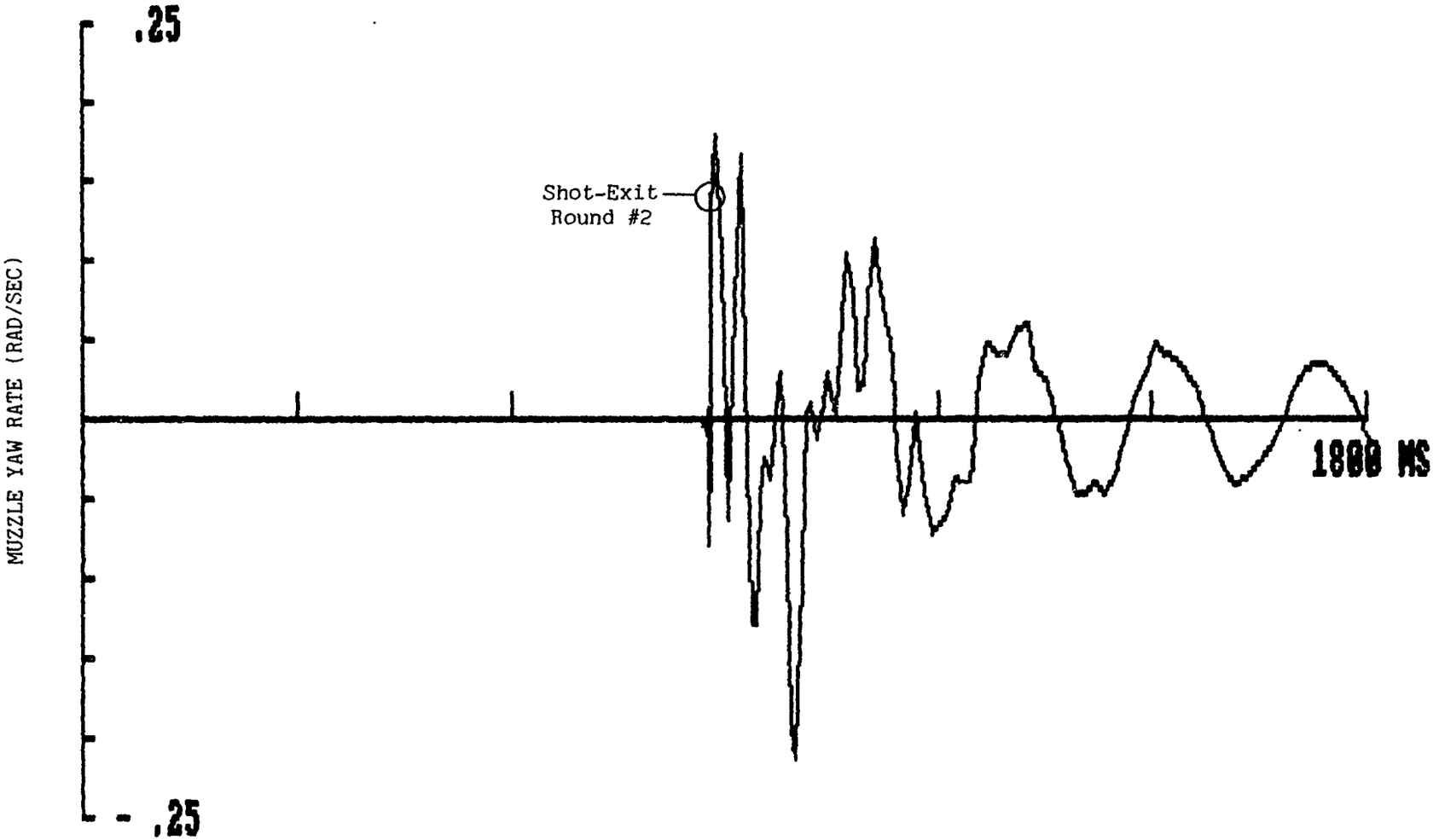

Fig. 34 (Cont'd.)

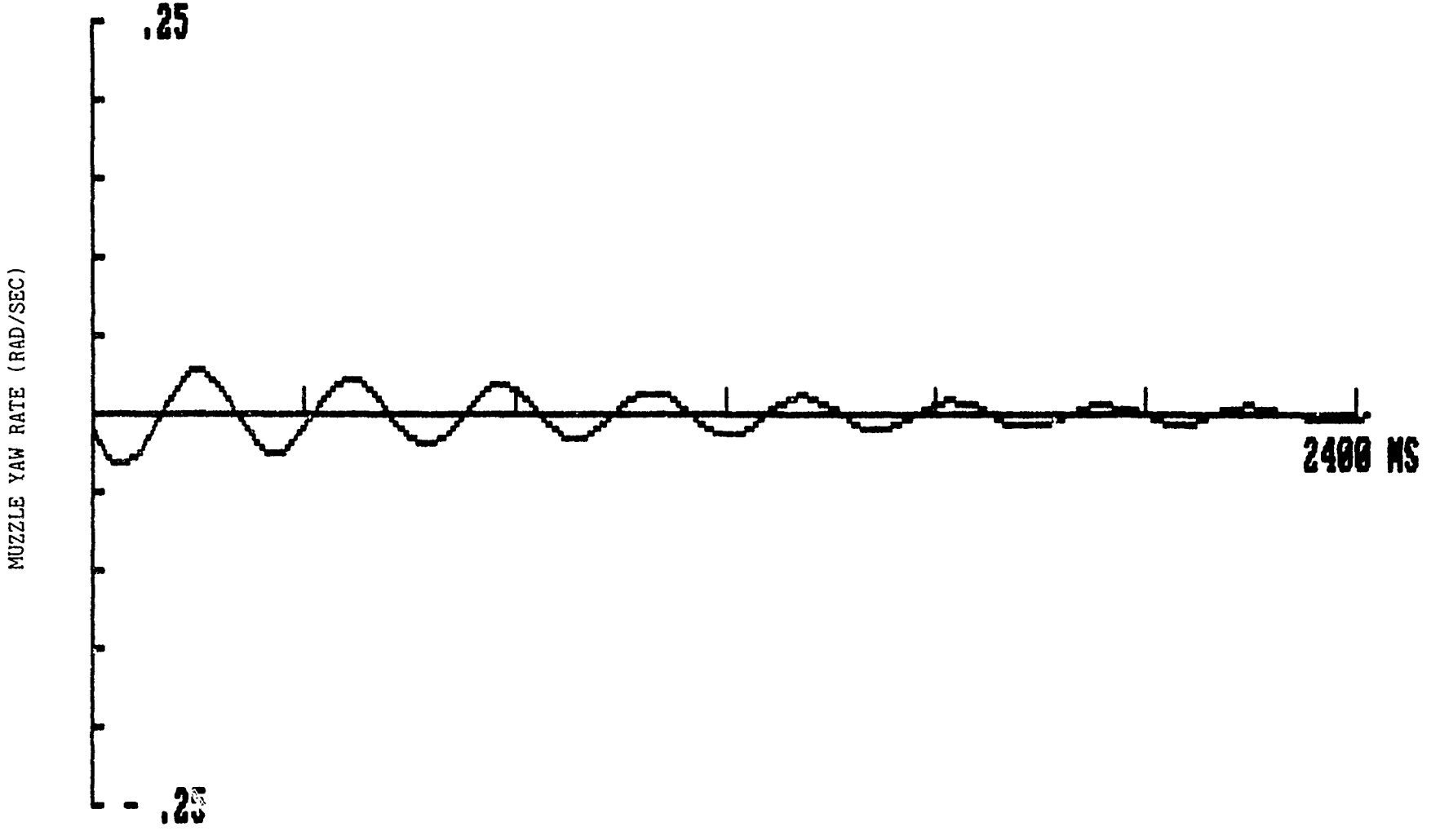

Fig. 34 (Cont'd.)

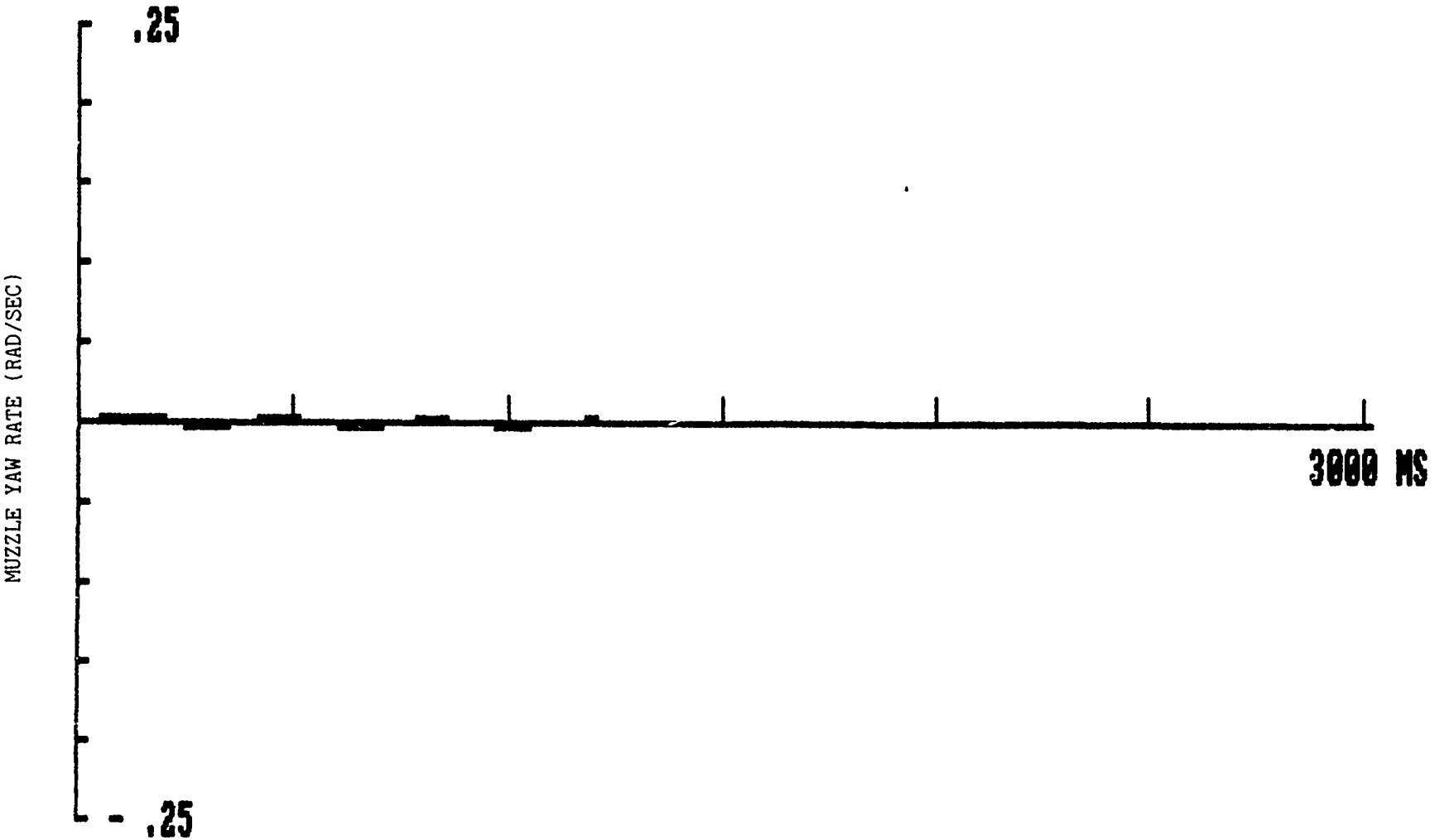

Fig. 34 (Cont'd.)

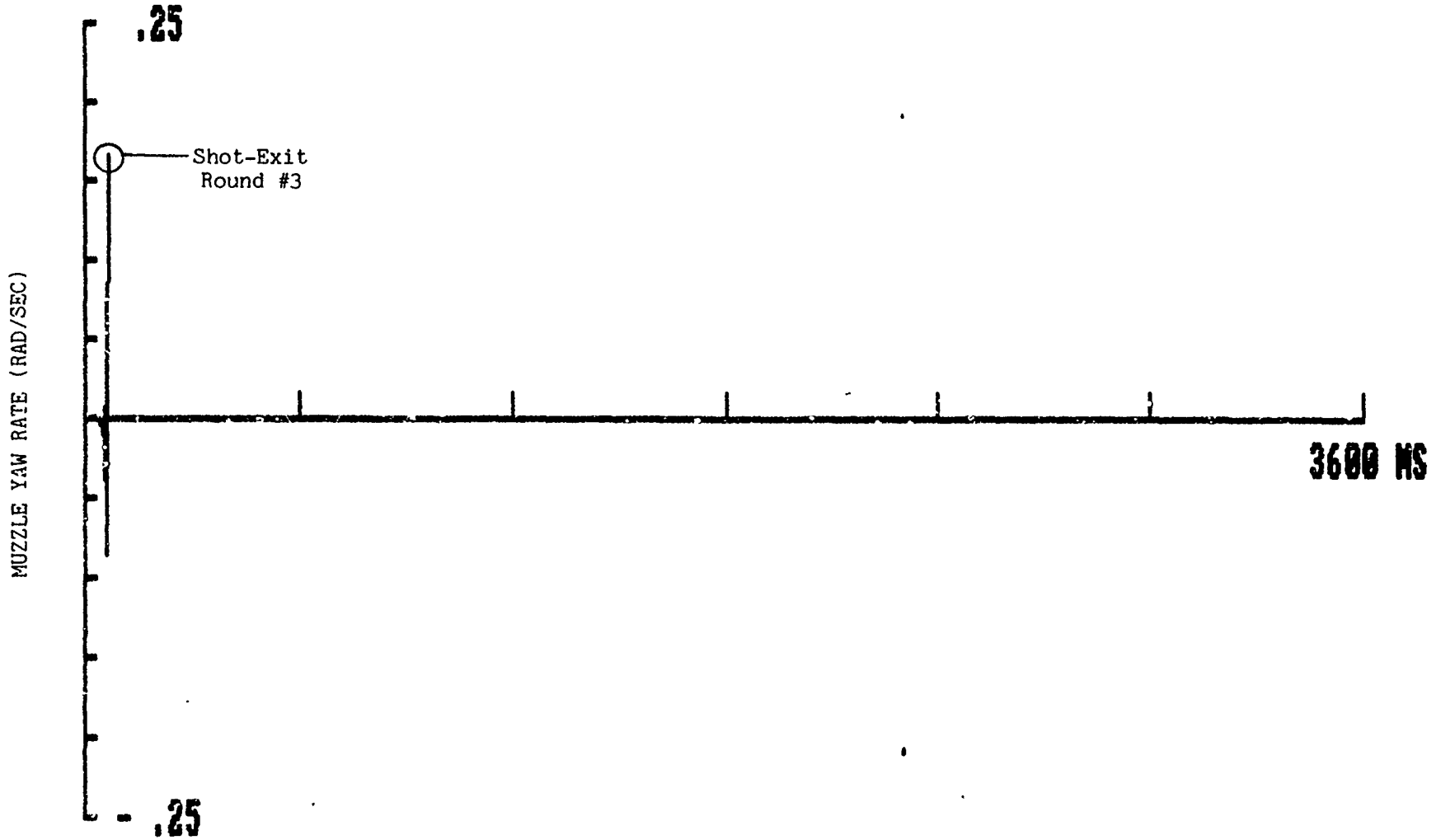

Fig. 34 (Cont'd.)

TABLE III - COMPARISON OF CONTROLLED VERSUS UNCONTROLLED THREE-ROUND BURST-MODE FIRE ON MOVING VEHICLE

		MUZZLE MOTION PARAMETERS AT SHOT-EXIT					
		VERTICAL-PLANE			HORIZONTAL-PLANE		
	Shot-Exit Time (ms)	Displacement (in)	Velocity (fps)	Pitch Rate (rad/sec)	Displacement (in)	Velocity (fps)	Yaw Rate (rad/sec)
Round 1							
U	6.3	- .004	- .048	- .007	- .004	- .792	+ .150
C1							
C2							
Round 2							
U	1006.2	+ .005	+ .139	+ .006	- .004	- .872	+ .155
C1	1023.6	+ .006	+ .181	- .009	- .007	- .788	+ .148
C2	1493.0	+ .001	+ .006	- .021	- .003	- .786	+ .128
Round 3							
U	2006.4	+ .006	+ .075	- .011	- .004	- .820	+ .143
C1	2022.8	+ .001	+ .102	- .006	- .004	- .815	+ .132
C2	3010.8	- .001	+ .108	- .005	- .005	- .826	+ .165

U - Without firing control signal
C1 - Vertical-plane "window" only
C2 - Combined vertical and horizontal-plane "windows"

6. CONCLUSIONS

Employing a Monte-Carlo routine and random number generator, DYNACODE-G has been modified such that based on a limited number of actual firings the user may now generate a statistically meaningful sample of "mathematical" firings in order to assess shot-to-shot variations in muzzle motion (or any other gun system response parameter of interest), for a particular class of ammunition. Although the 75mm ADMAG served as baseline gun system, with LAV firings as data base, the techniques developed are general and may be applied to any other gun system and data base of interest.

To simulate gun system response to vehicle motion over prescribed terrain, DYNACODE-G has been modified to accommodate acceleration inputs at the trunnion level. Using the 75mm ADMAG as baseline gun system, and M1 vehicle motion on the Munson straight, full and washboard courses as data base, typical cycles of vehicle motion data were simulated analytically and input into DYNACODE-G. Resulting output provides a means for assessing the effects of firing-on-the-move and the user may readily introduce a Monte-Carlo routine, with equally weighted random number generator, to predict probable gun tube muzzle motion prior to firing a vehicle mounted gun. The analyses performed are restricted to the vehicle motion data base provided; however, the techniques used in simulating vehicle motion should prove generally applicable to other vehicles and terrain.

In order to efficiently handle the computational requirements of tracking gun system response during burst-mode fire, an automated (self-determining) variable time-step numerical integration scheme has been developed and successfully implemented. This scheme could of course be introduced into the other versions of DYNACODE-G: however, the fixed time-step routine has proven to be of adequate computational efficiency when handling single-shot fire.

Finally, a version of DYNACODE-G with variable time-step integration and vehicle motion has been extended to incorporate an external firing signal and firing "windows" for controlled burst-mode fire. The program logic developed tracks muzzle motion subsequent to a firing and accepts a firing signal for the next round of a burst after sufficient time has elapsed (i) to load the next round and (ii) for muzzle motion to subside to acceptable "window" values. Using, for illustrative purposes, a load time of 1 sec for the 75mm ADMAG, muzzle motion has generally dissipated when firing on a fixed mount; however, muzzle motion is reinforced when firing on a moving vehicle. Using simulated M1 vehicle motion on the Munson full course, three three-round bursts, consisting of uncontrolled fire, controlled fire with a vertical plane "window" only, and controlled fire with both vertical and horizontal plane "windows" have been compared. The results of this comparison show that although it indeed seems plausible to introduce a firing "window" to optimize burst-mode fire, further study is needed to determine the parameters (and/or combinations thereof) which must be bounded, as well as acceptable "window" values. The latter will of course require a trade-off with delay time between firings to achieve burst-mode optimization. In addition, when firing-on-the-move, consideration must also be given to the nature of vehicle motion, the relative timing of the firing signal and phase relations between muzzle and vehicle motions.

ACKNOWLEDGEMENTS

The authors wish to express their appreciation to Mr. James O. Pilcher II, Interior Ballistics Division, U.S. Army Ballistic Research Laboratory, Aberdeen Proving Ground, MD, for his valuable technical assistance, critique and support during the course of this effort. The authors also wish to express their appreciation to Mrs. Melinda B. Krummerich and Miss Susan A. Coates, IBD, BRL, for their support in reducing the firing and vehicle motion data, and performing the required statistical analyses.

DISTRIBUTION LIST

No. of Copies	Organization
12	Administrator Defense Technical Info Center ATTN: DTIC-FDAC Cameron Station, Bldg. 5 Alexandria, VA 22304-6145
1	HQDA DAMA-ART-M Washington, D.C. 20310
1	Commander US Army Materiel Command ATTN: AMCDMD-ST 5001 Eisenhower Avenue Alexandria, VA 22333
10	CIA OIR/DB/Standard GE-47 HQ Washington, DC 20505
1	Commander U.S. Army Armament Research, Dev. & Engineering Center ATTN: SMCAR-MSI Dover, NJ 07801-5001
1	Commander U.S. Army ARDEC ATTN: SMCAR-TDC Dover, NJ 07801-5001
1	Commander U.S. Army AMCCOM, ARDEC, CCAC Benet Weapons Laboratory ATTN: SMCAR-CCB-TL Watervliet, NY 12189-4050
1	Commander U.S. Army BMD Advanced Technology Center ATTN: BMDATC-M, Mr. P. Boyd P.O. Box 1500 Huntsville, AL 35804
3	Commander U.S. Army AMCCOM, ARDC Dover, NJ 07801-5001
1	Commander U.S. Army Materiel Dev. and Readiness Command ATTN: AMCLDC 5001 Eisenhower Avenue Alexandria, VA 22333-0001
1	Commander U.S. Army AMCCOM, ARDC ATTN: Product Assuranc Directorate SMCAR-QAR-RIB, D. IMHOF Dover, NJ 07801-5001
1	Commander U.S. Army Armament, Munitions and Chemical Command ATTN: AMSMC-IMP-L Rock Island, IL 61299-7300
1	Commander U.S. Army Aviation Research and Development Command ATTN: AMSAV-ES 4300 Goodfellow Blvd. St. Louis, MO 63120-1798
1	Director U.S. Army Aviation Research and Technology Activity Ames Research Center Moffett Field, CA 94035-1099
1	Commander U.S. Army Communications Electronics Command ATTN: AMSEL-L Fort Monmouth, NJ 07703
1	Commander CECOM R&D Technical Library ATTN: AMSEL-IML (Rpts Section) B-2700 Fort Monmouth, NJ 07703-5300

DISTRIBUTION LIST

No. of Copies	Organization
1	Commander U.S. Army Missile Command ATTN: AMSMI-RX, M.W. Thauer Redstone Arsenal, AL 35898-5249
1	Director U.S. Army TRADOC Analysis Center ATTN: ATOR-TSL WSMR, NM 88002-5502
1	Commander U.S. Army Development and Employment Agency ATTN: MODE-ORO Fort Lewis, WA 98433-5000
1	Air Force Armament Laboratory ATTN: AFATL/DLODL Eglin AFB, FL 32542-5000
1	Commander U.S. Army Tank Automotive Cmd ATTN: AMSTA-TSL Warren, MI 48090
2	Director U.S. Army Materials and Mechanics Research Center ATTN: J. Mescall Tech. Library Watertown, MA 02172
2	Commander Naval Sea Systems Command (SEA-62R41) ATTN: L. Pasiuk Washington, DC 20362
1	Commander Naval Explosive Ordnance Disposal Facility ATTN: Lib Div Indian Head, MD 20640
1	Superintendent Naval Postgraduate School ATTN: Dir of Lib Monterey, CA 93940
1	Commander Naval Weapons Center ATTN: Code 3431, Tech Lib China Lake, CA 93555
1	AFELM, The Rand Corporation ATTN: Library-D 1700 Main Street Santa Monica, CA 90406
2	Project Manager Tank System ATTN: AMCPM-GCM-SV, Dr. M.R. Pattison Warren, MI 48397-5000
2	Project Manager Tank Main Armament Systems ATTN: AMCPM-TMA-PC, K. Rubin Dover, NJ 07801-5001

Aberdeen Proving Ground

Dir, USAMSAA
ATTN: AMXSY-D
AMXSY-MP, H. Cohen

Cdr, USATECOM
ATTN: AMSTE-TO-F

DIR, DRSTE-SG-H, Mr. Cole
Mr. Witt

Cdr, CRDEC, AMCCOM
ATTN: SMCCR-RSP-A
SMCCR-MU
SMCCR-SPS-IL